

Silja Bergitte Nordvik

Installation of Anchors for Mooring System of Floating Wind Turbines

June 2019



Norwegian University of
Science and Technology

Installation of Anchors for Mooring System of Floating Wind Turbines

Silja Bergitte Nordvik

Marine Technology

Submission date: June 2019

Supervisor: Kjell Larsen

Norwegian University of Science and Technology
Department of Marine Technology



MASTER THESIS SPRING 2019

for

Stud. tech. Silja Bergitte Nordvik

Installation of Anchors for Mooring System of Floating Wind Turbines – Comparison of Concepts

Installasjon av anker for forankringssystemer på flytende vindturbiner

Background

In order to be able to design, install and operate floating wind turbines and, in the future, large floating wind parks, cost-effective and safe marine operations are crucial. Capital expenditure of the marine operations for a floating wind park is large part of the total investment cost. An important building block for a floating wind turbine is the mooring system and installation of the anchors.

A key activity to successful subsea installation operations is the planning process. Lifting of subsea equipment, especially through the wave zone, is a weather critical activity. It is crucial that such operations are planned and understood properly and that effective equipment is used. This thesis shall specifically consider installation of anchor concepts for the, mooring system of floating wind turbines. Numerical simulations are an important part of the decision basis. The thesis shall use the tools available in the SIMA/SIMO program suite.

The main challenge of installation of the mooring system is the crane operation of the anchors. The state-of-art concept is the suction anchor. An alternative anchor concept is the Deep Penetrating Anchor (DPA) or the “torpedo” anchor. The thesis shall have a special focus on comparison of these anchor types.

Scope of Work

- 1) Review relevant literature and describe the main steps in the planning process of a marine operation in general. Describe briefly state-of-art subsea installation methods by use of crane vessels. For weather restricted operations, an overview of the planning process shall be described; the “alpha factor”-concept and how operability and weather windows can be optimized shall be described in detail.
- 2) Describe possible mooring systems for floating wind turbines. Focus on station keeping principles and main hardware components. Include an overview of the different anchor concepts available for the industry. A special comparison shall be given for the suction anchor and the DPA anchor concepts.
- 3) Familiarize with the numerical simulation suite SIMA/SIMO and describe the theory that is relevant for subsea lifting and installation of anchors.
- 4) Establish numerical simulation models in SIMA for a suction anchor and a DPA anchor. In particular, describe how important parameters like added mass, drag forces and slamming forces are defined in the simulation models. Propose parameters that may determine the design operational limit and estimate limits based on simulation results. The variability of the

design responses shall be assessed. Information on anchor concepts and simulation cases to be defined and discussed together with the supervisor.

5) Operability investigation. Based on simulation results from task 4) and weather data for the Barents Sea, typical operability figures shall be calculated. Cases to be discussed and agreed with supervisor.

6) Conclusions and recommendations for further work.

General information

The work scope may change or prove to be larger than initially anticipated. Subject to approval from the supervisor, topics may be changed or reduced in extent.

In the project the candidate shall present his personal contribution to the resolution of problems within the scope of work.

Theories and conclusions should be based on mathematical derivations and/or logic reasoning identifying the various steps in the deduction.

The candidates should utilise the existing possibilities for obtaining relevant literature.

Report/Delivery

The thesis report should be organised in a rational manner to give a clear exposition of results, assessments, and conclusions. The text should be brief and to the point, with a clear language. Telegraphic language should be avoided.

The report shall be written in English and edited as a research report including literature survey, description of relevant mathematical models together with numerical simulation results, discussion, conclusions and proposal for further work. List of symbols and acronyms, references and (optional) appendices shall also be included. All figures, tables and equations shall be numerated.

The original contribution of the candidate and material taken from other sources shall be clearly defined. Work from other sources shall be properly referenced using an acknowledged referencing system.

The report shall be submitted in Inspira, as specified by the department of Marine Technology. In addition, an electronic copy (pdf) to be sent to the supervisors.

Ownership

NTNU has according to the present rules the ownership of the project results. Any use of the project results has to be approved by NTNU (or external partner when this applies). The department has the right to use the results as if the work was carried out by a NTNU employee, if nothing else has been agreed in advance.

Thesis supervisor:

Prof. II Kjell Larsen, NTNU/Equinor

Deadline: June 11th, 2019

Trondheim, January 28th, 2019

Kjell Larsen (sign.)

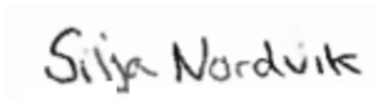
Silja Bergitte Nordvik (sign.)

Preface

This thesis is the final part of my master's degree in Marine Technology, with specialization within Marine System Design. The thesis is written during the spring semester of 2019, at the Department of Marine Technology(IMT) at the Norwegian University of Technology and Science(NTNU), Trondheim. The work has been done under the supervision of Professor Kjell Larsen, who works both at Equinor and as a professor at NTNU. The workload of the thesis corresponds to 30 ECTS.

During this master's thesis project, I have got the opportunity to investigate various interesting elements of marine operations with the main topic subsea lifting operations.

Trondheim, 11.06.2019

A handwritten signature in black ink that reads "Silja Nordvik". The signature is written in a cursive, slightly slanted style.

Silja Bergitte Nordvik

Acknowledgements

I would like to thank Professor Kjell Larsen for excellent advice and guidance as my supervisor during this master's project. Sharing of his knowledge and understanding of marine operations and hydrodynamics has been greatly appreciated. He has provided me with relevant data for developing the simulation model.

I would also like to thank PhD candidate Carlos Eduardo Silva de Souza for helping me set up the numerical simulations in SIMA.

S.B.N

Summary

Recovering energy from offshore wind is more expensive than inshore and thereby can cost-effective and safe marine operations be crucial to make Floating Offshore Wind Turbines (FOWT) competitive. The purpose of this thesis is to look at the marine operation of installing anchors used for FOWT by comparing a suction anchor and a deep penetration anchor. Relevant theory within mooring systems, lifting operations, hydrodynamics and operability is presented. Numerical simulation models of the anchors are made in SIMA, and numerical simulations and time domain analysis is performed. The lifting operation is done by use of a crane vessel, and the tension in the lifting line is primarily assessed. Weather data is taken from the Johan Castberg Field located in the Barents Sea, and the simulations are run with irregular waves and varying peak periods, significant wave height and directions.

From a marine operation view, the results show that the deep penetration anchor is recommended. This is because the tension in the wire is lower due to less influence from hydrodynamic forces compared to the suction anchor. This leads to a higher design criterion and operational limit. In addition, the reference time is shorter and thereby the required weather window is reduced.

For the suction anchor, the splash zone is a critical phase as the added mass is large compared to the structural mass due to entrapped water. Slamming forces appear typically for smaller peak periods and larger accelerations and gives large dynamics in the wire. A combined effect of the crane tip motion and wave kinematics will induce the overall largest vertical hydrodynamic force. The results show that lower peak periods gives a higher maximum tension in the wire. It is, therefore, important to assess the slamming and Morison's forces. Opposed to the deep penetration anchor, resonance in the wire is a risk. When assessing the operability, it can be seasonal challenges for the installation of a suction anchor when comparing July with October, and especially when installing several anchors in a row to avoid waiting on weather.

Sammendrag

Utvinning av havvind er dyrere enn vindkraft fra land, og dermed kan kostnadseffektiv og trygge marine operasjoner være avgjørende for å gjøre havvind konkurransedyktig. Hensikten med denne oppgaven er å se på den marine operasjonen å installere ankre som brukes til flytende vindturbiner ved å sammenligne et sugeanker og et droppanker. Relevant teori innen forankringssystemer, løfteoperasjoner, hydrodynamikk og operabilitet er presentert. Numeriske simuleringsmodeller av ankrene er laget i SIMA, og numeriske simuleringer og tidsdomeneanalyse er utført. Løfteoperasjonen er utført ved hjelp av et kranfartøy, og spenningen i løftelinen er først og fremst vurdert. Værdata er hentet fra Johan Castberg feltet i Barentshavet, og simuleringene er kjørt med uregulære bølger og varierende topperioder, signifikant bølgehøyde og retning.

Med tanke på den marine operasjonen, viser resultatene at droppankeret kan anbefales. Det skyldes at spenningen i løftewiren er lavere på grunn av mindre påvirkning fra hydrodynamiske krefter sammenlignet med sugeanker. Dette fører til et høyere designkriterium og operasjonsgrense. I tillegg er referansetiden kortere og dermed reduseres det nødvendige værvinduet.

For sugeanker er plaskesonen en kritisk fase siden tilleggsmassen er stor sammenlignet med den strukturelle massen på grunn av innesluttet vann. Slamming kreftene forekommer typisk for mindre topperioder og større akselerasjoner og gir mye dynamikk i løftewiren. En kombinert effekt av kranstipp bevegelsen og bølgekinematikk vil indusere den største vertikale hydrodynamiske kraften. Resultatene viser at lavere topperioder gir en høyere maksimal spenning i ledningen. Det er derfor viktig å vurdere slamming og Morisons krefter. I motsetning til droppankeret vil resonans i ledningen være en risiko. Når man vurderer tilgjengeligheten for installasjon, kan sesongvariasjoner være utfordrende for installasjon av sugeankeret og spesielt om man installerer flere ankre på rad for å unngå å vente på vær.

Contents

1	Introduction	1
1.1	Background	1
1.2	Objectives	2
1.3	Structure of The Paper	3
2	Mooring Systems	5
2.1	Mooring Lines	5
2.1.1	Chain	5
2.1.2	Steel Wire Ropes	6
2.1.3	Synthetic Fibre Ropes	7
2.2	Anchors	7
2.2.1	Drag Anchor	7
2.2.2	Plate Anchor	8
2.2.3	Suction Anchor	9
2.2.4	Dynamically Penetrating Anchors	10
	Deep Penetration Anchor	11
2.3	Mooring Systems	13
2.3.1	Catenary Mooring System	13
2.3.2	Taut Leg Mooring System	13
3	Subsea Lift and Crane Operations	15
3.1	Heavy- and Light lifts	15
3.2	Lifting Phases	16
3.2.1	Lift Off and Manoeuvring of Object	16
3.2.2	Splash Zone	17
3.2.3	Lowering	18
3.2.4	Landing on Seabed	18
3.3	Static and Dynamic Equilibrium	20
3.4	Crane Tip Motion	22

3.5	Slack and Snap Loads	23
3.6	Installation of Anchors	24
3.6.1	Installation of Deep Penetration Anchor	24
3.6.2	Installation of Suction Anchor	28
4	Hydrodynamic Theory	29
4.1	Linear Wave Theory	29
4.2	Irregular Waves	31
4.2.1	JONSWAP Spectrum	31
4.3	Equation of Motion	33
4.4	Response Amplitude Operator	34
4.5	Morison's Equation	34
4.6	Hydrodynamic Parameters	36
4.6.1	Added Mass	36
4.6.2	Drag Force	37
4.7	Water Entry Force	37
5	Planning of Marine Operations	39
5.1	The Planning Process	39
5.2	Weather Unrestricted Operations	42
5.3	Weather Restricted Operations	42
5.4	Operability and Weather Window	44
5.5	Weibull Distribution	45
6	Time domain analysis	47
6.1	Software	48
6.2	The Simulation Model	48
6.2.1	Design of The Anchors	48
6.2.2	Environmental Conditions	51
	Significant Wave Height and Peak Period	51
	Seed Numbers	53
6.2.3	Establishment of Hydrodynamic Coefficients	55
	Added Mass	55
	Drag Force	57
6.2.4	Installation Vessel	58
	RAO for Installation Vessel	60
6.2.5	Lifting Equipment	70
	Resistance and Capacity Checks	73
	Natural Period of The Hoisting Wire	73

7	Simulation Results	75
7.1	Static Equilibrium	75
7.2	Tension in Wire	76
7.2.1	Suction Anchor	76
7.2.2	Deep Penetration Anchor	80
7.3	Evaluating Resonance - Fast Fourier Transformation	82
8	Operability	89
8.1	Weather Hindcast for Johan Castberg	90
8.2	Probability Distribution	92
9	Conclusion	97
9.1	Recommendations for Further Work	98
A	Hardware properties	I
A.1	Diamond Blue	I
B	Hydrodynamic Coefficients	III
B.1	Added Mass Coefficients	III
B.1.1	Effect of height (3D structure)	IV
B.1.2	Effect of perforation	V
B.2	Drag Force Coefficients	VI
C	α-factor	VII

List of Figures

2.1.1 Stud-Link and Studless chain (Chakrabarti, 2005)	6
2.1.2 Steel wire rope construction (Chakrabarti, 2005)	6
2.1.3 Synthetic fibre rope which is built up by braided jacket, filter layer, rope cores, core strand and basic yarn (Chakrabarti, 2005)	7
2.2.1 Main components like shank, fluke and shackle of a drag anchor, from (American Bureau of Shipping, 2018)	8
2.2.2 Installation Process of a suction embadded plate anchor (American Bureau of Shipping, 2018)	8
2.2.3 Suction anchors (American Bureau of Shipping, 2018)	9
2.2.4 Dynamically penetrating anchor concepts	10
2.2.5 The OMNI-Max anchor (Randolph et al., 2011)	10
2.2.6 Deep penetration anchor (Deep Sea Anchors, 2019b)	11
2.3.1 Typical arrangement of mooring system. 1 shows the taut-leg mooring, 2 the catenary mooring and 3 shows the catenary mooring with buoyancy elements	14
2.3.2 Example on how to insert fibre rope in a catenary system, illustration based on Larsen (2018a)	14
3.2.1 Lifting phases: 1. In air, 2: Through splash zone, 3. Fully submerged, 4. Landing . .	16
3.2.2 Suction anchor in air and during manoeuvring. Pictures from Larsen (2018b) . . .	17
3.2.3 Splash zone (Larsen, 2018b)	18
3.2.4 How the offset varies with water depth. Picture from Larsen (2018b)	19
3.3.1 The relative vertical motion between the crane tip and a subsea structure for a dynamic system with stiffness K.	21
3.4.1 Vessel motion in six degree, translation and rotation about centre of gravity	22
3.5.1 Illustration of slack criterion	23
3.6.1 Alternative ways of installing deep penetration anchor.	25
3.6.2 Configuration of a DPA before anchor drop (Deep Sea Anchors, 2019a)	26
3.6.3 The configuration with two AHVs just before shooting operation (de Araujo et al., 2004)	27

3.6.4 Suction Anchor on deck of a vessel with installed suction pump (SPT Offshore, 2019)	28
3.6.5 Suction Anchor during suction operation, (SPT Offshore, 2019)	28
4.1.1 Water particles paths in deep water varying with water depth (TSI, 2019)	30
4.2.1 Examples of wave spectrum. $H_{1/3}$ is the significant wave height, T_2 the mean wave period. Modified Pierson Moskowitz spectrum, __, JONSWAP spectrum, ___. (Faltinsen, 1993)	32
4.3.1 System with one DOF in heave	33
4.5.1 Hydrodynamic classification of the marine structures using a circular cylinder as representative of structural elements and examining the dominant loads	35
5.1.1 The planning process of Marine Operations, based on DNV GL (2011a)	40
5.1.2 Weather window	41
5.4.1 Example on significant wave height as function of time measured every 3rd hour. Highlights a storm and a calm period based on measured H_s and a H_s limit H'_s	44
6.2.1 Main dimensions of the suction anchor and deep penetration anchor used in the simulation	49
6.2.2 Spectral peak period for given significant wave height at the Johan Castberg Field, downloaded from Dezecot et al. (2016)	52
6.2.3 How the most probable tension varies with number of seeds for the suction anchor at H_s 1 m and T_p 7.4 s	53
6.2.4 Comparison of the most probable maxima for H_s 1 and 2 meters for the suction anchor	54
6.2.5 Maxima and minima for deep penetration anchor for H_s 6 m and T_p 9.5 s	54
6.2.6 Depth dependency of added mass for suction anchors (Næss et al., 2014)	56
6.2.7 Vessel used in the simulation model	58
6.2.8 Illustration of the simulation model's origin, vessel's Centre of Gravity marked with COG and the location of the crane tip (the vessel is seen from the aft)	59
6.2.9 Given wave directions (vessel seen from above)	60
6.2.1 RAOs for surge motion	61
6.2.1 RAOs for sway motion	62
6.2.1 RAOs for heave motion	63
6.2.1 Decay test in heave, the natural period is shown	64
6.2.1 RAOs for roll motion	65
6.2.1 Decay test in roll	66
6.2.1 RAOs for pitch motion	67
6.2.1 Decay test in pitch	68
6.2.1 RAOs for yaw motion	69

6.2.1	The crane set up from crane tip to anchor. To the left: the set up with hook and three slings for the suction anchor. The DPA on the right connected directly to lifting wire.	70
6.2.2	The crane set up from crane tip to anchor. To the left: the set up with hook and three slings for the suction anchor. The DPA on the right connected directly to lifting wire.	72
6.2.2	The angle between sling and suction anchor	72
6.2.2	The stiffness in the lifting systems. To the left is the suction anchor and DPA to the right	74
6.2.2	Resonance period of hoisting cable with varying length	74
7.1.1	Static line force	75
7.2.1	Simulation of suction anchor with significant wave height 2 meters and varying peak periods	77
7.2.2	For significant wave height 2 meters and peak period 5.8 seconds	78
7.2.3	How the maximum tension varies with peak period and heading. This for significant wave height 1.5 m for suction anchor	79
7.2.4	Design criterion for the suction anchor varying with the peak period and wave heading	80
7.2.5	Simulation of deep penetration anchor with significant wave height 6 meters and varying peak periods	81
7.3.1	Natural period of the wire with varying length of crane wire for the suction anchor. A peak period of 4.6 s is highlighted.	82
7.3.2	H_s 1m, T_p 4.6 s and head sea waves	83
7.3.3	FFT for H_s 1 m T_p 4.6 s at water depth 150 and 100 meters. The wave period (T_p) and the natural period (T_n) are highlighted in the figures	84
7.3.4	Time series for H_s 1 m and T_p 4.6 s - water depth 150 and 100 meters. The red part is when lowering anchor to desired water depth, and the blue part is used for the FFT.	84
7.3.5	Wave elevation for H_s 1 m T_p 4.6 s at water depth 150 and 100 meters.	85
7.3.6	FFT for H_s 1.5 T_p 5.2 s at water depth 195 meters.	85
7.3.7	Time series for H_s 1.5 T_p 5.2 s - water depth 195 meters.	86
7.3.8	Crane tip movement for H_s 4m and T_p 14.4 s.	87
7.3.9	H_s 4m and T_p 14.4 s	87
8.1.1	Measurements of H_s for the Johan Castberg Field during 2010	91
8.1.2	Calm periods independent on season	92
8.2.1	Cumulative probability with respect to H_s	93

8.2.2 Cumulative probability with average length of calm for both July and October. . . .	95
8.2.3 Relationship between cumulative probability of H_s and $\bar{\tau}_c(h)$	95
8.2.4 Cumulative probability with respect to H_s	96

List of Tables

3.1	The lifting phases with associated issues	16
3.2	Overview of significant forces acting during different lifting phases	19
5.1	The acceptable return periods for H_s , obtained from DNV GL (2011a)	42
6.1	Total mass, volume and entrapped water for suction anchor and deep penetration anchor	48
6.2	Centre of Gravity with respect to origin	49
6.3	The length, specific volume and number of stripes for the slender element of the suction anchor.	50
6.4	The length, specific volume and number of stripes for the slender element of the suction anchor.	50
6.5	Mass moment of inertia about origin for the suction anchor and deep penetration anchor	51
6.6	Significant wave height and spectral peak period used in the simulation	52
6.7	Number of seeds suction anchor	55
6.8	Number of seeds for DPA	55
6.9	Calculated added mass values for suction anchor	55
6.10	Total added mass for the deep penetration anchor for the different directions.	56
6.11	Quadratic drag for fully submerged suction anchor and deep penetration anchor	57
6.12	Main dimensions of the installation vessel Scandi Acergy	58
6.13	Structural mass of installation vessel	59
6.14	Properties of the crane wire and the slings	70
6.15	Structural mass of the hook	71
6.16	Body points on suction anchor to connect anchor with slings	71
7.1	Significant wave height and peak periods that constitute the design criterion	79
8.1	Design criterion, α -factor, planned time for the operation, contingency time, reference time and operational criterion for suction anchor and DPA	90

8.2 Monthly Weibull parameters for significant wave height at the Johan Castberg Field.
Duration of event is 3 hours. Data from Dezecot et al. (2016) 92

Nomenclature

Abbreviations

CDF Cumulative Distribution Function

CFD Computational Fluid Dynamics

COG Centre Of Gravity

DNV GL Det Norske Veritas Germanischer Lloyd

DOF Degrees of freedom

DP Dynamic Positioning

DPA Deep penetration anchor

FD Frequency Domain

JONSWAP Joint North Sea Wave Project

MBL Minimum Breaking Load

PDF Probability Density Function

PM Pierson-Moskowitz

RAO Response Amplitude Operator

ROV Remotely Operated Vehicle

SHS Special Handling System

SWL Safe Working Load

TD Time Domain

ULS Ultimate Limit State

WF Weather Forecast

WOW Waiting On Weather

Greek Letters

α α -factor, a correlation factor between forecasted and observed values

β Shape Parameter in Weibull distribution

$\ddot{\eta}_3$ Acceleration in Heave

$\dot{\eta}_3$ Velocity in Heave

$\dot{\eta}_{ct}$ Crane Tip Vertical Velocity

$\dot{\zeta}_a$ Wave Velocity

η Single Amplitude Motion

η_3 Translation in Heave

η_{ct} Crane Tip Vertical Motion

γ Peakedness Parameter in JONSWAP spectrum

γ Scale Parameter in Weibull distribution

γ_{sf} Nominal Safety Factor

ω Wave Frequency

ω_0 Natural Frequency

ϕ Velocity Potential

τ_c Calm Period, calms

τ_s Storm Period, storms

ζ Wave Elevation

ζ_a Wave Amplitude

Roman Symbols

A_p Horizontal Projected Area of Lifted Object

A_p	Water plane Area of Lifted Object
A_{11}	Perpendicular Added Mass
A_{22}	Transverse Added Mass
A_{33}	Added Mass in Heave
A_{33}	Lonitudinal Added Mass
A_{ij}	Wave amplitude for wave component ij
c	Damping Coefficient
C_A	Dimensionless Added Mass Coefficient
C_D	Drag Coefficient
C_S	Slamming Coefficient
F_B	Varying Buoyancy Force
F_D	Drag Force
F_I	Inertia Force
F_S	Slamming Force
H_s	Significant Wave Height, defined as the mean of the one Third Highest Waves
K	Stiffness of Hoisting Cable
k	Restoring Coefficient
k	Wave Number
m	Mass of Lifted Object
m_a	Added Mass
OP_{LIM}	Design Criterion
OP_{WF}	Operational Criterion
q	Exitation Force
Re	Reynolds Number

T	Wave period
t	Time
T_C	Contingency Time
T_p	Peak period
T_R	Reference Period
T_{POP}	Planned Operation Period
u_c	Hoisting Velocity
u_r	Relative Velocity between Lifted Object and Water Particles
u_w	Water Particle Velocity
$u_{current}$	Average Current Speed
V_R	Reference Volume
z	Distance from Sea Surface to Lower Bound of Lifted Object

Chapter 1

Introduction

1.1 Background

In recent years, the floating offshore wind turbine (FOWT) market has gotten a bigger focus and has increased significantly. The demand for electricity is increasing steadily, and at the same time, the intention is to reduce global emissions (Cruz and Atcheson, 2016). To support the drive towards a reduction in carbon emissions, FOWT can play an important role with its renewable energy technology. According to IRENA (2016)'s analysis, wind power will have to become the leading power generation technology by 2030 to ensure a decarbonisation of the global economy. Fixed wind turbines cannot reach this goal alone. Fixed wind turbines have a limited water depth of about 40-50 m, while most of the world's oceans are deeper. Therefore, FOWTs are essential to utilize the offshore wind when reaching deeper water. Some of the main advantages of floating wind turbines are the high mean wind speed with more variations in time and space than onshore. Also, the large available areas offshore at a low price, and consequently large potentials to build larger turbines and wind farms is advantageous (Cruz and Atcheson, 2016). Although recovering energy from offshore wind is slightly more expensive, the resource provides up to 50% more energy than nearby onshore winds (PrinciplePower, 2018). Another important advantage of the floating structure is the possibility for greater standardisation in manufacturing since water depth and soil type have no impact on foundation design, leading to cost savings (IRENA, 2016).

In order to design, install and operate floating wind turbines and, in the future, large floating wind parks, cost-effective and safe marine operations are crucial. Capital expenditure (CAPEX) of the marine operations for a floating wind park is a large part of the total investment cost, and it is therefore important to optimize it to reduce the cost. An important building block for a floating wind turbine is the mooring system and installation of the anchors. Due to economical reasons, it is necessary to minimize mooring system costs, while not exceeding mooring line breaking strength and platform drift constraints. Factors like cheaper anchors with a cost-

effective design and production as well as decreased installation time are central.

A key activity to successful subsea installation is the planning process. Lifting of subsea equipment, especially through the splash zone, is a weather critical activity. The main challenge of installation of the mooring system is the crane operation of the anchors. It is crucial that such operations are planned and understood properly, and that effective equipment is used. The state-of-art concept is the suction anchor, and an alternative anchor concept is the deep penetration anchor (DPA).

1.2 Objectives

This thesis will look at the marine operation when installing anchors used for FOWT. Two possible concepts will be compared. This is a deep penetration anchor formed as an arrow with four fins at the top and a hollow suction anchor with a hatch on the top. The objective of this thesis is to compare the anchors and find the concept with the most cost-effective as well as the safest marine operation. This shall be done by looking at the lifting operations performed by a crane vessel. The tension in the lifting lines is to be assessed with a special focus on the splash zone. Numerical simulations and time domain analysis is to be utilized. The design criterion shall be found and discussed together with operational limits, reference time and operational availability.

The main objectives of this master's thesis are summarized by the bullet points below

- Present relevant literature and describe the main steps in the planning process of a marine operation in general. For weather restricted operations, an overview of the planning process shall be described; the α -factor concept and how operability and weather windows can be optimized.
- Give an overview of possible mooring systems for floating wind turbines. The focus to be on station keeping principles and main hardware components. Include an overview of the different anchor concepts available for the industry. A special comparison to be given for the suction anchor and the DPA anchor concepts.
- Familiarize with the numerical simulation software SIMA/SIMO and describe the theory that is relevant for subsea lifting and installation of anchors.
- Establish numerical simulation models in SIMA for a suction anchor and a DPA anchor.
- Perform operability investigations based on simulation results and weather data for the Barents Sea.

1.3 Structure of The Paper

- Chapter 2 presents the main mooring lines, different anchor concepts and mooring systems. Special comparison is given for the suction anchor and the deep penetration anchor.
- Chapter 3 presents the typical lift categories, different lifting phases, crane tip motion, and slack and snap loads. In the end, one alternative installation procedure of a deep penetration anchor and a suction anchor is presented.
- Chapter 4 focuses on the hydrodynamic theory. Linear wave theory and irregular waves are explained. Equation of motion and hydrodynamic parameters as added mass and drag are also described.
- Chapter 5 gives general information about marine operations, the planning process, the difference between weather restricted and unrestricted, operational criteria and weather window. In the end a description of the three-parameter Weibull distribution is given.
- Chapter 6 describes the domain analysis together with the software used during the simulations. The simulation model is presented with input data and environmental condition, lifting equipment and the installation vessel used during the simulations.
- Chapter 7 presents and discusses the simulation results and the anchor concepts are compared.
- Chapter 8 focuses on the operability for the two lifting operations. Comparing installation during summer with autumn. Operation availability is assessed.
- Chapter 9 presents the conclusions of this master thesis in addition to recommendations for further work

Chapter 2

Mooring Systems

Mooring systems gives position for a floating structure by use of mooring lines, and the aim is to control the horizontal offset to an acceptable limit. By this, station keeping is an important safety-critical system. A mooring system consists of several important parts. This chapter presents the main mooring lines, different anchor concepts and mooring systems with a focus on floating wind turbines. A special comparison is given for the suction anchor and the deep penetration anchor concepts.

2.1 Mooring Lines

2.1.1 Chain

Chain has relatively large weight and high stiffness and is a popular option for permanent mooring due to its high breaking strength. In addition, it has good abrasion characteristics to resist bottom dragged objects. On the other hand, chain is an expensive solution. There are two main types of chains, stud-link and studless chain (Chakrabarti, 2005). Studless is the simplest type and is made from straight metal bars that are bent to an oval shape, looped together, and welded shut. Stud-link has, in addition, a bar or stud across its inside width, see Figure 2.1.1. These studs add weight and help prevent deformation, making the stud-link chains stronger compared to the studless chain, however, the cost increases (Chakrabarti, 2005).

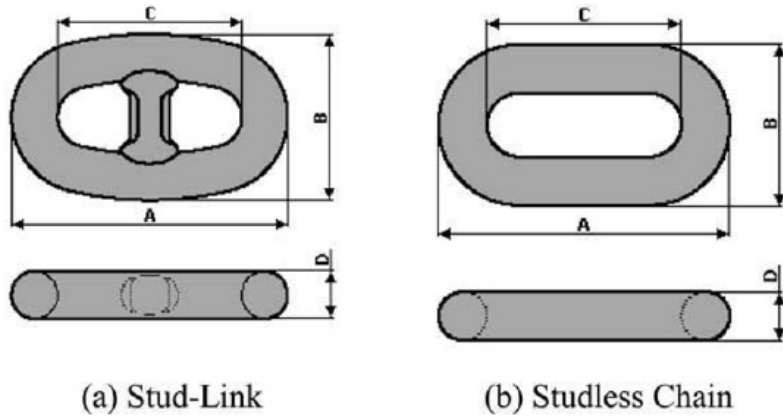


Figure 2.1.1: Stud-Link and Studless chain (Chakrabarti, 2005)

2.1.2 Steel Wire Ropes

Steel wire ropes in mooring systems consist of individual wires in a helical pattern called a strand (Chakrabarti, 2005). The configuration of the strands defines characteristics such as strength, fatigue life, etc. The pitch of the wires defines the elasticity and axial stiffness. Mooring line ropes typically consist of 12, 24, 37 or more wires per strand, and can be multi-strand or single-strand construction (Chakrabarti, 2005), see Figure 2.1.2 for different types of wire ropes. Mobile units with temporary wire rope moorings invariably use the more robust six-strand, while spiral strand which is more fatigue resistant is preferred for long-term permanent systems. The steel wire has a lower weight than chain for the same breaking load, and a higher elasticity, and is generally more prone to damage and corrosion than chain (Vryhof Anchors, 2010). In addition, it is cheaper and easier to handle with respect to installation.

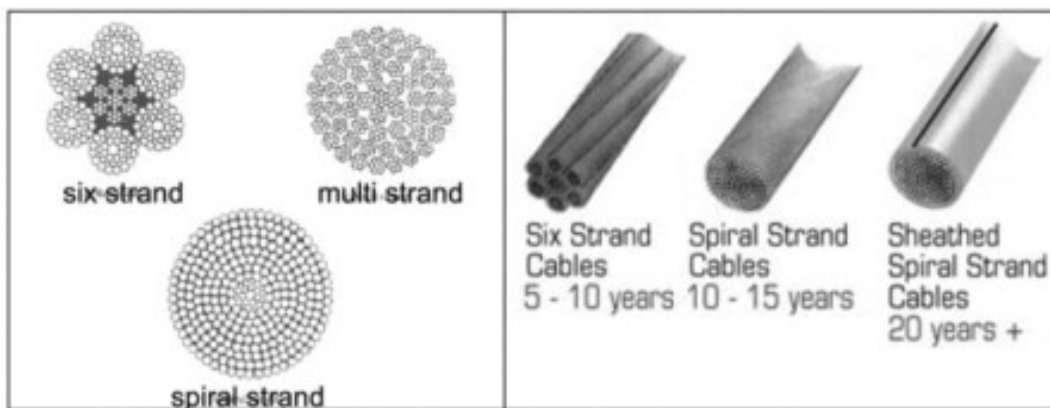


Figure 2.1.2: Steel wire rope construction (Chakrabarti, 2005)

2.1.3 Synthetic Fibre Ropes

Synthetic fibre ropes have lighter weight and are more elastic compared to chain and steel wire, which makes fibre ropes easier to handle. Especially in deep water it can be beneficial due to the weight and flexibility and it can absorb imposed dynamic motions through extension without causing an excessive dynamic tension (Chakrabarti, 2005). Moreover, the reduced line length will give a smaller footprint on the seabed and a reduced cost. The synthetic fibre ropes are built up by several layers with braided jacket, filter layer, rope cores, core strand and basic yarn as can be seen in Figure 2.1.3.

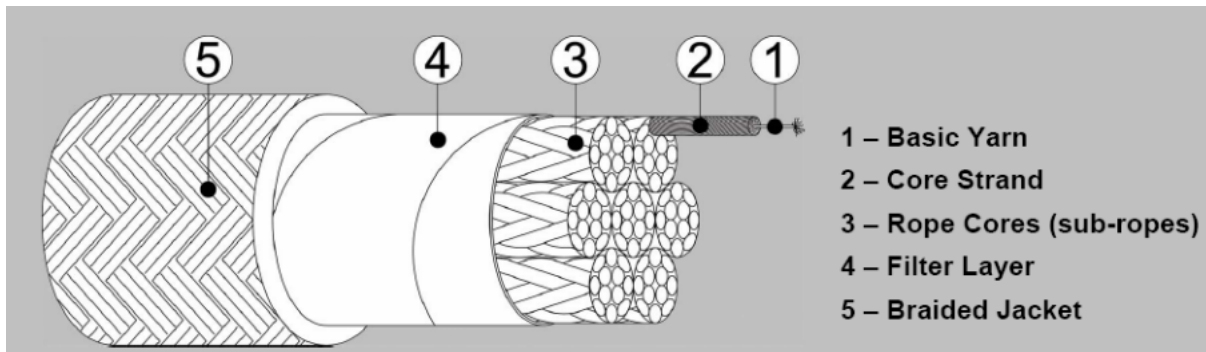


Figure 2.1.3: Synthetic fibre rope which is built up by braided jacket, filter layer, rope cores, core strand and basic yarn (Chakrabarti, 2005)

2.2 Anchors

This Section will give an overview of some available anchor concepts, including drag anchor, plate anchor, suction anchor and dynamically penetrating anchors.

2.2.1 Drag Anchor

The drag anchor is designed to penetrate partly or fully into the seabed (American Bureau of Shipping, 2018). They are installed by dragging the anchor through the ground. After installation, the anchor is capable of resisting loads equal to the installation load without further penetration. The drag anchor is more suitable of resisting large horizontal loads than large vertical loads (Vryhof Anchors, 2010). A drag anchor with the main components fluke, shank, shackle and chain can be seen in Figure 2.2.1. Drag anchors are used for the WindFloat Atlantic project to be installed outside Portugal during 2019 (Froese, 2018).

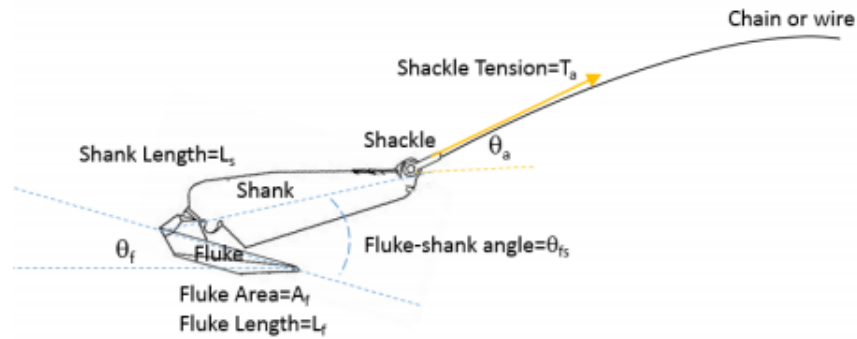


Figure 2.2.1: Main components like shank, fluke and shackle of a drag anchor, from (American Bureau of Shipping, 2018)

2.2.2 Plate Anchor

Plate anchors can be divided into two categories: drag-in plate anchor and push-in plate anchor (American Bureau of Shipping, 2018). For the drag-in plate anchor, the anchor is dragged into the soil during installation. Gravity, hydraulic, propellant, impact hammer or suction is used to install the push-in plate anchor. The plate anchor has a high holding capacity and high vertical capacity and is mostly used in cohesive soil. To achieve the maximum resistance, the anchor is rotated to a position perpendicular to the loading direction after penetration. The suction embedded plate anchor (SEPLA) is a type of push-in plate anchor, and the installation of this is illustrated in Figure 2.2.2. First, the anchor self-weight penetrates before the suction anchor gives a further penetration by pumping out water. The suction anchor is then retrieved and the SEPLA is rotated to develop its full capacity by pulling the mooring line.

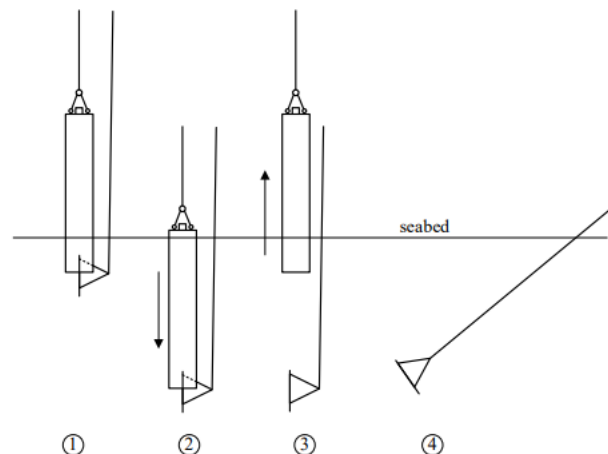


Figure 2.2.2: Installation Process of a suction embedded plate anchor (American Bureau of Shipping, 2018)

2.2.3 Suction Anchor

A typical suction anchor is a hollow steel cylinder with closed top (Vryhof Anchors, 2010), see Figure 2.2.3. In order to evacuate air during water entry and to provide ventilation during lowering and soil penetration, one or more hatches are placed on top of the anchor (Solaas and Sandvik, 2017). After completed self-penetration, the top hatch covers are closed and the pressure inside gets lower than outside (Vryhof Anchors, 2010). The anchor is sucked into the seabed with help from the valves for its final penetration and levelling. In most cases the vertical side-walls are without perforation, however, in some cases, the lower part of the walls may be with holes to reduce the risk for soil fracture when landing and during the initial part of the soil penetration. The friction of the soil along the suction anchor and lateral soil resistance constitute the holding capacity, and the anchor is capable of withstanding both horizontal and vertical loads (Solaas and Sandvik, 2017). The diameter to height ratio for a suction anchor can vary considerably, depending on usage and soil conditions. Suction anchors are used at the Hywind Scotland Pilot Park (Equinor, 2017).



Figure 2.2.3: Suction anchors (American Bureau of Shipping, 2018)

2.2.4 Dynamically Penetrating Anchors

Over the last few decades, numerous mooring concepts have been developed, one of these being dynamically penetrating anchors. Several companies have designed such anchors, and the designs vary from company to company. Dynamically penetrating anchor can be divided into three depending on the shape (Gao et al., 2015): torpedo anchor, deep penetrating anchor (DPA) and OMNI-Max anchor. DPA and the torpedo anchor are quite a similar concept with an arrow-shaped body and fins located at the upper part. Also, the installation procedure is the same for these concepts. The DPA has shorter and wider fins attached on the cylindrical pile. Figure 2.2.4a shows a typical torpedo anchor with four fins and Figure 2.2.4b shows a DPA.



(a) Torpedo anchor (de Aguiar et al., 2009)



(b) Deep penetration anchor (Deep Sea Anchors, 2019a)

Figure 2.2.4: Dynamically penetrating anchor concepts

For the OMNI-Max anchor, both the geometry, size and weight are somewhat different. Here, a double set of fins are placed on the anchor, the large fins on the top and the smaller at the bottom. Further, the anchor features an arm that transmits the loading point closer to the anchor tip (Randolph et al., 2011), see Figure 2.2.5.

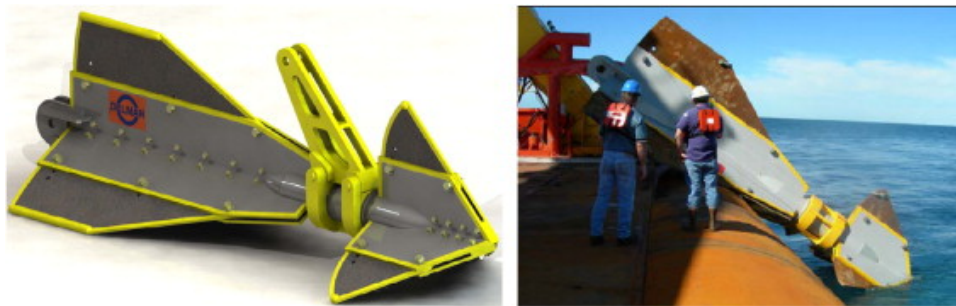


Figure 2.2.5: The OMNI-Max anchor (Randolph et al., 2011)

This thesis focuses on DPA, and a more detailed description of this anchor concepts follows.

Deep Penetration Anchor

DPA's are familiarized as cone-tipped, cylindrical steel pipes filled with concrete and scrap metal, and can be used for anchoring both mobile drilling units as well as permanent facilities (Gilbert et al., 2008). DPA works best in soft to medium clay soil conditions (WILDE, 2009). They are equipped with tail fins to provide good directional and non-rotational stability. This gives a precise horizontal landing and a vertical configuration of the anchor in the soil. The anchors are installed as projectiles penetrating the sea floor under velocity (Gilbert et al., 2008), relying on the kinetic energy they acquire while free falling from heights of between 30 and 150 meters above the seabed. The size and weight of a DPA affect the height that ensures the right terminal velocity before penetrating the sea floor, and the amount of kinetic energy increases proportionally to the velocity squared. For the anchor to achieve the necessary seabed penetration and holding capacity, a certain amount of kinetic energy is required at the time instant it hits the seabed. The penetration depth, measured between the mudline and top of the anchor, is typically 9 to 15 meters. No external forces are acting on the anchor during the installation. Figure 2.2.6 illustrates a DPA.



Figure 2.2.6: Deep penetration anchor (Deep Sea Anchors, 2019b)

Comparing Deep Penetration Anchor and Suction anchor

The main reason for using DPA is its simplicity and speed of installation. Installation can be executed by nearly any offshore vessel by either using the moonpool, stern roller or a crane. In general, the installation procedure is less time consuming than a suction anchor installation. The anchor concept can be used for a wide range of water depths, and the installation is not

dependent on the water depth considering the equipment needed for the installation. For the suction anchor, challenges regarding positioning will increase with the water depth. Due to the simple design of the DPA, the fabrication is easy and economic. Likewise, the compact design allows several anchors to be transported at one offshore vessel compared to suction anchors, and fast installation is possible using one or two vessels and limited use of ROVs.

The no need for external energy is also an advantage during the installation of DPA. The anchor is fully driven by its own weight. The requirement for extra equipment and manpower is therefore reduced. The only external equipment required is a remotely operated underwater vehicle (ROV) used for line observation and initiation of anchor drop. On the contrary, when installing suction anchors external energy and umbilicals are needed to run the pump skid (Hagen et al., 1998). Also, drag embedded anchors require external energy during installation where the anchors are dragged into the soil by an anchor handling vessel (AHV). These factors make DPA a cost-effective anchor concept throughout fabrication, transportation and installation.

A critical phase of a subsea installation is when lowering equipment and constructions through the splash zone. In this phase, a structure is exposed to large hydrodynamic forces such as added mass, drag and slamming forces. Regarding the DPA, the small cross-section area ensures a low drag force which is an advantage during splash zone crossing (Lieng et al., 2000). Suction anchors have, on the other hand, a much larger cross-section area and entrapped water. Therefore, the dynamic motions in the splash zone are limited and installation in more harsh weather is feasible for DPAs compared to suction anchors. In addition, the increased acceptable weather window reduces downtime of the DPA installation, a positive effect on the operational costs.

DPA has a much smaller footprint compared to other concepts like a suction anchor, which requires a relatively large diameter to obtain the embedment pressure under control. Drag-embedded plate anchors may be used for the same purpose but only if the location and depth are not critical. Since the drag-embedded plate anchors are dragged into the soil, which leaves a large footprint, they are not suitable for fields with large amounts of subsea infrastructure (WILDE, 2009).

For DPAs there are challenges associated with the prediction of the embedment depth and set-up after installation (Gao et al., 2015). The anchor cannot be tilted in the soil since it will lead to reduced loading capacity. These factors are connected to the soil properties as well as the characteristics and geometry of the anchor and will reduce the capacity of the anchor. To prevent unacceptable vertical tilt angles after penetration in the soil, it is necessary to insert heavier material or ballast at the bottom of the pile to keep the centre of gravity (COG) low (WILDE, 2009). This is generally achieved by the use of lead ballast near the tip, a section of cast iron above the lead, and possibly concrete above the iron. It is, however, easier to predict the holding capacity and control the penetration into the soil for a suction anchor. In addition, there are more data available since there are several suction anchors installed.

2.3 Mooring Systems

2.3.1 Catenary Mooring System

Catenary lines are considered the traditional mooring lines and are the most common mooring system in shallow water. Due to the gravity, the mooring lines are installed as a hanging line from the floating structure and down to the anchor. The catenary mooring is compiled of chain and steel wire where the geometric stiffness is of major importance. Geometric stiffness can be obtained by adding weight or buoyancy from line weights or buoys.

2.3.2 Taut Leg Mooring System

The taut leg system or taut system has pre-tensioned mooring lines that keep the lines in a linear shape from the anchor to the floating structure and is dominated by elastic stiffness. This is because the modulus of elasticity of polyester is much lower compared to steel and reduces wave and drift frequency forces (Chakrabarti, 2005). An other advantage of the low weight is the easy handling during installation. The stiffness of synthetic line ropes is not constant but varies with the load range and the mean load. One drawback with taut mooring is the use in shallow water due to challenges regarding scaling down. This means that the line length must be long independent of the water depth. This is because the elasticity is provided by cable length, the cross section and its elastic modulus, and the system stiffness needed does not change significantly from deep to shallow water (Larsen, 2018a). To avoid that the taut mooring line touches the ground due to low tension, a buoyancy element can lift it from the seabed.

For taut leg mooring, the lines reach the anchor at the seabed with an angle, while in a catenary system the lines arrive the seabed horizontally. Consequently, for taut leg mooring, the anchor must be able to withstand both horizontal and vertical forces, while it must only resist horizontal forces in a catenary system. Figure 2.3.1 illustrates a typical arrangement of the mooring system, where 1 shows the taut-leg mooring. Nr 2 and 3 show the catenary mooring system, however, 3 has additional buoyancy elements.

It is also possible to use a mooring system with a combination of chain and synthetic fibre rope. This system will be lighter than full chain and steel wire systems, and less expensive due to the cost of fibre ropes. Since the stiffness of a taut mooring rope system is only dependent on the axial stiffness, the lines need to be long enough to provide the required elasticity to get the system to be able to absorb the environmental loads. By inserting fibre rope to the catenary system, as shown in Figure 2.3.2, the geometric stiffness will decrease as well as the total stiffness. With a chain-polyester line configuration, the pre-tension of the mooring line will be lower and due to the weight of the suspended chain, and the polyester section will always satisfy the criterion to be in tension. This can also be accomplished by clump weights and buoys.

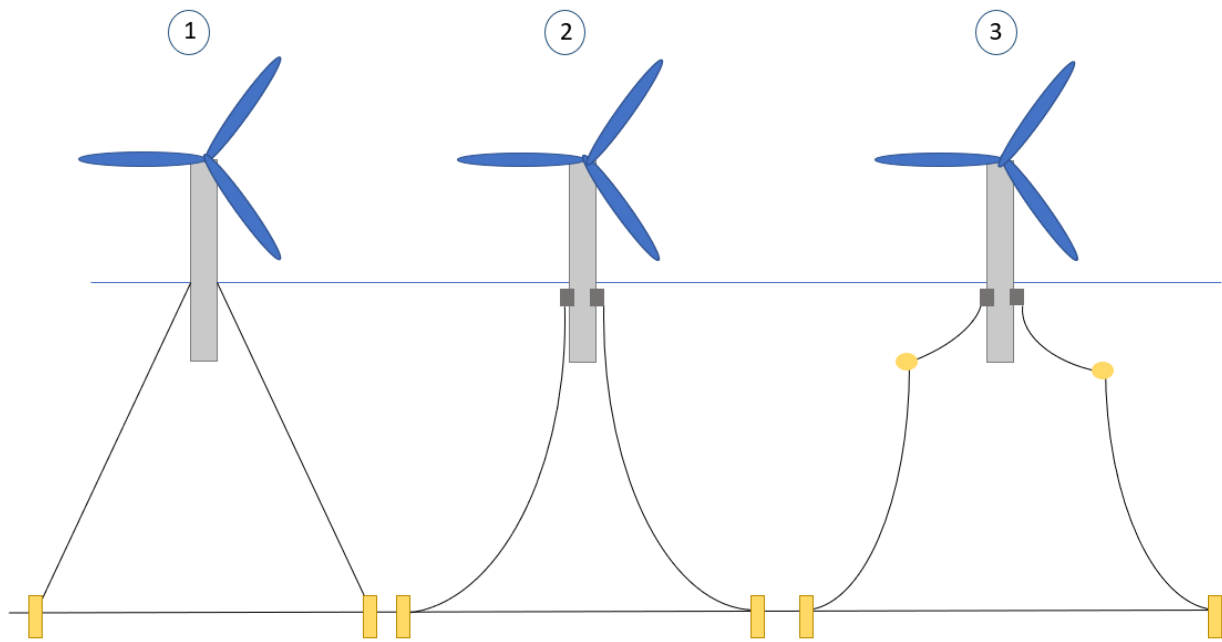


Figure 2.3.1: Typical arrangement of mooring system. 1 shows the taut-leg mooring, 2 the catenary mooring and 3 shows the catenary mooring with buoyancy elements

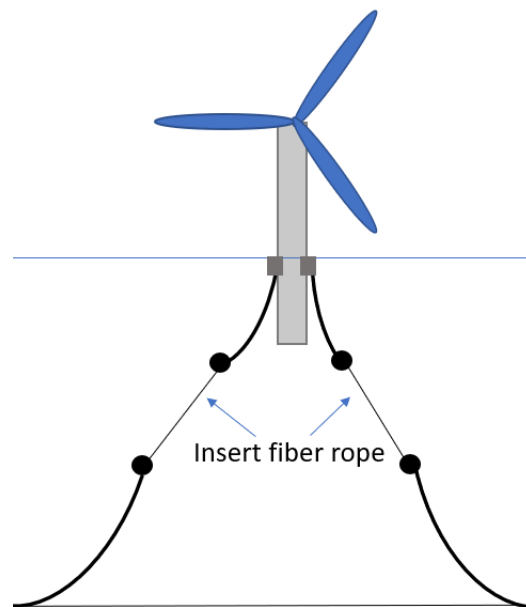


Figure 2.3.2: Example on how to insert fibre rope in a catenary system, illustration based on Larsen (2018a)

Chapter 3

Subsea Lift and Crane Operations

There are several ways to perform an offshore lift, and dependent on the lifted object and its geometry an appropriate method and suitable equipment are needed. During a subsea operation, it is important that the lifted object always shall be handled in a safe way. Likewise, to wait on weather can be costly and should, therefore, be avoided without affecting the safety of personnel or equipment. This chapter describes the difference between heavy and light lifts, lifting phases and their respective challenges, slack and snap loads and how to establish limits for the lift. In addition, a description of the static and dynamic equilibrium of the lifting system and the crane tip motion is described. In the end, examples of installation procedures of a DPA and a suction anchor are presented.

3.1 Heavy- and Light lifts

The weight of the object is an important factor when planning the operation. Based on the weight ratio between lifted object and the vessel, DNV GL (2011b) classifies a lift as light or heavy. A light lift is when the weight of the object is typically less than 1-2% of the vessel displacement, and thus the weight of the object will not affect the motion of the vessel. Heave compensation, which is a system that can compensate for an object's vertical motion, can be used during a light lift operation. When the weight of the object is above 1-2% of the vessel's weight, the lift is classified as a heavy lift. In this case, there will be dynamic coupling between the lifted object and the vessel together with hydrodynamic coupling from the environment. This leads to a more complex operation and heave compensation cannot be used.

3.2 Lifting Phases

A lifting operation does usually involve a vessel, a crane and the lifted object. DNV GL (2011b) divides a typical subsea operation into the following phases; lift off from deck and manoeuvring object, lowering through the wave zone, further lowering down to seabed and positioning and landing. These phases should be assessed during the planning. In the following subsections, the different phases will be described in detail and the challenges that one can be exposed to during each phase will be highlighted. Table 3.1 sums up the lifting phases with associated issues, and Figure 3.2.1 illustrates the different lifting phases.

Table 3.1: The lifting phases with associated issues

Lifting phases	Issues
Lift-off and in air	Snap loads, pendulum motions, impact
Splash zone	Large dynamic loads, snap loads, large rotations due to instability
In water column	Vertical resonance in deep water
Landing	Position accuracy, soil disturbance, snap loads

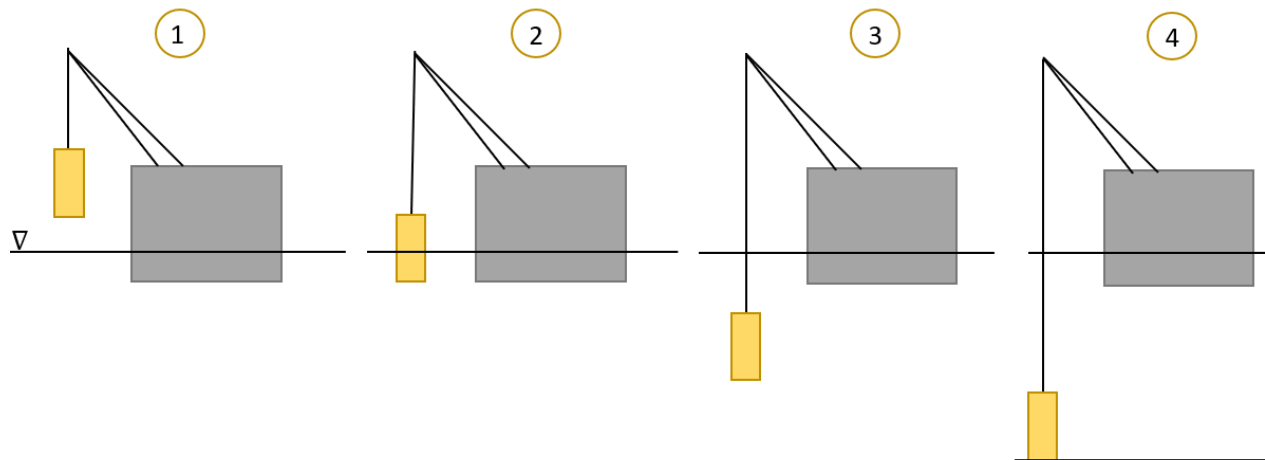


Figure 3.2.1: Lifting phases: 1. In air, 2: Through splash zone, 3. Fully submerged, 4. Landing

3.2.1 Lift Off and Manoeuvring of Object

The lift-off phase starts with cutting the sea fastening. The duration of this depends on the sea fastening used, whether it is strapped or welded. The object is then lifted off from a nearby vessel, from a deck or from shore. Dynamic motions become important as the object is lifted off deck, and to control this motion is essential. The vertical and horizontal motion in the crane tip might introduce an unacceptable slack in lifting line and subsequent snap loads, and therefore

the tension in the lifting wire shall be controlled. To move the object over the side of the vessel presents challenges regarding the stability of the vessel and extended crane capacity, where the centre of gravity will increase. To counteract heeling moment due to crane slewing, ballast operations are executed (Larsen, 2018b). During this phase, parameters like hoisting speed of the crane, the stiffness of the wire and mass of the object are important. To attach several tugger lines to provide horizontal stiffness can be a risk mitigating measure to prevent pendulum motion in the air. To ensure safe deck handling is important during the operation to protect structures and people. Also, the weather condition can determine whether the lifting operation is possible (DNV GL, 2011b). Figure 3.2.2a shows a suction anchor when lifted from deck and Figure 3.2.2b when the anchor is manoeuvred and ready for the lowering into the water.



(a) Lift-off from deck



(b) Manoeuvring anchor

Figure 3.2.2: Suction anchor in air and during manoeuvring. Pictures from Larsen (2018b)

3.2.2 Splash Zone

An object lowered into or lifted out of water will be exposed to a number of forces (DNV GL, 2011b), and this phase is usually the most critical. Forces like the weight of the object in the air, buoyancy, inertia, wave damping, drag, wave excitation, slamming and water exit forces are central. Also, lowering through the splash zone can lead to snap loads due to slack in lifting lines, so tension in lifting line and slings are important. By using special handling systems (SHS), the motion of the lifted object can be improved through the splash zone. During this phase, both sea elevation and crane tip motion are important parameters (Larsen, 2018b). Asymmetrical submergence or filling of the object can cause instability and critical forces in lifting wire. Figure 3.2.3 illustrates the splash zone.



Figure 3.2.3: Splash zone (Larsen, 2018b)

3.2.3 Lowering

The lowering phase is when the object submerges and there is variation in water depth. This phase is mainly driven by current forces in the horizontal plane and added mass, drag, inertia and crane tip forces in the vertical plane. The cable weight and the weight of the lifted object can lead to cable stretch. The static weight at the crane tip will increase as the water depth and cable length increases (Larsen, 2018b). Wave-induced motion of the vessel crane tip can lead to vertical oscillations of the lifted object. The mass-spring system has a natural period, if the crane tip oscillates with the same period, dynamic resonance can appear. This can be critical for the lifting operation. The stiffness of the cable will decrease with cable length, which increases the vertical resonance period of the lifting system. Heave compensation can be used to control the vertical motion of the object and tension in the lifting line during a light lift operation, and thereby reduce the chance of resonance. For deep water or strong current, ocean current can cause large horizontal offset.

3.2.4 Landing on Seabed

The final step is to place the object in the correct position and retrieve the lifting cable. As mentioned, for large water depths placing the object correctly can be difficult due to current loads. The ocean current is time-dependent and its magnitude and direction can vary with water depth. This can lead to difficulties with manoeuvring and accurate positioning on the seabed. Figure 3.2.4 shows how the offset will increase with water depth.

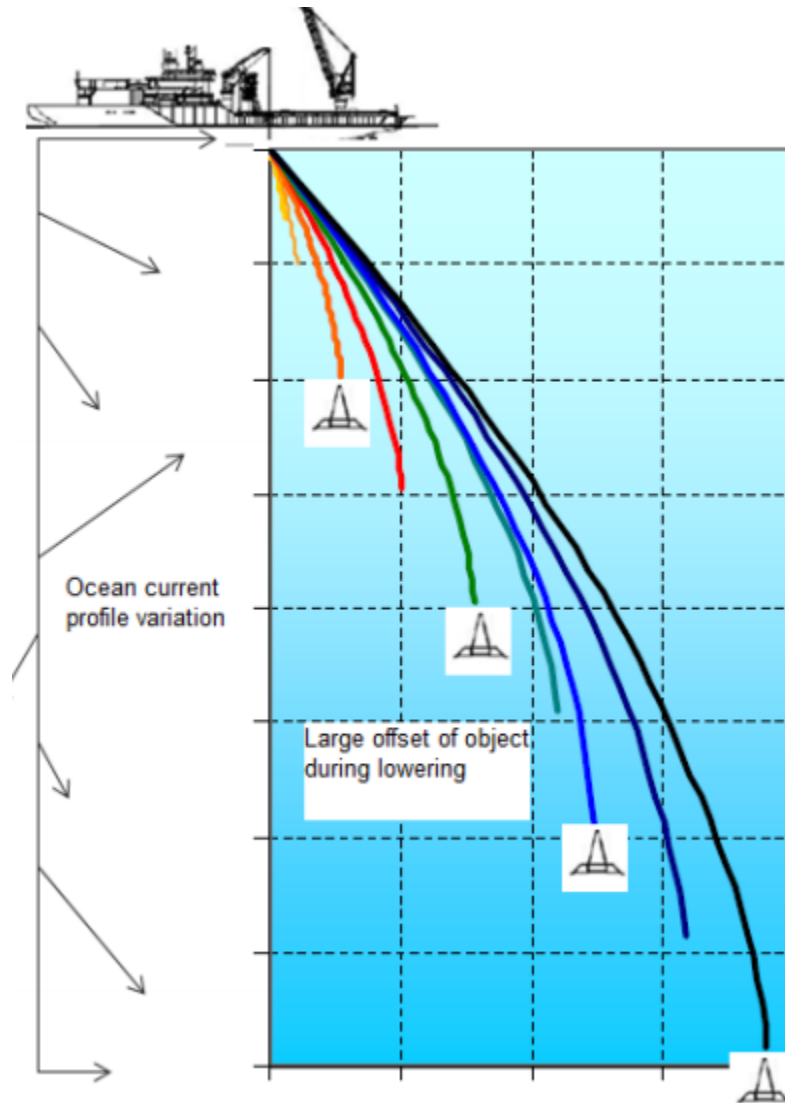


Figure 3.2.4: How the offset varies with water depth. Picture from Larsen (2018b)

The lifting phase determines the hydrodynamic forces acting on the system. Table 3.2 shows the phases when the object is in air, in the splash zone and fully submerged with the associated forces connected to the phase.

Table 3.2: Overview of significant forces acting during different lifting phases

	Drag	Slamming	Inertia	Buoyancy	Varying Buoyancy	Mg
In air			×			×
Slash zone	×	×	×	×	×	×
Fully submerged	×		×	×		×

As can be seen from Table 3.2, the inertia force and the weight are present during all phases.

When a object passes the splash zone, the hydrodynamic force will be a combination of the drag force F_D , slamming force F_S , inertia force F_I and varying buoyancy F_B . This is presented in Equation 3.1 based on the simplified method from DNV GL (2011b).

$$F_{Hyd} = \sqrt{(F_D + F_S)^2 + (F_I - F_B)^2} \quad (3.1)$$

The resulting force in the lifting line can be calculated from Equation 3.2

$$F_{Res} = Mg + F_{Hyd} - F_{buoy} \quad (3.2)$$

3.3 Static and Dynamic Equilibrium

The static load in the hoisting line $F_{line,stat}$ is given from Equation 3.3, and is expressed through the total weight, Mg , the time-dependent mass due to water filling, $m(t)g$, and the buoyancy force, $F_{B,mean}$.

$$F_{line,stat} = Mg + m(t)g - F_{B,mean} \quad (3.3)$$

The total weight of the lifting system includes the lifted object, the hoisting line and rigging equipment. The buoyancy force is acting in the opposite direction. Equation 3.4 shows the definition of the total line force $F_{line,tot}$, which is the sum of static and dynamic forces acting on the line. The dynamic line force $F_{line,dyn}$ is determined by the stiffness of the line and the relative vertical movement between the crane tip and the object. Figure 3.3.1 shows the relative vertical motion between the crane tip and a subsea structure for a dynamic system with stiffness K .

$$F_{line,tot} = F_{line,stat} + F_{line,dyn} = Mg + m(t)g - F_{B,mean} + K(\eta_{ct} - \eta) \quad (3.4)$$

By summing the dynamic line force and the hydrodynamic forces (inertia, drag, slamming and varying buoyancy), the dynamic equilibrium can be found. This is set out in Equation 3.5 from Larsen (2018b) assuming water entry.

$$\begin{aligned} M\ddot{\eta} = & \underbrace{-\rho C_A V \ddot{\eta} + \rho V (1 + C_A) \dot{v}}_{\text{Inertia}} + \underbrace{\frac{1}{2} \rho C_D S (v - \dot{\eta}) |v - \dot{\eta}|}_{\text{Drag}} \\ & + \underbrace{\frac{1}{2} \rho C_s A_p (\dot{\zeta} - \dot{\eta})^2}_{\text{Slamming}} + \underbrace{\rho g A_w \zeta}_{\text{Varying Buoyancy}} + \underbrace{K(\eta_{ct} - \eta)}_{F_{line,dyn}} \end{aligned} \quad (3.5)$$

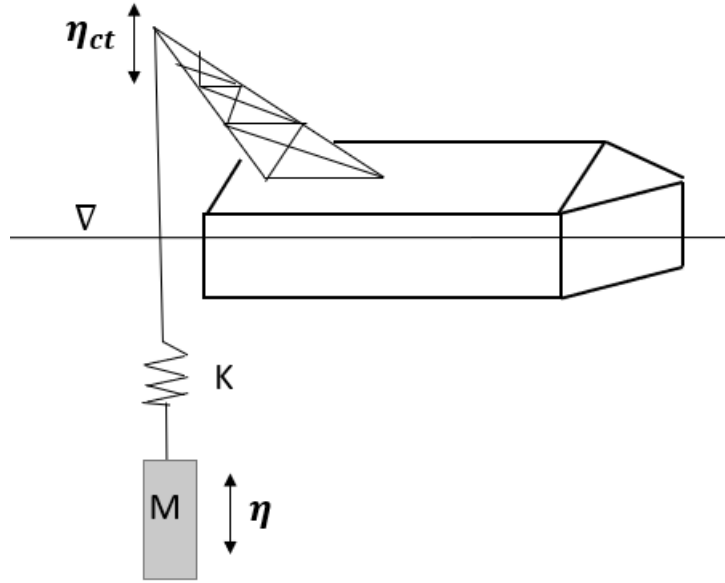


Figure 3.3.1: The relative vertical motion between the crane tip and a subsea structure for a dynamic system with stiffness K .

By reformulating Equation 3.5, the vertical motion η can be found for dynamic equilibrium in Equation 3.6. Here added mass A can be written as $\rho C_A V_R$.

$$(M + A)\ddot{\eta} + K\eta = \rho V_R(1 + C_A)\dot{v} + \frac{1}{2}\rho C_D S(v - \dot{\eta})|v - \dot{\eta}| + \frac{1}{2}\rho C_S A_p(\dot{\zeta} - \dot{\eta})^2 + \rho g A_W \zeta + K\eta_{ct} \quad (3.6)$$

M = mass of lifted object

ρ = sea water density

C_A = added mass coefficient

V_R = added mass reference volume

K = Stiffness of hoisting cable

C_D = drag coefficient in oscillatory flow

S = projected area normal to force direction

C_S = slamming coefficient

A_p = horizontal projected area of object

A_w = waterplane area of object

ζ = wave elevation

$\dot{\zeta}$ = wave velocity

η_{ct} = crane tip vertical motion

η = dynamic vertical motion of object

$\dot{\eta}$ = dynamic vertical velocity of object

$\ddot{\eta}$ = dynamic vertical acceleration of object

v = fluid particle vertical velocity

\dot{v} = fluid particle vertical acceleration

3.4 Crane Tip Motion

The vessel motions consist of translatory displacements in the x -, y - and z -direction with respect to the origin and angular displacements of the rotational motion about the x -, y - and z -axis. The translatory displacements in the x -, y - and z -direction are called surge, sway and heave, denoted η_1 , η_2 and η_3 . The rotational motion about the x -, y - and z -axis are called roll, pitch and yaw, denoted η_4 , η_5 and η_6 . The vessel motions are shown in Figure 3.4.1. Equation 3.7 shows the motions of any point on the ship when the position relative to the Centre of Gravity is known (Faltinsen, 1993). i , j and k are unit vectors along the x -, y - and z -axis, respectively.

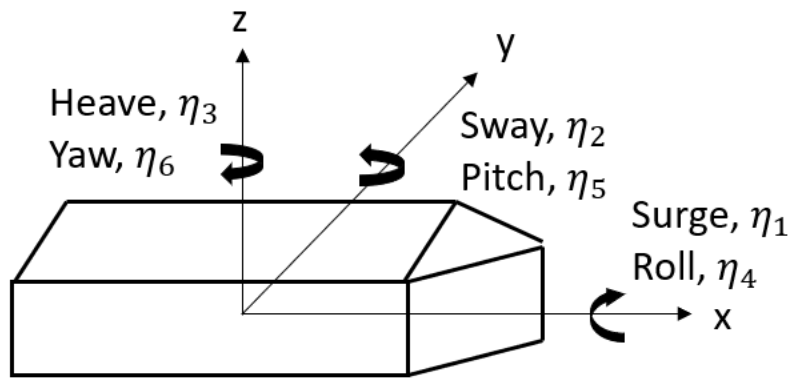


Figure 3.4.1: Vessel motion in six degree, translation and rotation about centre of gravity

$$s = (\eta_1 + z\eta_5 - y\eta_6)\mathbf{i} + (\eta_2 - z\eta_4 + x\eta_6)\mathbf{j} + (\eta_3 + y\eta_4 - x\eta_5)\mathbf{k} \quad (3.7)$$

In this thesis the motion characteristics of the vessel are not affected by the lifted object since the weight difference between the anchor and the installation vessel is categorized as a light lift. Hence, the motion of the crane tip can be determined directly from the wave-induced rigid body motion of the crane vessel. To control the rope tension, the vertical motion of the crane tip (η_{ct}) is of high interest. η_{ct} can be found from Equation 3.7, and is a function of the vessel motions in heave, roll and pitch.

3.5 Slack and Snap Loads

Marine lifting operations are usually performed with a crane wire and lifting slings. Lifting wire and slings do not allow compression and do only have capacity in tension. When there is no tension in lifting lines, the lifting system will be exposed to slack. Slack will take place when the hydrodynamic forces exceed the submerged static weight of the lifted object. The combination of the vessel and crane tip motion and vertical velocity can lead to slack. This takes typically place during lowing through the splash zone or when the object is fully submerged. This shock load can have a magnitude many times greater than the dynamic forces resulting from the steady-state response of the system (Thurston et al., 2011). Because of the large magnitude of the snap load, it can be very critical for the lifting operation if slack in the lifting wire or slings occurs. Among other things can the snap loads exceed the sling's or wire's yield strength and break the material. Another critical situation is that the sling can be deformed and bent causing damage to the fibres and defect the sling.

From DNV GL (2011b)'s Recommended Practice of Modelling and Analysis of Marine Operations, it states that snap forces as a consequence of slack shall be avoided and that the weather criteria should be adjusted to ensure this. The recommendation is that the tension force in the lifting slings shall not become less than 10% of the static submerged weight of the lifted structure. A 10% margin is assumed to be an adequate safety level with respect to the load factors and load combinations stated in the Ultimate limit state (ULS) criteria. This is illustrated in Figure 3.5.1.

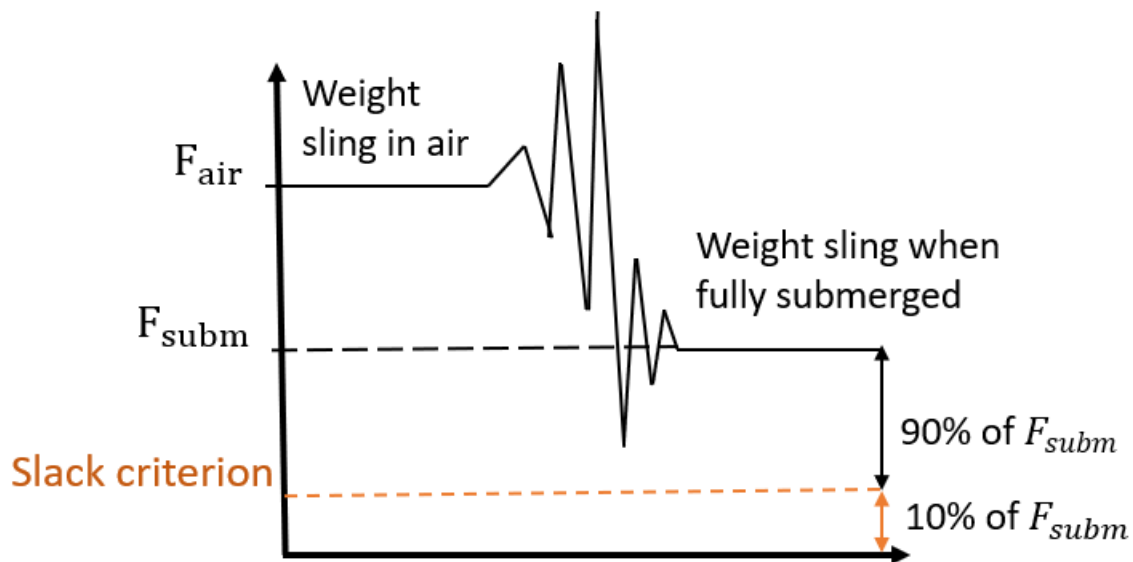


Figure 3.5.1: Illustration of slack criterion

In addition to the slack criterion, the lifting equipment needs to go through a capacity check before an operation can be executed (DNV GL, 2014). The maximum dynamic load in a single sling shall be adjusted for skew loads and sling capacity is checked against a certified Minimum Breaking Load (MBL). The maximum dynamic sling load F_{sling} should fulfil Equation 3.8. This equation will be used for the weakest link in the lifting system, either the slings or the hoisting line.

$$F_{sling} < \frac{MBL_{sling}}{\gamma_{sf}} \quad (3.8)$$

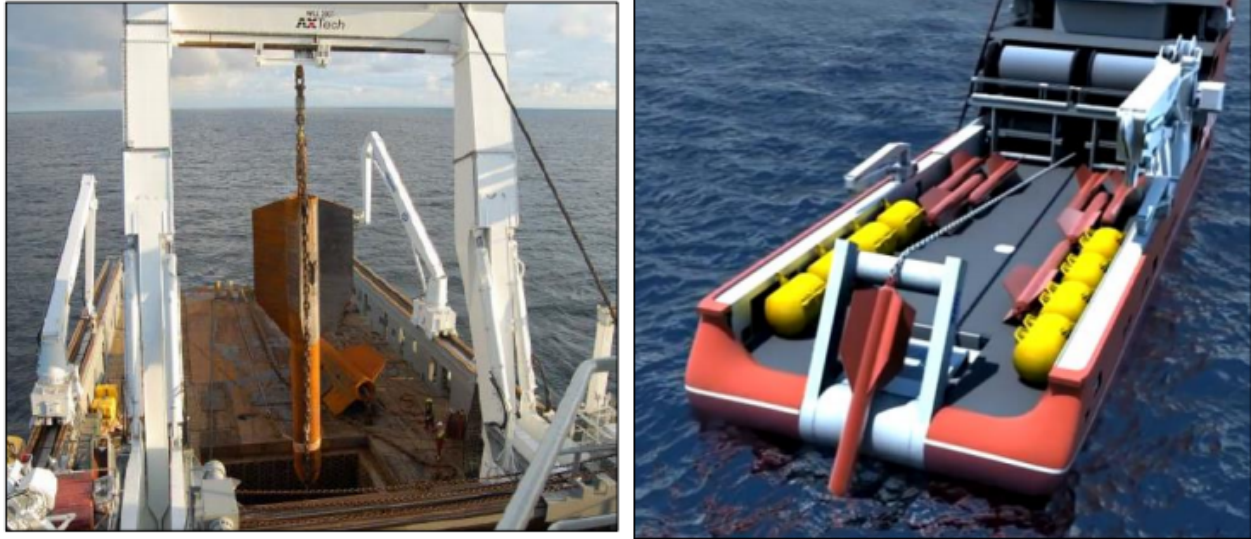
γ_{sf} is the nominal safety factor. The safety factor consists of a number of factors (load, material, consequence etc.) and is often set to 3.0 (Larsen, 2018b).

3.6 Installation of Anchors

Before the installation can take place, the operation has to be planned in details. Essential information must be gathered, analyses carried out and different installation scenarios considered. It is important to investigate the soil for the specific site before deciding the design of the anchor. Together with the anchor geometry and kinetic energy, the penetration depth of the DPA can be estimated. This is important for the holding capacity of the system. The drop height and anchor velocity during the drop phase must also be determined. In this section, alternative installation procedures for a DPA and a suction anchor are described. These are used as a basis further in the thesis.

3.6.1 Installation of Deep Penetration Anchor

Depending on the installation procedure, either one or two anchor-handling vessels (AHV) can be used to lower the DPA to a determined height above the seabed. The deep penetration anchor can be linked directly to the floating unit or be pre-laid with or without permanent mooring lines. There are several ways to install the anchor; lowered into the water through the vessel's moonpool (Figure 3.6.1a), deployed over the stern roller by use of an A-frame (Figure 3.6.1b), lowered by a winch along the ship's side or by use of a crane.



(a) DPA lifted through a moonpool, from Landhaug (2015) citing Deep Sea Anchors and Equinor (2009) and skidding winches (Deep Sea Anchors, 2019a)

Figure 3.6.1: Alternative ways of installing deep penetration anchor.

The anchor is installed by releasing the anchor from an installation wire at a calculated height above the seafloor. A release unit is connected to the lower end of the installation wire and receives an acoustic signal from the ROV that detaches the wire from the mooring line. Then, the anchor is free to fall towards the seabed. This is illustrated in Figure 3.6.2 where the anchor is released at $t=0$ and reaches the sea floor after x seconds.



Figure 3.6.2: Configuration of a DPA before anchor drop(Deep Sea Anchors, 2019a)

One can then either install only bottom chain (pre-lay) or most of the mooring lines before it later will be connected to the floating structure. For FOWT, pre-lay is most common practice. If anchor installation is performed without the permanent mooring line, only one vessel is required for the operation. Two vessels are normally preferred when laying down permanent mooring lines. This will especially be the case if the installation is done in deep water due to the weight of the mooring line. Accordingly, the anchor is lowered using an installation wire from the first AHV while the second AHV holds the permanent mooring line that is attached to the anchor and forms a loop. Figure 3.6.3 shows the installation of DPA using two AHVs.

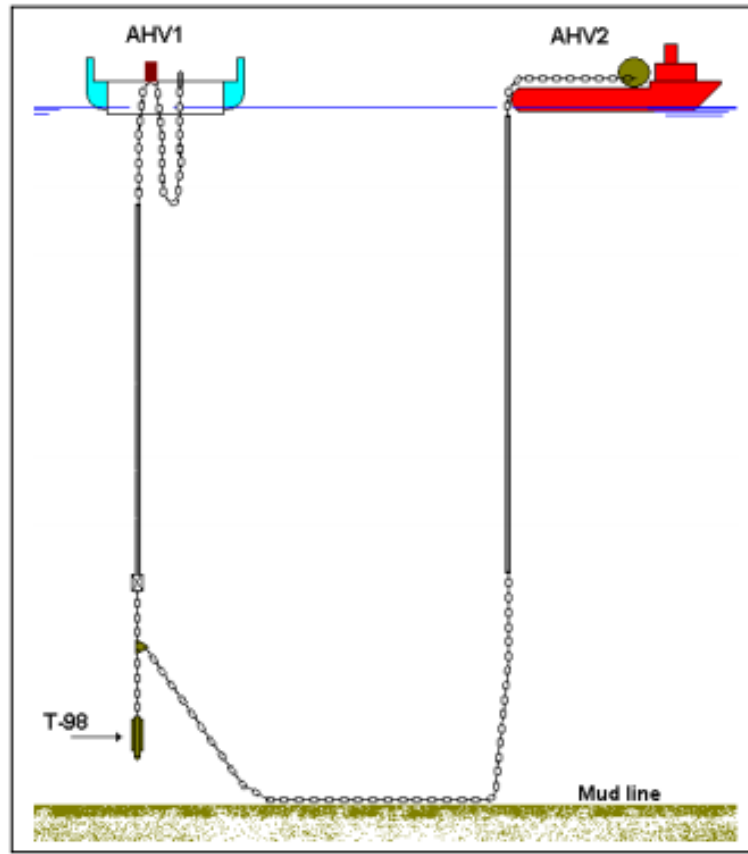


Figure 3.6.3: The configuration with two AHVs just before shooting operation(de Araujo et al., 2004)

In the following, one method is described. The installation procedure used further in this thesis is based on using a crane and one crane vessel.

1. Pick up the DPA by use of a vessel crane.
2. Connect one end of mooring chain to the top of the anchor and the other end to a release unit which is again connected to crane wire.
3. Lift the anchor from vessel deck.
4. Rotate crane over vessel side.
5. Lower anchor to the desired drop height.
6. Inspect mooring line and anchor with ROV.
7. When the configuration is approved, the ROV sends out an acoustic signal that opens the release unit. The anchor is free to fall and will penetrate into the seabed.
8. The ROV checks that everything is fine, and if so, the installation is complete.
9. The bottom chain is then connected to a buoy for later pick up and connection to the permanent mooring line and the floating wind turbine.

3.6.2 Installation of Suction Anchor

Below is one alternative installation procedure of a suction anchor presented.

1. Pick up the suction anchor and install a suction pump on the top, see Figure 3.6.4.
2. Lift the anchor from the deck and into the water.
3. Lower to the seabed, position and orientate with ROV.
4. Lower suction pile to self-weight penetration.
5. Close vent valve in suction pump and perform suction operation, see Figure 3.6.5.
6. Open vent valve and remotely recover suction pump to deck.



Figure 3.6.4: Suction Anchor on deck of a vessel with installed suction pump (SPT Offshore, 2019)

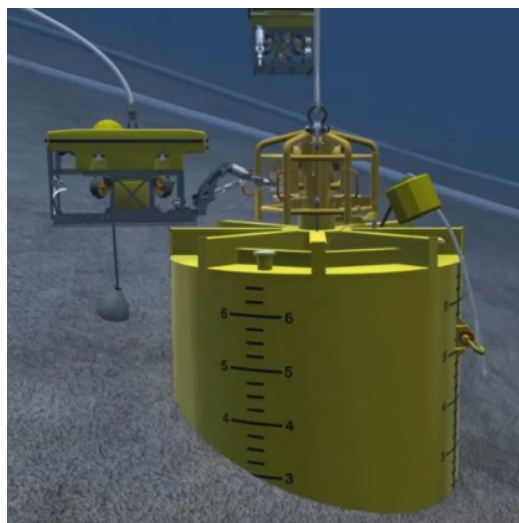


Figure 3.6.5: Suction Anchor during suction operation, (SPT Offshore, 2019)

Chapter 4

Hydrodynamic Theory

This chapter focuses on the hydrodynamic theory that is of importance in the context of this thesis. Linear wave theory with a focus on fluid particle motions is presented as well as irregular waves and wave spectrum which will give a more realistic description of a sea state during the simulation. Equation of motion is used to evaluate the dynamic and natural periods of the lifting system, and the Morison's equation for calculating wave loads with drag and inertia forces and their related coefficients are described.

4.1 Linear Wave Theory

The linear theory represents a first order approximation in satisfying the free surface conditions (Faltinsen, 1993). For linear wave theory, propagating waves are assumed with a horizontal sea bottom and a free-surface of infinite horizontal extent.

Regular waves can be described by a single circular frequency $\omega = \frac{2\pi}{T}$ and a single wavelength $\lambda = \frac{2\pi}{k}$ where T is the wave period and k is the wave number. The steepness, H/λ , of a linear wave is small. This means that linear waves do not exhibit second order behaviour, such as breaking. The wave profile for a regular sinusoidal incident wave is given by Equation 4.1

$$\zeta = \zeta_a \sin(\omega t - kx) \quad (4.1)$$

where x is the distance from the origin to the point of interest in the X direction, and t is time.

The velocity potential ϕ for a regular wave under the assumptions of incompressible and inviscid sea water, irrotational fluid motion, infinite water depth and that the pressure follows the Bernoulli equation can be found from Equation 4.2. ζ_a is the wave amplitude and z the vertical coordinate positive upwards z .

$$\phi = \frac{g\zeta_a}{\omega} e^{kz} \cos(\omega t - kx) \quad (4.2)$$

Further, the vertical particle velocity and acceleration can be expressed from Equation 4.3 and 4.4 respectively.

$$w = \omega\zeta_a e^{kz} \cos(\omega t - kx) \quad (4.3)$$

$$a_3 = -\omega^2\zeta_a e^{kz} \sin(\omega t - kx) \quad (4.4)$$

with wave amplitude ζ_a , time variable t , the wave number k , direction of wave propagation x , wave frequency ω and the vertical coordinate positive upwards z . The wave number can be found by Equation 4.5

$$k = \frac{2\pi}{\lambda} \quad (4.5)$$

where λ is the wavelength, and for infinite water, it can be expressed using wave period T demonstrated in Equation 4.6

$$\lambda = \frac{g}{2\pi} T^2 \quad (4.6)$$

The wave energy makes the water particles move in an orbital motion, and Figure 4.1.1 shows water particle movement in deep water. Near the surface, the diameter of the movement of the orbits will be approximately equal to the wave height, and the diameter and the wave energy will decrease with depth. In deep water, for a depth below half the wavelength, water is unaffected by the wave energy (TSI, 2019).

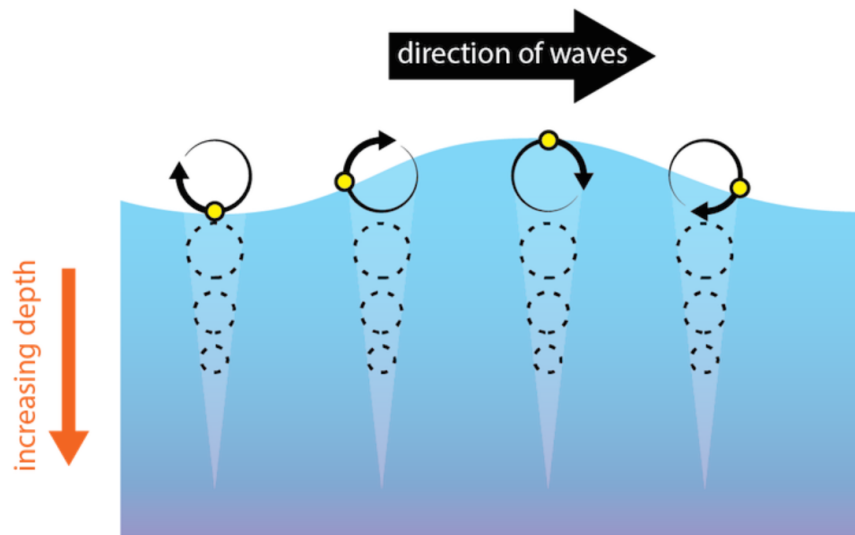


Figure 4.1.1: Water particles paths in deep water varying with water depth (TSI, 2019)

4.2 Irregular Waves

The sea state cannot be described with such a simple model as regular or periodic waves since ocean waves are irregular with random shape, height, length and propagation on the surface of the sea. The waves have several frequencies and amplitudes and can be described as a sum of sine- and/or cosine functions. By use of linear wave theory, the superposition principle is valid and the random wave elevation can be split into several regular wave components (Faltinsen, 1993). In other words, it is possible to study the response of irregular waves as the sum of the response of regular waves.

As the waves are random in reality, the wave spectrum is introduced to capture the randomness by assuming stationary sea state for a few hours, typically 3 hours. Stationary means the statistical properties of the sea state such as mean, variance are constant (Pettersen, 2007). If the wave components are long-crested, it is sufficient to represent the waves in a wave spectrum. However, if the waves are short crested, a directional spectrum is needed.

4.2.1 JONSWAP Spectrum

In design, one usually does not have access to the real wave spectrum for that area and the weather to calculate the desired response for a ship or a construction. Therefore, one uses standardized wave spectrum for which there are several. The standardized spectrum becomes a form of the average spectrum, and will thus not be valid for all frequencies (Pettersen, 2007). This is important to take into account when considering the results.

The JONSWAP ('Joint North Sea Wave Project') spectra came as a result of a multinational project in the south-eastern parts of the North Sea in 1968 and 1969 (Pettersen, 2007), and is a modification of the Pierson-Moskowitz (PM) Spectrum. In the area where it was measured, one found that the spectrum had a very sharp peak. The JONSWAP spectrum is a five parameter spectra with $\alpha, \gamma, \sigma_a, \sigma_B, \omega_p$, and the structure of the spectrum is as follows:

1. With the PM spectrum as a basis, a top frequency, ω_p is introduced instead of the wind velocity, V .

$$A = \alpha g^2 \quad (4.7)$$

where α is 0.0081 for PM spectra and describes the shape on the spectra in the high frequency part. This gives the following relation between ω_p and V

$$\omega_p = 0.87 \frac{g}{V} \quad (4.8)$$

and the PM spectrum gets the following shape

$$S(\omega) = \alpha \frac{g^2}{\omega^5} \exp \left[-\frac{5}{4} \left(\frac{\omega_p}{\omega} \right)^4 \right] \quad (4.9)$$

2. The spectrum from Equation 4.9 is then multiplied with

$$\gamma^{\exp[-\frac{1}{2}(\frac{\omega-\omega_p}{\sigma\omega_p})^2]} \tag{4.10}$$

where γ is the peakedness parameter, and σ is equal to σ_a for $\omega \leq \omega_p$ and is equal to σ_b for $\omega > \omega_p$. The peakedness parameter is proportional to the relation between the maximum energy in JONSWAP spectrum and maximum energy in the PM spectrum, ie.

$$\gamma = \frac{S_{JONSWAP,max}}{S_{PM,max}} \cdot \text{constant} \tag{4.11}$$

γ varies between 1 and 7, and for γ equal to 1 the JONSWAP spectrum is identical to the PM spectrum. If a PM spectrum and JONSWAP spectrum is used to describe the same sea state, the total energy for the sea state will be equal, meaning that the area under the graph is the same. However, the main difference is how the energy is distributed on the frequencies. In the JONSWAP spectrum, more energy will appear around the peak frequency and less energy on frequencies away from the peak frequency compared to the PM spectrum. A modified PM spectrum and a JONSWAP spectrum are shown in Figure 4.2.1.

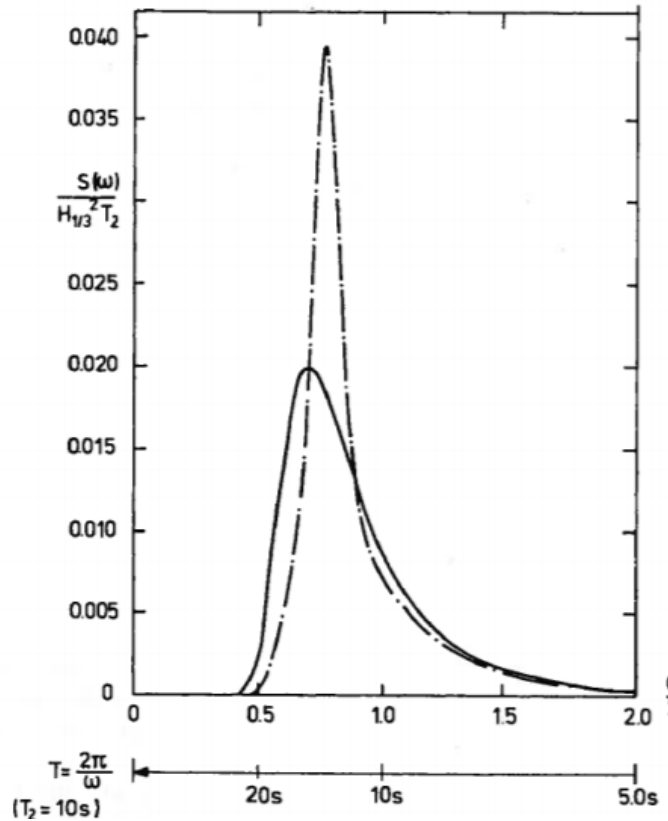


Figure 4.2.1: Examples of wave spectrum. $H_{1/3}$ is the significant wave height, T_2 the mean wave period. Modified Pierson Moskowitz spectrum, —, JONSWAP spectrum, -.-.(Faltinsen, 1993)

4.3 Equation of Motion

The equation of motion describes the behaviour of a system in terms of its motion as a function of time, and a general expression can be found in Equation 4.12.

$$M\ddot{x} + C\dot{x} + B_1\dot{x} + B_2\dot{x}|\dot{x}| + kx = q \quad (4.12)$$

M is the structural mass including the frequency dependent added mass matrix. C represents the frequency dependent potential damping coefficient, B_1 and B_2 is the linear and quadratic damping coefficient and K is the hydrodynamic stiffness coefficient. Position, velocity and acceleration is denoted x , \dot{x} , \ddot{x} respectively, while q is the excitation force. Figure 4.3.1 shows a system with one degree of freedom (DOF) in heave.

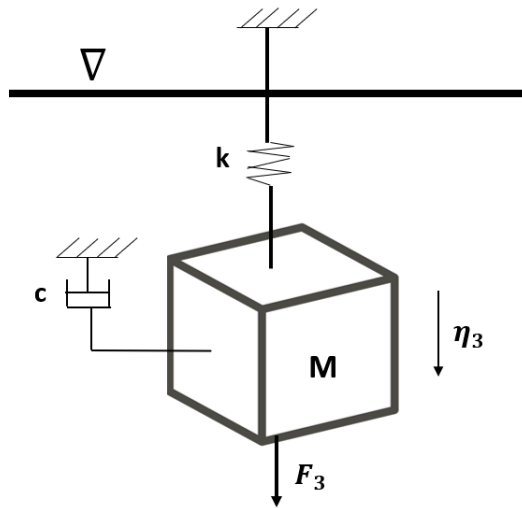


Figure 4.3.1: System with one DOF in heave

For a un-damped system with one DOF in heave the damping coefficient c equals zero. The system will then oscillate with the natural frequency and a constant amplitude. The natural frequency ω_0 is expressed by Equation 4.13

$$\omega_0 = \sqrt{\frac{k}{M + A_{33}}} \quad (4.13)$$

with the mass M , added mass in heave A_{33} and stiffness of system k . The corresponding natural period T_n in heave is given by Equation 4.14

$$T_n = \frac{2\pi}{\omega_0} = 2\pi\sqrt{\frac{(M + A_{33})}{k}} \quad (4.14)$$

The stiffness of a hoisting system may be calculated by (DNV GL, 2011b):

$$\frac{1}{k} = \frac{1}{k_{rigging}} + \frac{1}{k_{line}} + \frac{1}{k_{soft}} + \frac{1}{k_{block}} + \frac{1}{k_{boom}} + \frac{1}{k_{other}} \quad (4.15)$$

k is the total stiffness of a hoisting system, $k_{rigging}$, k_{soft} and k_{boom} are stiffness for respectively the rigging system, of soft strops or a passive heave compensation system and the crane boom. If multiple lines in a block are used, k_{boom} is to be added. Further, other stiffness contributors are counted for by adding k_{other} . k_{line} is the stiffness of hoisting line which may be calculated by

$$k_{line} = \frac{EA}{L} \quad (4.16)$$

where E is the modulus of rope elasticity, A the effective section area of line and L the length of the line.

The natural period of a pendulum depends on the length of the wire L and the gravitational acceleration g and can be found from Equation 4.17

$$T_n = 2\pi \sqrt{\frac{L}{g}} \quad (4.17)$$

4.4 Response Amplitude Operator

A Response Amplitude Operator (RAO) is used to determine the likely behaviour of a ship or a floating structure when at sea. The RAOs are given in six DOF and is defined at the vessel's COG and is usually calculated for all wave headings. RAOs are transfer functions used to determine the effect that a sea state will have upon the motion of a ship through the water. RAO is the linear transfer function between a wave and the vessel motion and is known as $|H(\omega, \beta)|$ (Greco, 2018). This defines the relationship between input and output and is known as the response amplitude per unitary incident-wave amplitude: $|H(\omega, \beta)| = \frac{\eta_a}{\zeta_a}$.

4.5 Morison's Equation

Structures or parts can be classified as small and large volume, and where the constructions ability to generate waves are important when calculating forces on large volume structures (Petersen, 2007). Based on a vertical cylinder placed at the sea floor and up through the water surface in regular sinus waves, the two cases can be classified. The structure is called small volume if the relation between wavelength λ and diameter D is larger than 5. Small volume constructions can further be divided into inertia and drag dominated structures. For a cylinder, the

structure can be defined as drag dominated if $H/D > 4\pi$. Figure 4.5.1 shows the classification of marine structures.

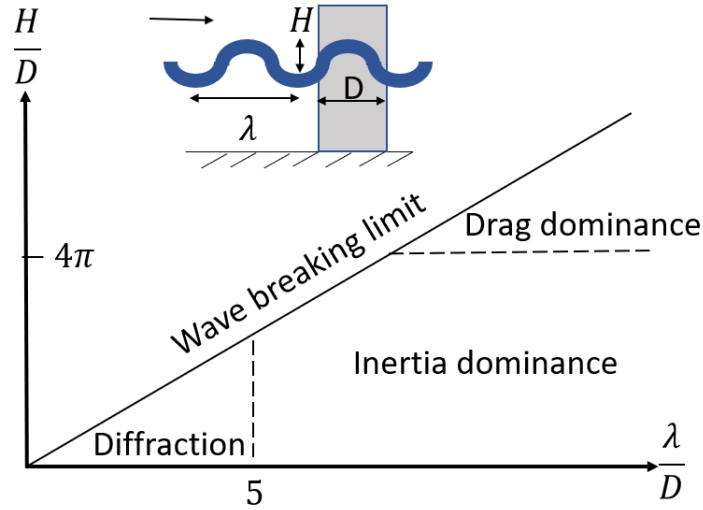


Figure 4.5.1: Hydrodynamic classification of the marine structures using a circular cylinder as representative of structural elements and examining the dominant loads

Morison's equation can be used for small volume structures to estimate wave loads. The general Morison's equation is the sum of inertia and a drag force and can be found from Equation 4.18.

$$F_M = F_D + F_I = 0.5\rho AC_D u|u| + \rho VC_M \dot{u} \quad (4.18)$$

The first part is the drag force, F_D , proportional to the square of the instantaneous flow velocity u with the mass density of the water ρ , drag coefficient C_D and cylinder area A . The inertia force F_I is in phase with the local flow acceleration \dot{u} , and is the sum of the Froude–Krylov force $\rho V \dot{u}$ and the hydrodynamic mass force $\rho C_a V \dot{u}$. The inertia coefficient can be found from $C_m = 1 + C_a$ where C_a is the added mass coefficient. In reality, the mass and drag coefficients C_M and C_D have to be empirically determined since they are dependent on many parameters like Reynolds number, Keulegan-Carpenter number, a relative current number and surface roughness ratio.

The inertia force will decay with depth like $e^{2\pi z/\lambda}$ and the drag force like $e^{4\pi z/\lambda}$. This applies to deep water regular sinusoidal incident waves when assuming C_M and C_D constant with depth (which might not be realistic) (Faltinsen, 1993). When there is a wave node at the cylinder axis the inertia force will have a maximum absolute value and the drag-force will then be zero. While the drag force will have a maximum absolute value when there is a wave crest or a wave trough at the cylinder axis.

4.6 Hydrodynamic Parameters

Hydrodynamic parameters can be determined theoretical or by experimental methods, and are depend on the body geometry, perforation, sharp edges, oscillation, wave height, water depth, wave period and the vicinity of free surface or sea bottom. DNV GL (2011b) recommends to carry out models test for achieving most accurate hydrodynamic coefficients of a 3-dimensional subsea structure with complex geometry.

4.6.1 Added Mass

Added mass is defined as the inertia added to a system due to an accelerating or decelerating body when it moves fluid as it penetrates the water. Added mass is dependent on the body shape, current, depth, oscillation frequency and a motion mode. It is shown that reliable estimates on the added mass for the subsea structure is important to be able to estimate the lifting forces during installation and to asses the likelihood of slack in the lifting wire (Nielsen, 2012). When the structure is lowered through the splash zone, the added mass will start to increase as the project area of the structure increases, while in deeply submerged condition (submergence greater than about twice the characteristic dimension of the structure) the added mass is no longer position dependent. In fully submerged condition, the submerged volume obviously is constant, but as the structure approaches the seafloor, the added mass becomes a function of the distance to the bottom (Nielsen, 2012).

The total added mass for a three-dimensional body can be found from Equation 4.19

$$A_{ij} = \rho C_A V_R \quad (4.19)$$

where A_{ij} is the added mass force in i -direction due to acceleration in j -direction, C_A is the dimensionless added mass coefficient and V_R is the reference volume in m^3 . DNV GL (2011b) has in the standard DNV-RP-H103 described how to find added mass coefficients for simple geometries theoretically. This can be found in Appendix B.1.

Effect of height and perforation shall be accounted for, and the procedure is presented in Appendix B.1.1 and B.1.2 respectively.

Added Mass for a Suction Anchor

Nielsen (2012) has presented one alternative way of estimating the added mass for a suction anchor since the values from DNV GL can be some conservative. This method assumes a suction anchor with a central hole at the top with radius a , the radius of the anchor R and the height H , and gives the horizontal added mass as shown in Equation 4.20

$$A_{11} = \rho \pi R^2 H \quad (4.20)$$

and the vertical added mass from

$$\frac{A_{33}}{\rho \pi R^2 H} = 1 + \frac{4}{3} \left(\frac{R}{H} \right) - \frac{8}{\pi^2} \frac{a}{H} \frac{(1 + \frac{H}{2R})(1 + \pi \frac{H}{2R})}{1 + \frac{2}{\pi} \frac{Ha}{R^2}} \quad (4.21)$$

The expressions are derived under the assumption that $a \ll R$ and $H \gg R$.

4.6.2 Drag Force

Drag forces are due to braking against upstream surfaces, which gives an overpressure on the front and a negative pressure on the back, and where the sum of these provides the drag force. The drag force can be divided into quadratic and linear drag, where linear drag is connected to friction and viscous forces while quadratic is connected to pressure forces. The linear drag is often neglected since the vortex shedding is small compared to the friction.

Appendix B.2 contains data to find the drag force theoretically for simple geometries. The drag force with the drag coefficient C_D can be calculated from Equation 4.22

$$F_D = \frac{1}{2} \rho C_D v^2 A \quad (4.22)$$

where ρ is the density of the sea water, A is the projected area of the submerged part of the object, and v is the flow velocity relative to the object.

4.7 Water Entry Force

The impulse loads with high-pressure peaks that occur when objects hit water surface are often called slamming forces (Faltinsen, 1993). This happens during the water entry and can therefore also be called the water entry force. This is a non-linear phenomenon and lasts for milliseconds. Slamming can among other things lead to slack in slings which shall be avoided. The slamming force can be found from Equation 4.23 (DNV GL, 2011b)

$$F_s(t) = \frac{1}{2} \rho C_s A_p v_s^2 = \frac{1}{2} \rho C_s A_p (\dot{\zeta} - \dot{\eta})^2 \quad (4.23)$$

C_s is the slamming coefficient and can be found from $C_s = \frac{2}{\rho A_p} \frac{dA_{33}^{\infty}}{dh}$ where $\frac{dA_{33}^{\infty}}{dh}$ is the rate of added mass with submergence, ρ is the water density, A_p is the horizontal projected area of the object and h is the submergence relative to surface elevation. $\dot{\zeta}$ is the wave velocity and $\dot{\eta}$ is the object velocity.

Chapter 5

Planning of Marine Operations

This chapter is based on the offshore standard DNV-OS-H101 'Marine Operations, General' by DNV GL (2011a) which gives guidance and instructions for planning, preparations and performance of marine operations. This standard shall be considered in relation to the structural and operational complexity and sensitivity as well as the type of marine operation to be performed. The intention is to ensure structural failures less than 1/1000 per operation, meaning a probability of less than 10^{-4} . All the DNV offshore standards covering marine operation are named the VMO Standard. In 2016, the «VMO» standards were merged into one, called DNVGL-ST-N001.

In the standard, a marine operation is defined as a non-routine operation in the marine environment which takes place in a limited duration of time. The aim is to bring an object from one defined safe condition to another. Here, the object shall be exposed to normal risk, in other words, exposed to risks that are expected in the permanent condition. A marine operation consists of two phases; the design and planning phase and the execution of the operation phase (DNV GL, 2011b).

At the end of the chapter, the Weibull three-parameter distribution is described as a statistical model.

5.1 The Planning Process

The planning process is important to satisfy requirements for cost, operation efficiency and safety. As far as possible, planning should be based on well-proven principles, techniques, systems and equipment. Operations within an unknown environment or with new technology shall be documented through acceptable qualification processes. The planning process can be divided into five as illustrated in Figure 5.1.1. The organisation of key personnel involved in the operation shall be established prior to the execution. The first part of the planning process is to identify relevant regulations, rules and specifications for the given operation. In addition, physical limitations shall be found by for example doing a survey of offshore, inshore or quay

sites. During the overall planning, operational concepts, available vessels and equipment, as well as cost and risk assessment shall be considered. Physical limitations and environmental conditions shall be evaluated when developing the design basis. While, for the design brief, the activities planned with available tools and acceptance criteria shall be decided. Further, the load effects and required structural resistance shall be decided during the engineering and design. In the end, the operational procedures are prepared. As seen in Figure 5.1.1, the planning and design can be seen as an iterative process.

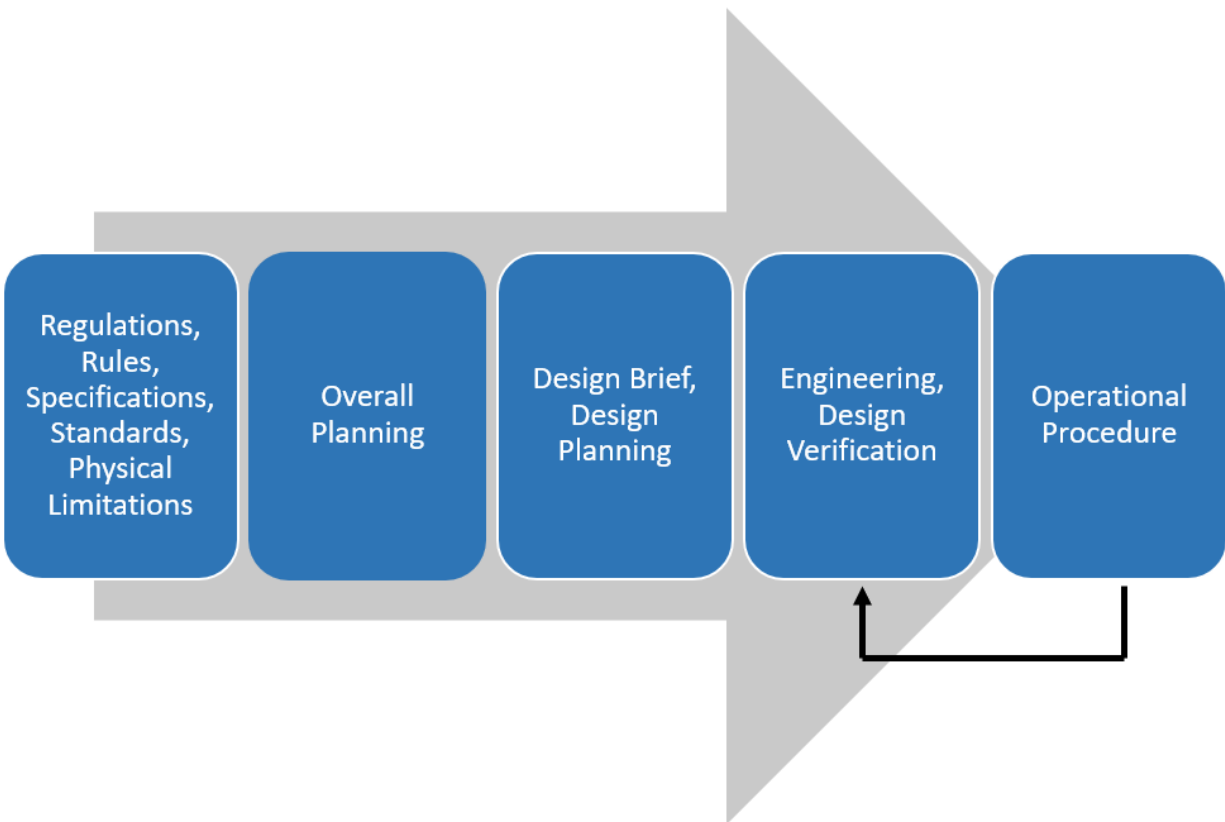


Figure 5.1.1: The planning process of Marine Operations, based on DNV GL (2011a)

The duration of marine operations shall be defined by an operation reference period, written as

$$T_R = T_{POP} + T_C, \quad (5.1)$$

where T_C is the estimated maximum contingency time and T_{POP} the planned operation period. T_{POP} should usually be based on a detailed schedule for the operation. By use of knowledge from similar tasks or operations, reasonable conservative assessment can be made to estimate the time. In addition, frequently experienced time delaying incidents should be included.

There is a general uncertainty in the planned operation time, and to compensate for this, T_C is added. T_C shall also cover the required additional time to complete the operation if a possible contingency situation appears. Normally, an applied T_C of less than 6 h is not acceptable. For some operations, a contingency time of 50% of T_{POP} may normally be accepted, this is typically for operations with good experience. If uncertainties and required time for contingency situations is not assessed in detail, T_C should be taken at least equal to T_{POP} , i.e. $T_R \geq 2 \cdot T_{POP}$. The defined start for weather restricted operations will be when the latest weather forecast (WF) is published. The relation between T_{POP} , T_C and T_R is shown in Figure 5.1.2.

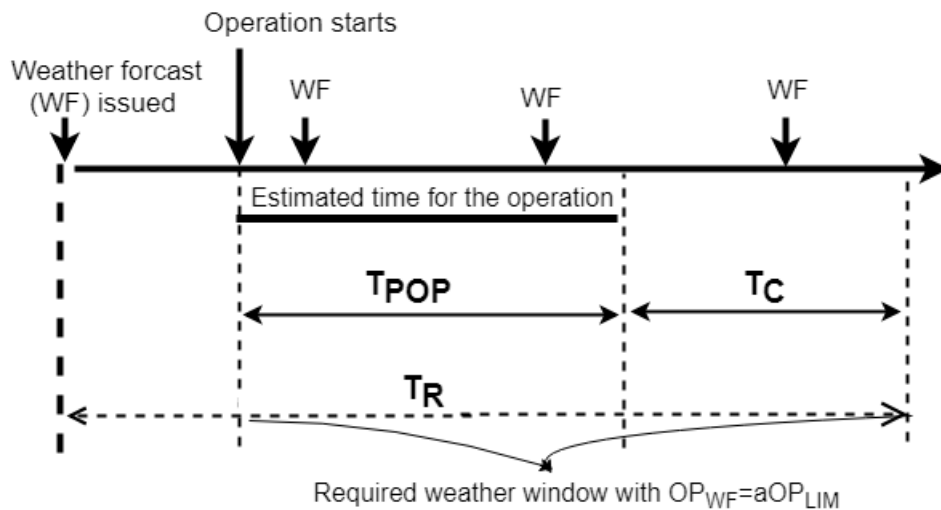


Figure 5.1.2: Weather window

The standard gives rules for the planning and execution of marine operations to ensure that the operation is performed within a given safety level. In the planning process, the operation or sub-operation may either be classified as restricted or unrestricted. This will impact the safety and cost of the operation.

5.2 Weather Unrestricted Operations

Unrestricted operations are characterized by longer duration, and T_R is normally more than 96 h and T_{POP} more than 72 h. These operations must be able to be carried out in any weather condition that can be encountered during the season. When planning weather unrestricted operations, local and seasonal statistics should be used, and the design criteria will be based on extreme value statistics. The minimum acceptable return period, T_d should be defined according to the operation reference period, T_R , see Table 5.1 with criteria for significant wave height (H_s) (DNV GL, 2011a).

Table 5.1: The acceptable return periods for H_s , obtained from DNV GL (2011a)

Reference Period, T_R	Return Period, T_d
$T_R \leq 3$ days	$T_d \geq 1$ month
$3 \text{ days} \leq T_R \leq 7$ days	$T_d \geq 3$ months
$7 \text{ days} \leq T_R \leq 30$ days	$T_d \geq 1$ year
$30 \text{ days} \leq T_R \leq 180$ days	$T_d \geq 10$ years
$T_R > 180$ days	$T_d \geq 100$ years

5.3 Weather Restricted Operations

For operations with a shorter duration, the operation is defined as weather restricted, and T_{POP} is usually less than 72 hours. These operations should be planned based on weather forecasts for the selected design environmental condition for the operation. The operations are designed and planned for a considerably lower environmental condition than the seasonal, statistical extremes used for weather unrestricted. A shorter reference period should be considered for areas and seasons where the corresponding reliable weather forecast is not considered realistic.

Forecasted and Monitored Operational Limits

To account for uncertainty in both monitoring and forecasting of the environment, a forecasted operational criterion, OP_{WF} , is defined to find the maximum weather condition to execute the marine operation. The operational criterion is determined during the planning process and controlled by the weather forecast and can be found from

$$OP_{WF} = \alpha \cdot OP_{LIM}, \quad (5.2)$$

where α is a factor used to account for the uncertainty in the weather forecast, and OP_{LIM} is the design criterion. OP_{LIM} is based on weather restrictions used for calculating the design

load effects. OP_{LIM} should never be greater than; maximum environmental criteria, the conditions for safe working of personnel, or position keeping. Based on the weather uncertainty for the actual site and the planned period of the operation the α -factor can be estimated. The α -factor is determined based on OP_{LIM} , T_{POP} and the weather forecast. Planned operation time shall be used as a minimum time for the selection of a α -factor. The α -factor is an important parameter for safety and cost for offshore operations and should be as reliable as possible in order to maintain high operation operability. The α -factor should be calibrated to ensure that the probability of exceeding the design criterion with more than 50% is less than 10^{-4} . It includes the fact that it is harder to estimate the wave height for small sea conditions than for larger seas. The α -factor does always have a magnitude less than one and will rise with increased quality of weather forecasts and the use of on-site monitoring systems. Further, it will decrease with the length of the planned operation, meaning that the difference between OP_{LIM} and OP_{WF} increases with increased T_{POP} . Since waves are considered to be the most influencing parameter during the execution of marine operations, H_s is a preferred assessment parameter.

In the standard DNV-OS-H101, various tables for estimating the α -factor are listed. These tables are based on the North Sea and the Norwegian Sea, however, they can be used as a guideline for other offshore areas.

Weather Forecast Levels

The weather forecast level for restricted marine operations shall be area specific. It is classified into different levels (A, B and C) by use of operational sensitivity to weather conditions and T_R . Every category has its own requirements that have to be fulfilled before the operation can take place.

Level A: larger marine operations that are sensitive to environmental conditions. It can be mating operations, multi barge towing or jack-up rig moves.

Level B: operations that are environmentally sensitive regarding value and consequences, like offshore lifting and sensitive barge towing.

Level C: is less affected by the weather conditions, carried out on a regular basis, such as on-shore/inshore lifting or loadout operations

The weather forecast level indicates whether a dedicated meteorologist is required on site, the number of independent WF sources and the maximum WF interval. This will affect the α factor used. Appendix C shows the various α -factor for the different weather forecast levels.

5.4 Operability and Weather Window

A weather window is defined as the period of time which is sufficient in length to safely carry out a marine operation. When assessing the available weather window, T_R is used. For restricted operations, the OP_{WF} shall be less than the weather forecasted environmental conditions during the entire period. Since waiting on weather is expensive, it is crucial to understand weather limitations and to have knowledge of weather at site.

Operability is the operation availability and can be defined as the ability to keep an object or a system in a safe and reliable condition, in agreement with pre-defined operational requirements. Calm periods also called calms (τ_c), is defined as the working period, where the H_s is lower than the operational limit, OP_{WF} . While, for a H_s higher than OP_{WF} , a storm period or storm (τ_s) occurs, and the operation must wait. Normally we denote periods of storms and calms by the significant wave height and with weather forecasts every third hour. See Figure 5.4.1 for an illustration of a time series of wave elevation with examples of calm and storm periods for a given operational criterion. The duration of the calm period can be found to be $\tau_c = t_2 - t_1$. An operation can only take place when the weather forecast predicts a calm period that is of longer duration than T_R .

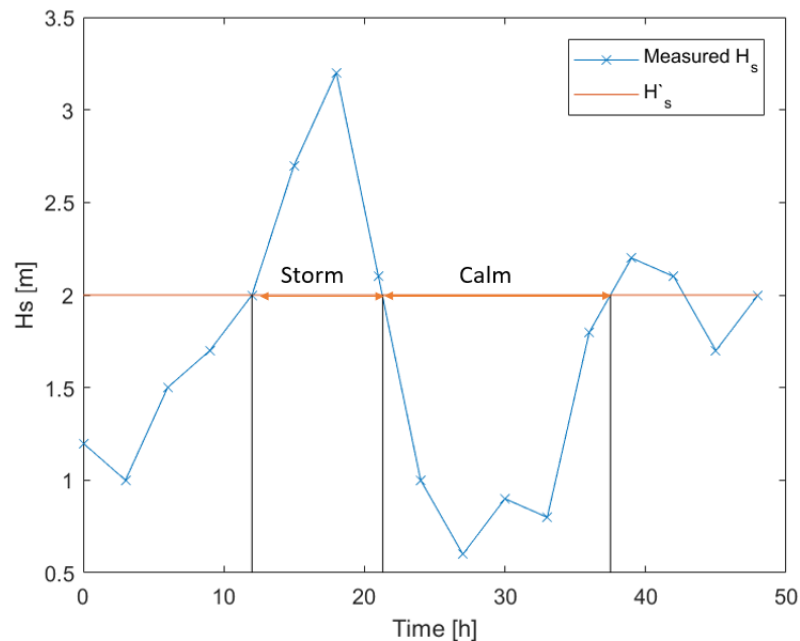


Figure 5.4.1: Example on significant wave height as function of time measured every 3rd hour. Highlights a storm and a calm period based on measured H_s and a H_s limit H'_s

Wait periods are storm periods or calm period of shorter duration than T_R also referred to as calm-wait periods. The probability of being able to work is equal to the probability that H_s is lower than the operational criteria OP_{WF} and that the calm period, τ_c , is longer than the

operation reference period, T_R . The total operational time can be formulated as

$$T_{op} = T_{tot} * P[(H_s \leq OP_{WF}) \cap (\tau_c > T_R)] \quad (5.3)$$

where T_{tot} is the total number of days in the period evaluated, OP_{WF} is the operational limit, τ_c is calm while T_R is the reference period. A weather window is sufficient duration of a calm where the operation can be performed. It is therefore important to evaluate whether the length of the calm period is long enough for the planned operation.

Marine operations can either be temporarily stopped (like drilling or offshore loading) or they are such short duration that they will be started only when it can be guaranteed that acceptable weather conditions will persist until the operation is finished (platform or crane operations). For the planning and design of a marine operation, it may be necessary to halt the operation by reversing the operation and bring the object to a safe condition. Therefore, all points of no return (PNR) shall be documented, which are places in the operation that cannot be reversed. The first safe condition after passing a PNR shall be defined and considered in the planning.

5.5 Weibull Distribution

To account for the uncertainty, a probability distribution is used to show the relationship between the outcome of an event and its frequency of occurrence. The three-parameter Weibull distribution can be used to find the probability distribution with the probability density function (PDF) and a cumulative probability function (CDF) (McCool, 2012). The CDF for a three-parameter version of the Weibull distribution can be found in Equation 5.4 and describes the probability p that X is less than or equal to a given value x .

$$F(x) = 1 - \exp\left[-\left(\frac{x-\gamma}{\eta}\right)^\beta\right]; \quad x > \gamma \quad (5.4)$$

γ is the location parameter, β is the shape and η is the scale that can be defined by a geographical area. The shape value is equal to the slope of the regression line in a probability plot.

The PDF, $f(x)$, is found in Equation 5.5 as the derivative of $F(x)$. The area underneath a PDF is always equal to 1.

$$f(x) = \frac{dF(x)}{dx} = \frac{\beta}{\eta} \left[\frac{x-\gamma}{\eta}\right]^{\beta-1} \exp\left[-\left(\frac{x-\gamma}{\eta}\right)^\beta\right]; \quad x > \gamma \quad (5.5)$$

Chapter 6

Time domain analysis

When dealing with dynamic analysis and stochastic processes, the terms time domain (TD) and frequency domain (FD) are often referred to. The two domains represent alternative ways to describe processes and carry out dynamic analyses (Larsen, 2015). The FD-method is described by a energy spectrum. All non-linearities are eliminated and it is possible to avoid the time dependency from the problem and solve a one-shot problem only dependent on the frequency (Greco, 2018).

If the load type is not harmonic and linearly linked to the wave height, or the principle of linear superposition is not valid, time domain analyses have to be carried out (Larsen, 2015). The TD-method is based on the realisation of the response over time and takes non-linearity effects into account. Forces can then be found from a simple version of Morison's equation. All the dynamic loads are calculated for each time step which is a time consuming, and therefore complex simulation programs are needed in order to achieve adequate results.

Fast Fourier Transform (FFT) is an algorithm that converts the time domain results to a representation in the frequency domain. Based on the FFT, one can evaluate where most of the energy is and consider whether resonance dominates the load.

In this thesis, the simulations are performed in a TD software, but FFT is also used for evaluating the distribution of the energy. The software used for the simulations are SIMO and SIMA which are described later in this chapter. Also, the simulation models with the design of the DPA and suction anchor, the environmental conditions, the hydrodynamic parameters, the lifting equipment and the installation vessel with associated parameters and data are presented.

6.1 Software

In this thesis, SIMO and SIMA developed by SINTEF Ocean are used for time domain analyses of the lifting operation. These systems work together where SIMA is the simulation workbench and SIMO is the analysis engine used for marine operations and floating systems (Reinholdtsen et al., 2018). SIMO is a numerical tool and builds on non-linear time domain analysis which makes it able to deal with advanced structures and operations, and most of the forces that are present in a marine operation can be modelled. SIMO solves the equation of motion to calculate the load and responses with respect to time. In addition, it takes into account the environmental forces as wind, waves and current. The output from SIMO includes time series of forces and motions, statistics and spectral analysis for all forces and motions. Through SIMA one get access to 3D graphics, post-processing, instant model validation, analysis workflow, batch simulation and scripting. Meaning, it supports the entire process of the analysis - from modelling and definition of the simulation and its execution to the results. A more detailed software description can be found in the SIMO User Guide (SINTEF Ocean, 2018).

For this thesis, the body of the anchors are modelled using SIMA and the forces are calculated by SIMO. It is used for both static and dynamic simulations.

6.2 The Simulation Model

6.2.1 Design of The Anchors

In this thesis, a suction anchor and a DPA are compared, and the simulation models are based on the anchors illustrated in Figure 6.2.1. As can be seen from the figure, both of the anchors have a weight of 110 tons. The DPA is massive, while the suction anchor is hollow which will give an increased weight of trapped water. On the top of the suction anchor, a hatch with diameter 1 meter is placed which gives a penetration of 11%. Table 6.1 shows the total mass, volume and entrapped water for the suction anchor and DPA. It is assumed that the entrapped water constitutes the entire internal volume of the suction anchor. This is conservative as some water will flow through the hatch at the top of the anchor (DNV GL, 2011b).

Table 6.1: Total mass, volume and entrapped water for suction anchor and deep penetration anchor

	Suction Anchor	Deep Penetration Anchor
Total mass [t]	110.00	110.00
Total volume [m^3]	12.54	28.95
Entrapped water [t]	421.86	-

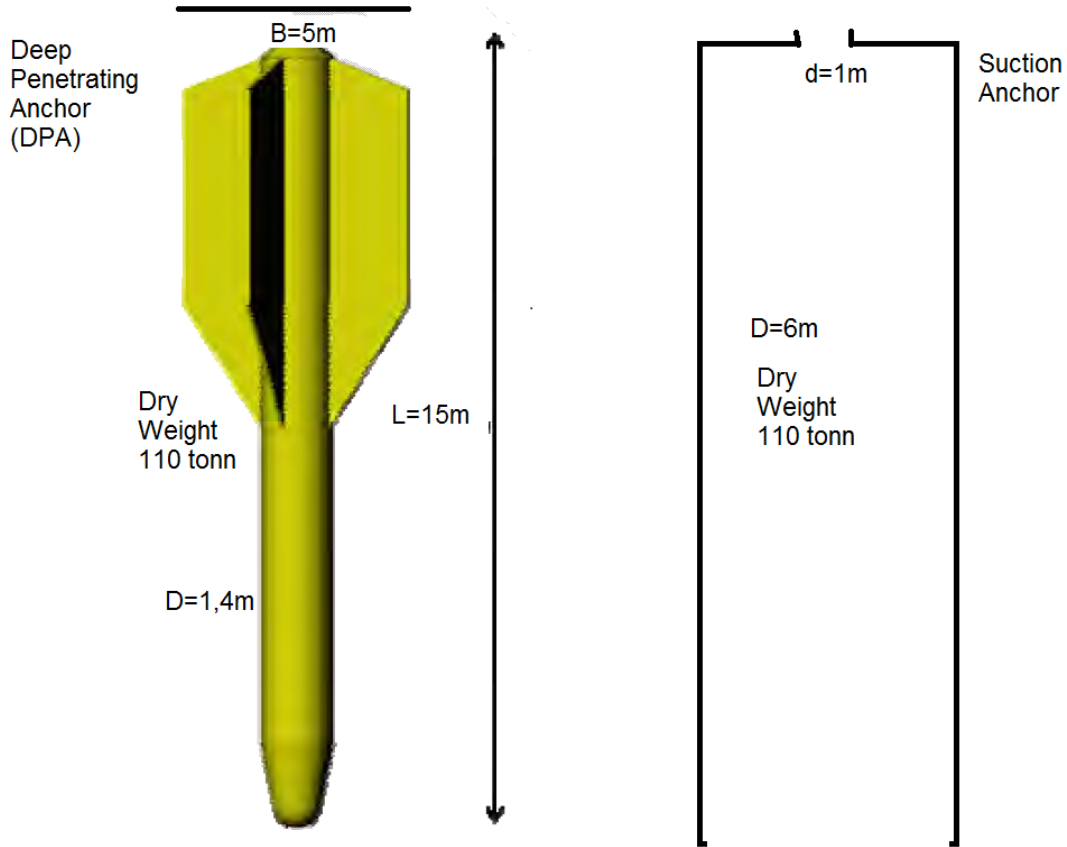


Figure 6.2.1: Main dimensions of the suction anchor and deep penetration anchor used in the simulation

The COG of the suction anchor is assumed to be half of the length of the anchor, 7.5m . In fact, this point will be slightly higher due to the top which will contain valves. For DPA, heavy filling material with a higher density than steel is used to move the COG towards the tip. COG should be placed as close to the tip as possible and is calculated to be 4.29 m .

The COG coordinates with respect to the simulation model's origin are listed in Table 6.2. The initial position of the DPA is higher compared to the suction anchor due to the lift setup.

Table 6.2: Centre of Gravity with respect to origin

Suction Anchor	(x, y, z)	(-24.5, 27.9, 2.3)
DPA	(x, y, z)	(-24.5, 27.9, 5.8)

The anchors are modelled as slender elements in SIMA. The suction anchor consists of one slender element, while for the DPA two elements are used: one for the upper part with the fins, and one for the lower part. This is to compensate for varying weight inside the anchor to keep the centre of gravity low. Table 6.3 shows the length, specific volume and number of stripes for

the slender element of the suction anchor.

Table 6.3: The length, specific volume and number of stripes for the slender element of the suction anchor.

Slender Element	Length (m)	Specific Volume (m^2)	Number of Strips
Suction Anchor	15	0.84	10

The number of stripes tells how many parts the element is divided into. In this case, the anchors are divided into 10 strips. For the DPA, the slender elements are listed in Table 6.4, and both of the slender elements have 5 stripes.

Table 6.4: The length, specific volume and number of stripes for the slender element of the deep penetration anchor.

Slender Element	Length (m)	Specific Volume (m^2)	Number of Strips
Top	7.04	2.37	5
Bottom	7.96	1.54	5
Total	15	3.91	10

The mass of the suction anchor is placed under kinetics together with mass moment of inertia of origin of the anchor. This is found in Table 6.5. The mass moment of inertia for the suction anchor is calculated from Equation 6.1 and 6.2. These formulas are based on thin shells along the z-axis with radius r and length L and mass M . For the vertical direction, the mass moment of inertia is given as

$$I_z = MLr^2 \quad (6.1)$$

and in the horizontal direction as

$$I_x = I_y = \frac{1}{2}MLr^2 + \frac{1}{12}ML^3. \quad (6.2)$$

For DPA, the mass moment of inertia is based on a circular cylinder, and the vertical direction is given in Equation 6.3 and horizontal in Equation 6.4.

$$I_z = \frac{1}{2}MLr^2 \quad (6.3)$$

$$I_x = I_y = \frac{1}{12}ML(3r^2 + L^2) \quad (6.4)$$

Table 6.5: Mass moment of inertia about origin for the suction anchor and deep penetration anchor

	Mass moment of inertia about origin (kgm^2)					
	I_{xx}	I_{yx}	I_{yy}	I_{zx}	I_{zy}	I_{zz}
Suction Anchor	$3.79 \cdot 10^8$	0.00	$3.79 \cdot 10^8$	0.00	0.00	$2.72 \cdot 10^7$
Deep Penetration Anchor	$3.11 \cdot 10^7$	0.00	$3.11 \cdot 10^7$	0.00	0.00	$1.21 \cdot 10^6$

6.2.2 Environmental Conditions

Excitation loads are environmental loads from waves, wind and current. Wind and current loads were neglected in this thesis. The wind would affected the lift when in air, while the current could give the anchors a offset during the lowering phase. This applies most to the suction anchor as it is lowered to the seabed and relocation can increase the planned operational time. For the lifting operation, Metocean Design Basis for the Johan Castberg Field from Dezecot et al. (2016) is used to establish environmental data. It is mainly used to find the significant wave height and the corresponding spectral peak period. The Johan Castberg Field is located (at 72.493° N, 20.334° E) in the Barents Sea with a water depth typically between 370 and 390 meters.

Significant Wave Height and Peak Period

For the H_s measured, three different T_p values are presented, the mean value and a 90% confidence bands as illustrated in Figure 6.2.2. This is done to represent the uncertainty in the estimated data due to limited or noisy data. P5 means that 5% of the registered T_p s are equal or less than this value, and for P95 is 95% of the T_p s qual or less to this value. The simulation is done for different H_s values (between 1 and 6 meters), and Table 6.6 shows the corresponding T_p values used. However, the findings will also be transferable and relevant to other offshore areas. The wave conditions implemented in SIMA is thereby location dependent.

The environment was characterised by a JONSWAP wave spectrum with no swell, wind or current. The short crested waves with spreading exponent of 2 were given for 11 directions. The significant wave height, peak period and seed number were all variables during the simulations. Cosine series were used as a representation of the waves in order to take care of the depth-dependent water particle motion.

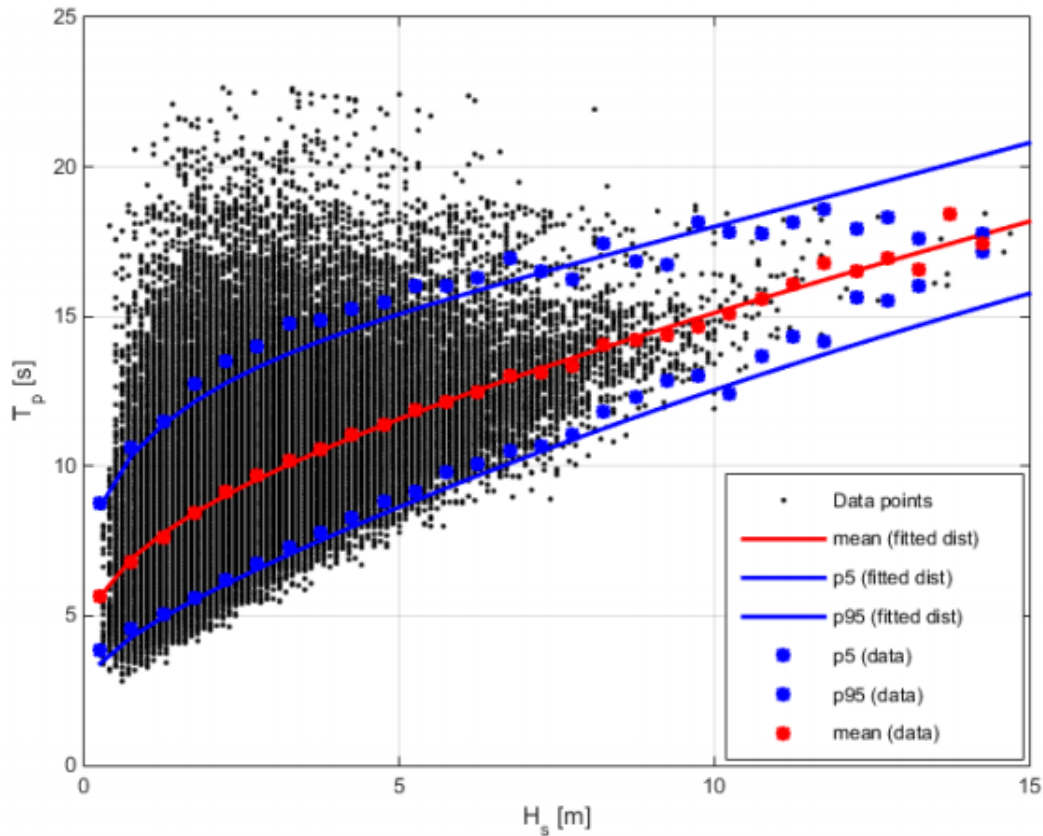


Figure 6.2.2: Spectral peak period for given significant wave height at the Johan Castberg Field, downloaded from Dezecot et al. (2016)

Table 6.6: Significant wave height and spectral peak period used in the simulation

Significant Wave Height, H_s (m)	Spectral Peak Period, T_p (s)		
	P5	Mean	P95
1.0	4.6	7.4	10.9
1.5	5.2	8.1	11.7
2.0	5.8	8.7	12.5
2.5	6.3	9.3	13.0
3.0	6.8	9.8	13.5
4.0	7.7	10.7	14.4
5.0	8.6	11.6	15.1
6.0	9.5	12.4	15.7

Seed Numbers

Further, the correct number of seeds for each weather condition is found. Random irregular waves are not only determined by the significant wave height and peak period but also the regular waves' phase. To account for this, random seeds are introduced. Various seed numbers result in different irregular waves based on the same significant wave height and peak period, within the same wave spectrum. To find an appropriate number of seeds for the different weather conditions, 30 simulations with different seed numbers and constant H_s and T_p are performed and plotted to see if there are large deviations or a trend. This is done with respect to the tension in the lifting wire. This is done by first finding the maxima and minima of simulation one, then the average of the maxima and minima for the two first simulations and so on. Then the most probable maxima and minima load, T_c^{MPM} is plotted.

Head sea waves are used with mean T_p for the suction anchor and P5 T_p for the DPA as a basis, while H_s varies. It is thus assumed that the same number of seeds are needed for the other periods and headings of the waves with the same H_s . For the suction anchor with significant wave height 1 meter and peak period 7.4 seconds, Figure 6.2.3 shows the most probable maxima and minima for an increasing number of seeds.

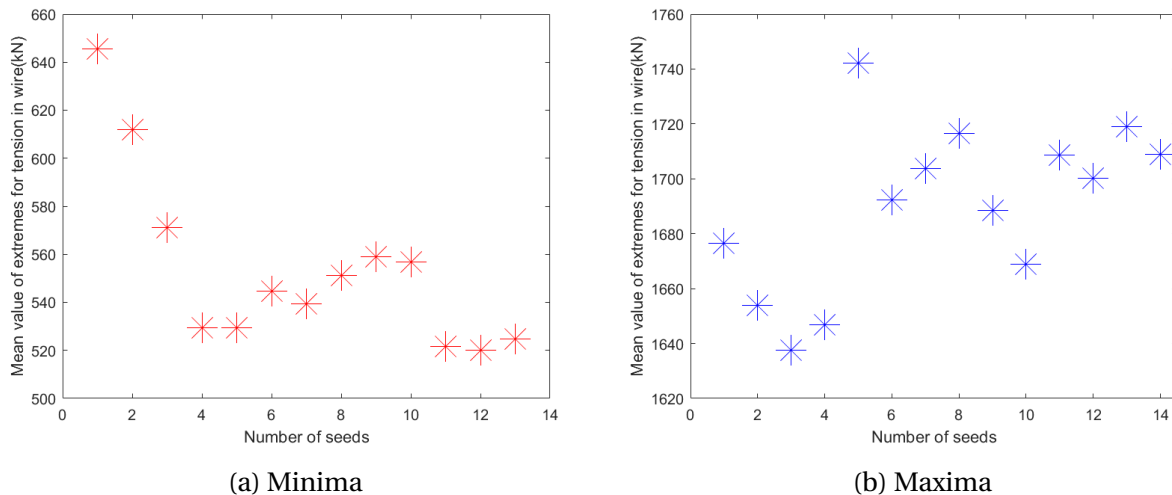


Figure 6.2.3: How the most probable tension varies with number of seeds for the suction anchor at H_s 1 m and T_p 7.4 s

It might look like large spreads but comparing it to the simulation for H_s 2 m and T_p 8.7 s, the spread is smaller. Figure 6.2.4a and 6.2.4b shows the most probable maxima for these cases with the same values along the y-axis. One can clearly see that it forms a pattern in both cases, but later for the case with H_s 2 m due to a high peak in the start. Based on this, it is concluded to use five seeds for the simulation with H_s 1 meter and ten for H_s 2 meters.

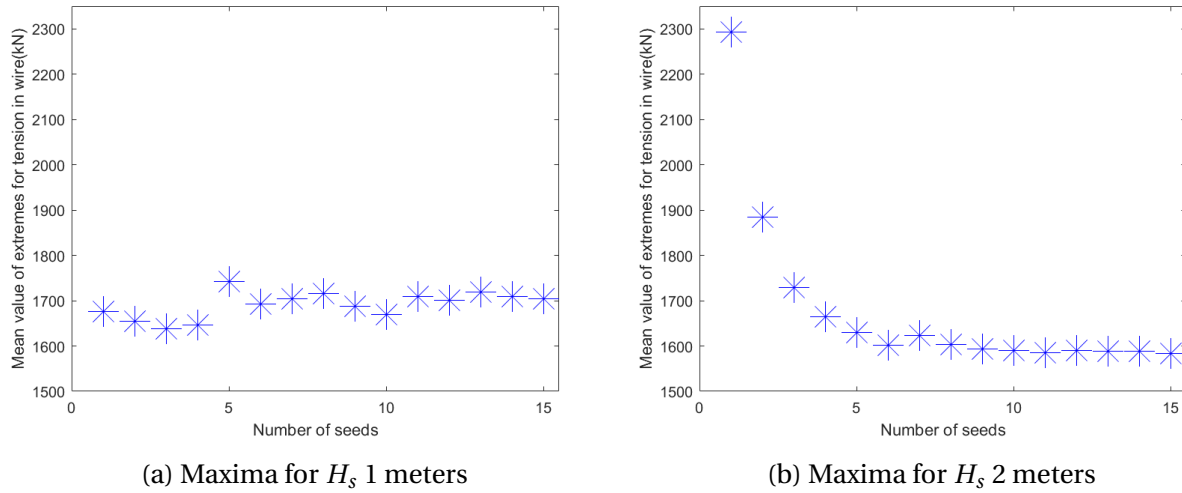


Figure 6.2.4: Comparison of the most probable maxima for H_s 1 and 2 meters for the suction anchor

Figure 6.2.5 presents the most probable maxima and minima for the deep penetration anchor for H_s 6 m and T_p 9.5 s. Even though the weather is high the variations along the y-axis is minimal. For this H_s , it is decided to use seven seeds.

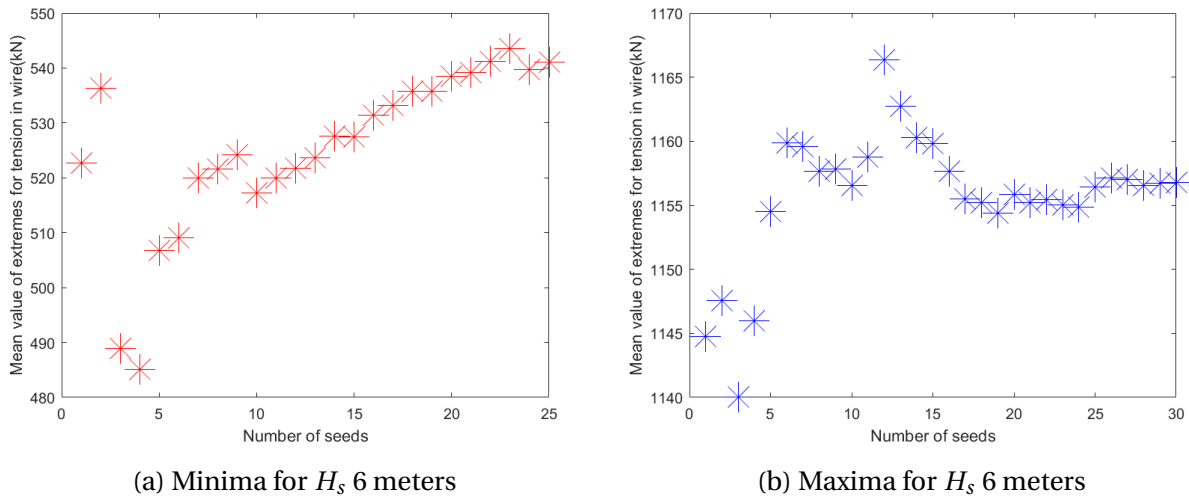


Figure 6.2.5: Maxima and minima for deep penetration anchor for H_s 6 m and T_p 9.5 s

Based on the simulations with varying maxima and minima tension and due to computational available power, the number of seeds are decided. Table 6.7 and 6.8 presents the number of seeds used for the different weather conditions during the simulation. An increased number of seeds could maybe give different simulations results as the results will be more reasonable.

Condition	Seeds
$H_s = 1.0$ m	5
$H_s = 1.5$ m	5
$H_s = 2.0$ m	10
$H_s = 2.5$ m	9
$H_s = 3.0$ m	9
$H_s = 4.0$ m	9

Table 6.7: Number of seeds suction anchor

Condition	Seeds
$H_s = 3.0$ m	7
$H_s = 4.0$ m	5
$H_s = 5.0$ m	10
$H_s = 6.0$ m	7

Table 6.8: Number of seeds for DPA

6.2.3 Establishment of Hydrodynamic Coefficients

The added mass and drag coefficients for DPA and suction anchor is described in this section.

Added Mass

For the suction anchor, the added mass is found from the paper presented in Section 4.6.1 by Nielsen (2012). An estimate of the added mass based on (DNV GL, 2011b) had a higher value and thus agreed with the paper. The added mass in the three directions for a fully submerged suction anchor is given in Table 6.9. The entrapped water is included in the vertical direction. Based on this, one can see that the added mass for the suction anchor is large compared to the structural mass.

Table 6.9: Calculated added mass values for suction anchor

Added Mass direction	Value
A_{11}	856.58 t
A_{22}	856.58 t
A_{33}	619.30 t

For an object in the splash zone in irregular waves, the following expression is implemented for the water entry phase (Næss et al., 2014):

$$(M + A_{33})\ddot{\eta} = B_{33}^{(1)}(v_3 - \dot{\eta}) + B_{33}^{(2)}(v_3 - \dot{\eta})|v_3 - \dot{\eta}| + (\rho V + A_{33}\dot{v}_3) + \frac{dA_{33}^{\infty}}{dh}(\dot{\zeta} - \dot{\eta}) + \rho g V(t) - Mg + F_{line}(t) \quad (6.5)$$

As can be seen from Equation 6.5, the slamming force is dependent upon the change in added mass with the depth and the relative velocity between the object and the water surface (Næss et al., 2014). Consequently, how added mass varies with the water depth is a critical factor when modelling the slamming force in SIMO. The added mass for a suction anchor is distributed with depth using depth-dependent coefficients, and Figure 6.2.6 shows the depth dependency

implemented on the added mass for the suction anchor. The depth dependent coefficients are applied to the total added mass included entrapped water.

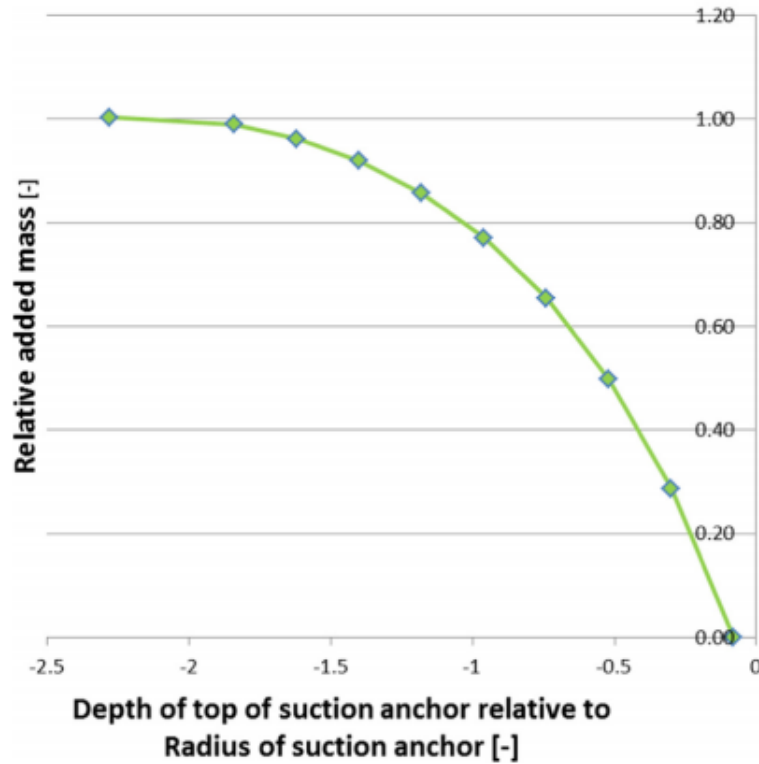


Figure 6.2.6: Depth dependency of added mass for suction anchors (Næss et al., 2014)

This is used for the added mass in the vertical direction which is zero until the top of the anchor is under water. From here it starts to increase until a water depth of about 7 m where the added mass reaches its maximum value. The vertical added mass is laid in a plane at the top of the anchor modelled as fixed body elements in SIMA. The horizontal added mass is laid into the slender element and will increase linearly as the anchor reaches the water surface.

For the DPA, Appendix B.1 with added mass calculation from DNV GL is used as a basis to find the added mass. The total calculated value for added mass on the DPA can be found in Table 6.10. For the DPA, there is not added any water depth independent coefficients in SIMA.

Table 6.10: Total added mass for the deep penetration anchor for the different directions.

Added Mass direction	Value
A_{11}	85.23 t
A_{22}	85.23 t
A_{33}	3.20 t

Drag Force

The quadratic drag for both the suction anchor and DPA is estimated using the guidelines in DNV GL, found in Appendix B.2. The total quadratic drag force can be found in Table 6.11.

Table 6.11: Quadratic drag for fully submerged suction anchor and deep penetration anchor

	Quadratic Drag direction	Value ($\frac{Ns^2}{m^2}$)
Suction Anchor	C_{21}	11012.85
	C_{22}	23985.00
	C_{23}	23985.00
Deep Penetration Anchor	C_{21}	414.47
	C_{22}	15200.27
	C_{23}	15200.27

The DPA is divided into two parts in SIMA, the upper part consisting of rectangular plates and the lower section a cylindrical part. The linear drag is neglected for both the suction and DPA.

6.2.4 Installation Vessel

The vessel used in the simulation model is Skandi Acergy which is a typical crane vessel and is illustrated in Figure 6.2.7 from SIMA. The vessel have a length of 138 meters, a breadth of 27 meters and a draught of 6 meter as can be seen in Table 6.12. A typical crane vessel does usually have a Dynamic Positioning (DP) system that uses its own propellers and thrusters to maintain the vessels position and heading during installation. To recreate a DP system that is independent of mooring and anchors into a simulation model is challenging. The vessel in the simulation model is kept in position by use of a horizontal mooring system that consists of four mooring lines with stiffness and damping equivalent to the ones that would have arisen due to a DP system (Solaas et al., 2017).



Figure 6.2.7: Vessel used in the simulation model

Table 6.12: Main dimensions of the installation vessel Scandi Acergy

Parameters	Values
Length (L_{pp})	138 m
Breadth	27 m
Draught	6 m

The installation vessel's given mass properties are as listed in Table 6.13 where the mass moments of inertia are defined about the origin.

Table 6.13: Structural mass of installation vessel

Parameters	Values	Units
Mass	$1.69 \cdot 10^7$	<i>kg</i>
I_{xx}	$1.93 \cdot 10^9$	<i>kgm²</i>
I_{yx}	0	<i>kgm²</i>
I_{yy}	$2.35 \cdot 10^{10}$	<i>kgm²</i>
I_{zx}	$8.78 \cdot 10^6$	<i>kgm²</i>
I_{zy}	0	<i>kgm²</i>
I_{zz}	$2.31 \cdot 10^{10}$	<i>kgm²</i>

The COG of the vessel is located at (0.12, 0.00, 4.25), and the crane tip at (-24.50, 27.90, 32.60). The relative distance between the crane tip and the vessel is then (-24.62, 27.90, 28.35). The origin in the simulation model is the intersection between the water plane and the vessel for $y = 0$. The origin, the vessels COG and the crane tip are illustrated in Figure 6.2.8.

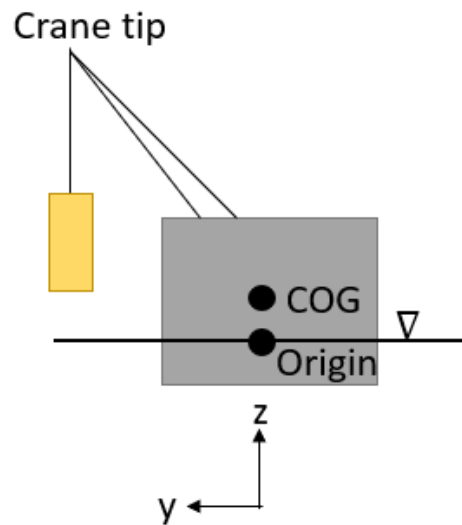


Figure 6.2.8: Illustration of the simulation model's origin, vessel's Centre of Gravity marked with COG and the location of the crane tip (the vessel is seen from the aft)

RAO for Installation Vessel

The RAO of the vessel is dependent on the direction of the waves and the vessel motion is defined in six degrees of freedom. The first order motion transfer functions for the vessel is presented in this section. The RAOs between 0° and 180° are equal to the RAOs between 180° and 360° due to symmetry about the x-axis. The wave direction and vessel motions defined in the simulation model is illustrated in Figure 6.2.9. Waves propagating 90° to the vessel is called beam sea, whereas incoming waves from 0° and 180° to the vessel is called following sea and head sea respectively.

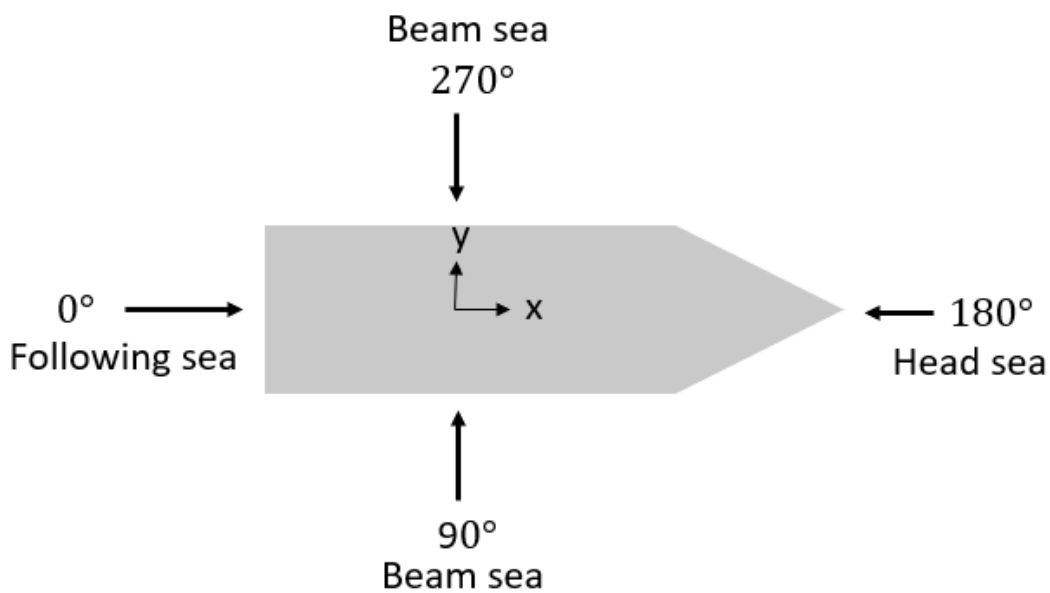


Figure 6.2.9: Given wave directions (vessel seen from above)

A motion decay test, or sometimes called a free oscillation test, is carried out by giving the system an initial displacement and then leaving the system free to oscillate. From this, the damping level and the natural periods of the system can be evaluated. In this case, it is done for verification of the model.

RAO in surge

Figure 6.2.10 shows the RAOs for the vessel surge motion for following sea, (0°), beam sea (90°) and head sea (180°). From the Figure, one can see that the beam sea has limited impact on the surge motion for the vessel. Though, head sea and following sea can have a small impact. Waves with a peak period around 7 seconds will give the vessel a surge amplitude of 0.1 meters per meter wave height (m/m), which is a negligible motion. The crane tip motion in the longitudinal direction will be dependent on the vessel's surge, pitch and yaw motion. Small surge motions will not be of huge risk during the lifting operation because the lifted object will move along the vessel side.

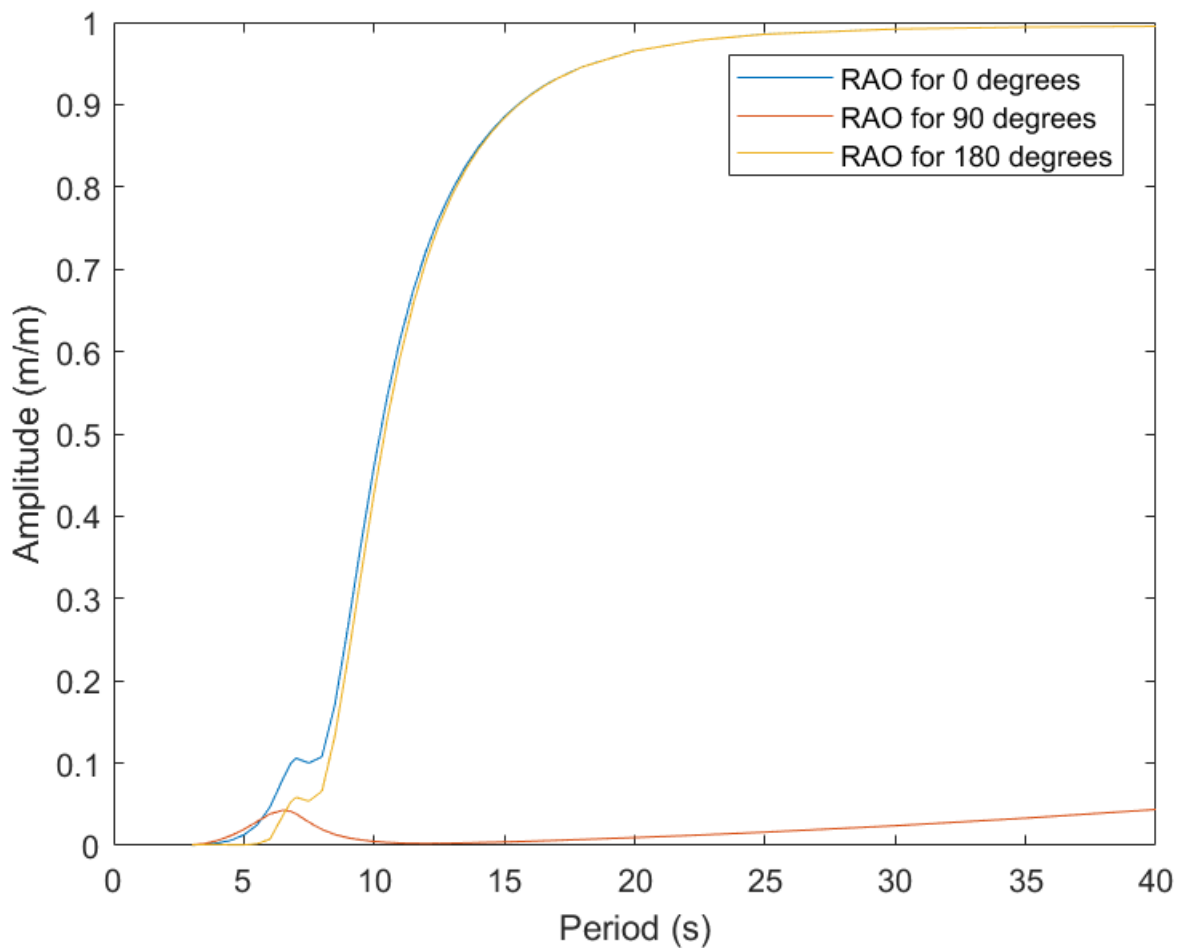


Figure 6.2.10: RAOs for surge motion

RAO in sway

The RAOs for the vessel in sway motion are shown in Figure 6.2.11 for 0, 90 and 158 degrees. Beam sea with a peak period of 15 seconds will result in a sway amplitude of approximately 1.5 m/m before it converges towards 1 m/m for peak periods around 19 seconds. A top appears for the peak period around 15 seconds and illustrates the vessels' natural period. Resonance will arise in sway for this peak period. The RAO for 158° has about the same shape, however, peak amplitude converges towards 0.4 m/m . Following sea and head sea will not have any significant impact on the vessel's sway motion. The sway, roll and yaw motion of the vessel will be important for the translational direction of the crane tip, and since the lifted object will move along the y-axis, sway motion can be a risk during the lifting operation which can lead to a collision between the object and the vessel.

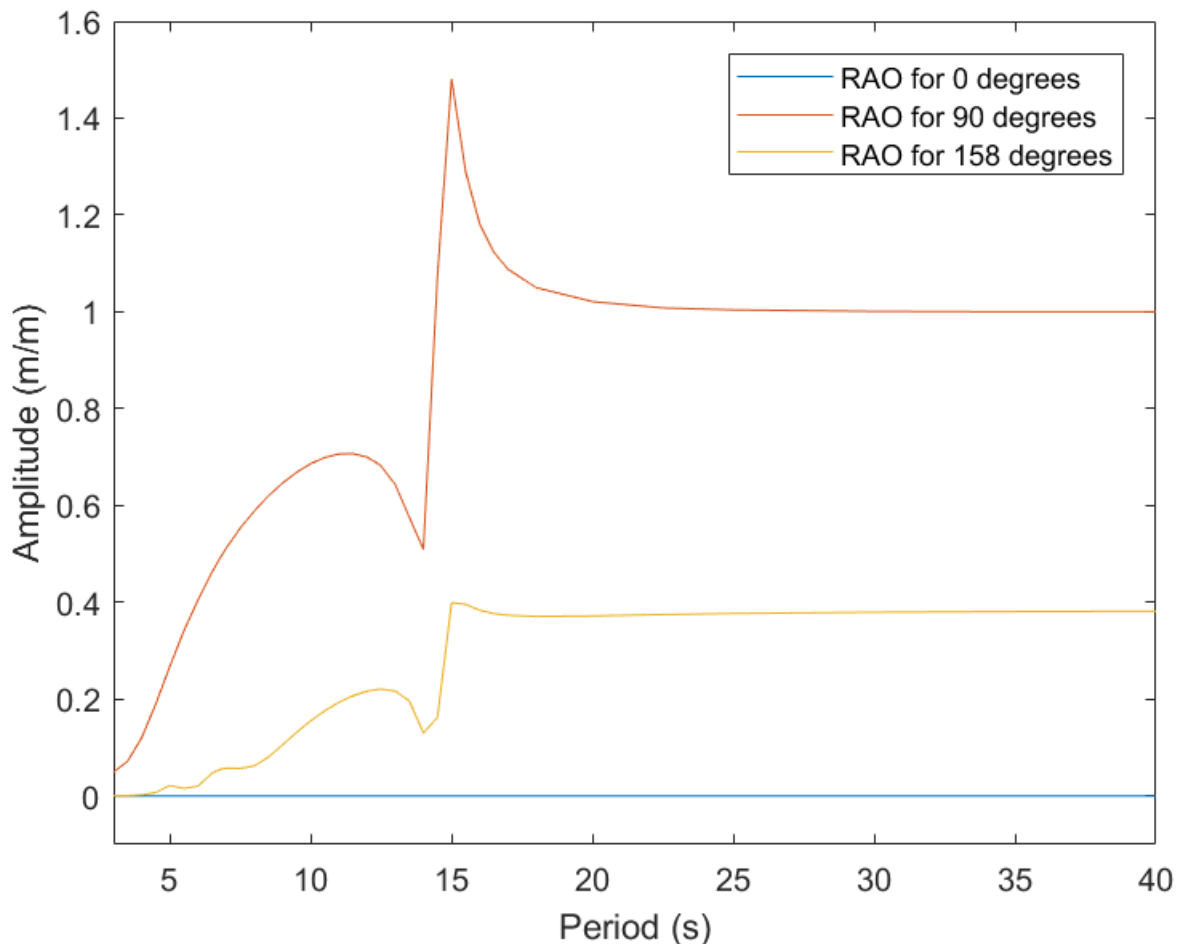


Figure 6.2.11: RAOs for sway motion

RAO in heave

RAOs for the vessel's heave motion is shown in Figure 6.2.12. For beam sea, a T_p of around 8 seconds constitutes a heave amplitude of 1.2 m/m and will go towards 1 m/m for 13 seconds. For waves propagating with a heading of 68° , the RAO will converge towards 1 m/m around 12 seconds. For the vertical crane tip motion, the vessel's heave, roll and pitch are crucial. Heave motions can be a danger during a lifting operation due to sudden submergence of the lifted object, large slamming forces in the splash zone and possible slack in lifting lines that may result in large snap forces.

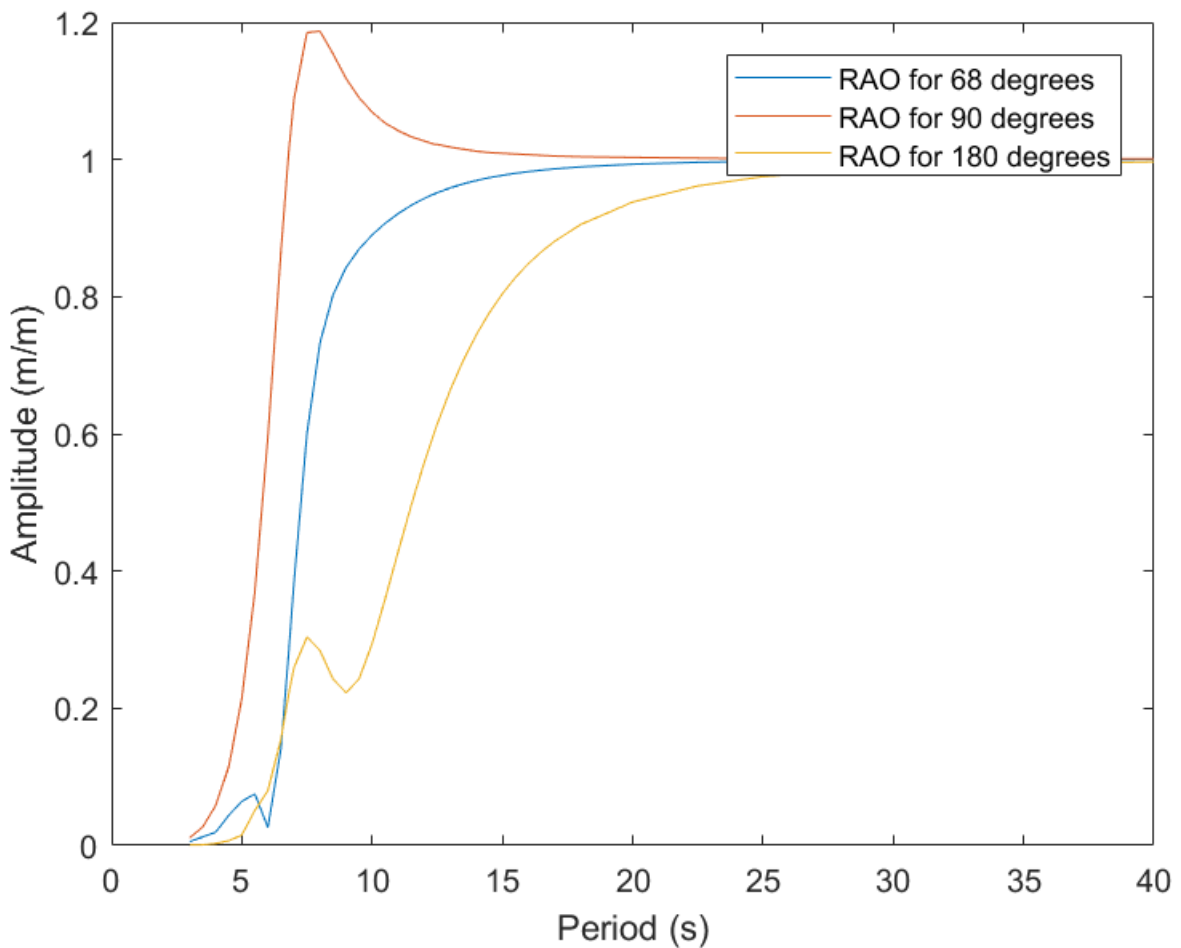


Figure 6.2.12: RAOs for heave motion

A decay test is performed by applying a large specified force in the COG of the vessel, and then releasing it. Here the initial displacement is set as 100 m, and the structure is released without any external environmental effects. Only the effect of linear damping drives the structure to do the pendulum action and stop at the original point gradually. From the decay test presented

in Figure 6.2.13, one can see that the natural period in heave is 7.4 s This corresponds to the RAO.

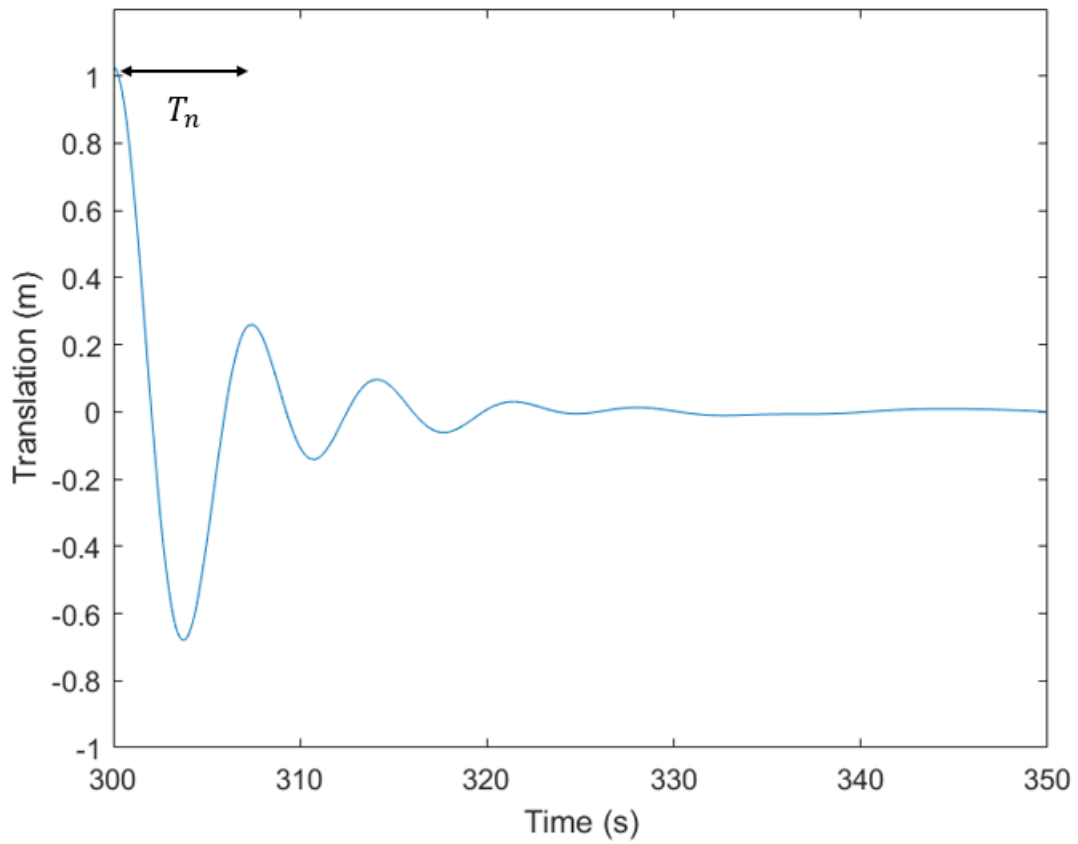


Figure 6.2.13: Decay test in heave, the natural period is shown

RAO in roll

Figure 6.2.14 presents the RAOs for the roll motion for the vessel. Here, the beam sea will have a considerable impact on the vessels motion for the peak period of 14.5 seconds where the roll amplitude is approximately 12 degrees per meter wave height (deg/m). The RAO for waves 158° to the vessel have also a similar curvature, however, with a smaller maximum roll amplitude laying around $5deg/m$ for a T_p of 14.5 seconds. Large roll motions will result in sway and heave motions for the crane tip and hence for the lifted object. This is not desirable and should, therefore, be avoided. The roll motions affect the translational and vertical motion of an object.

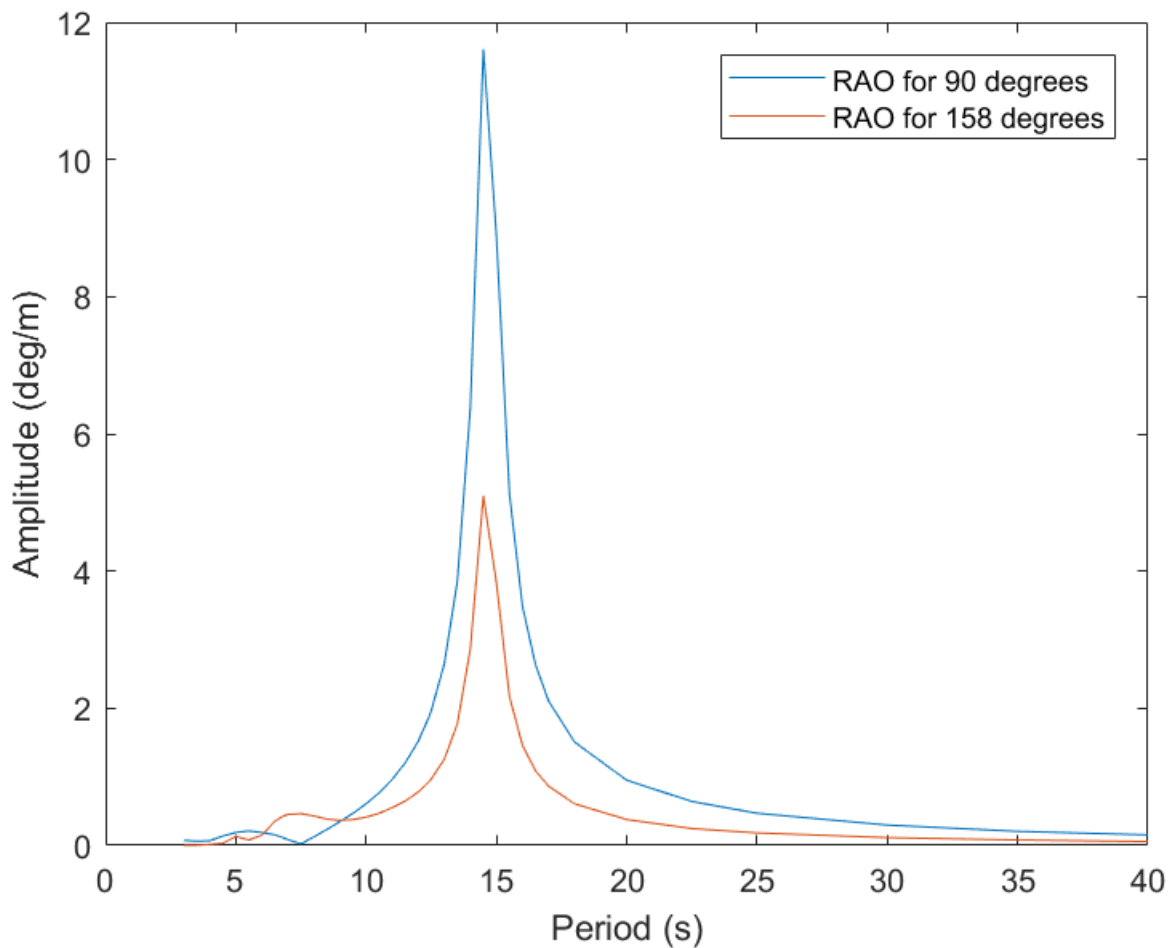


Figure 6.2.14: RAOs for roll motion

Figure 6.2.15 shows the decay test in roll with the natural period 14.7 s, which confirms the RAO. Hence, resonance in roll is likely to happen for this wave period.

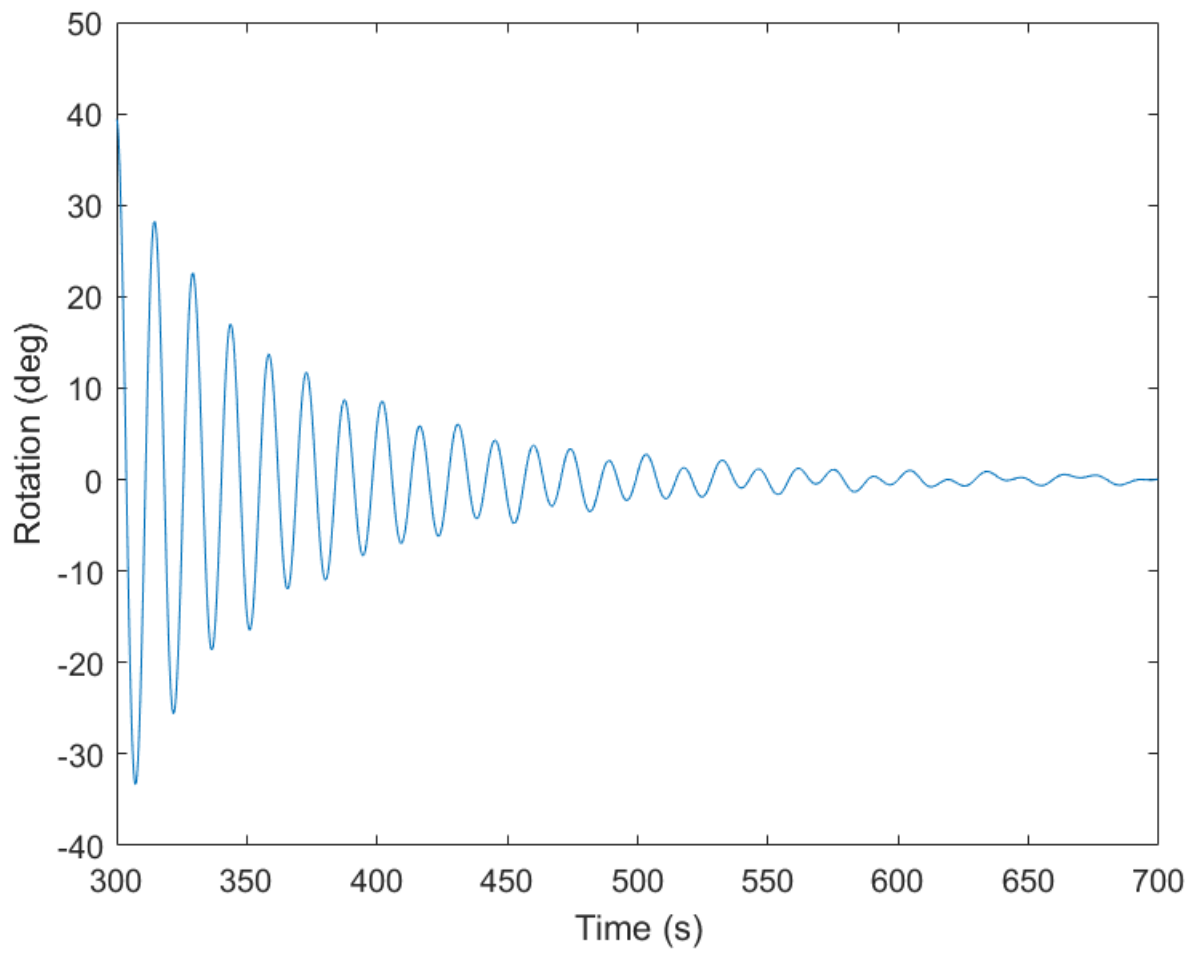


Figure 6.2.15: Decay test in roll

RAO in pitch

From Figure 6.2.16, the RAOs for the pitch motion of the vessel is given. For incoming waves 68° to the vessel with T_p of about 7 seconds, the resulting pitch amplitude will be of 1.4 deg/m . In similar manner has the wave with a heading of 135° a similar curvature as the aforementioned ones but with a pitch amplitude of 1.3 deg/m for peak periods of 9 s. Beam sea will, on the other hand, have an insignificant impact on the pitch motion. Large pitch motions will result in surge and heave motions of the crane tip which are further transferred to the lifted object. As mentioned above, small surge motions do not have a large impact on the lift, but heave motions can be critical and should be prevented. Comparing to the RAO for the heave motion, one can see that they have the same period for the peak. The natural period is 6.5 seconds. This is found from the decay test illustrated in Figure 6.2.17

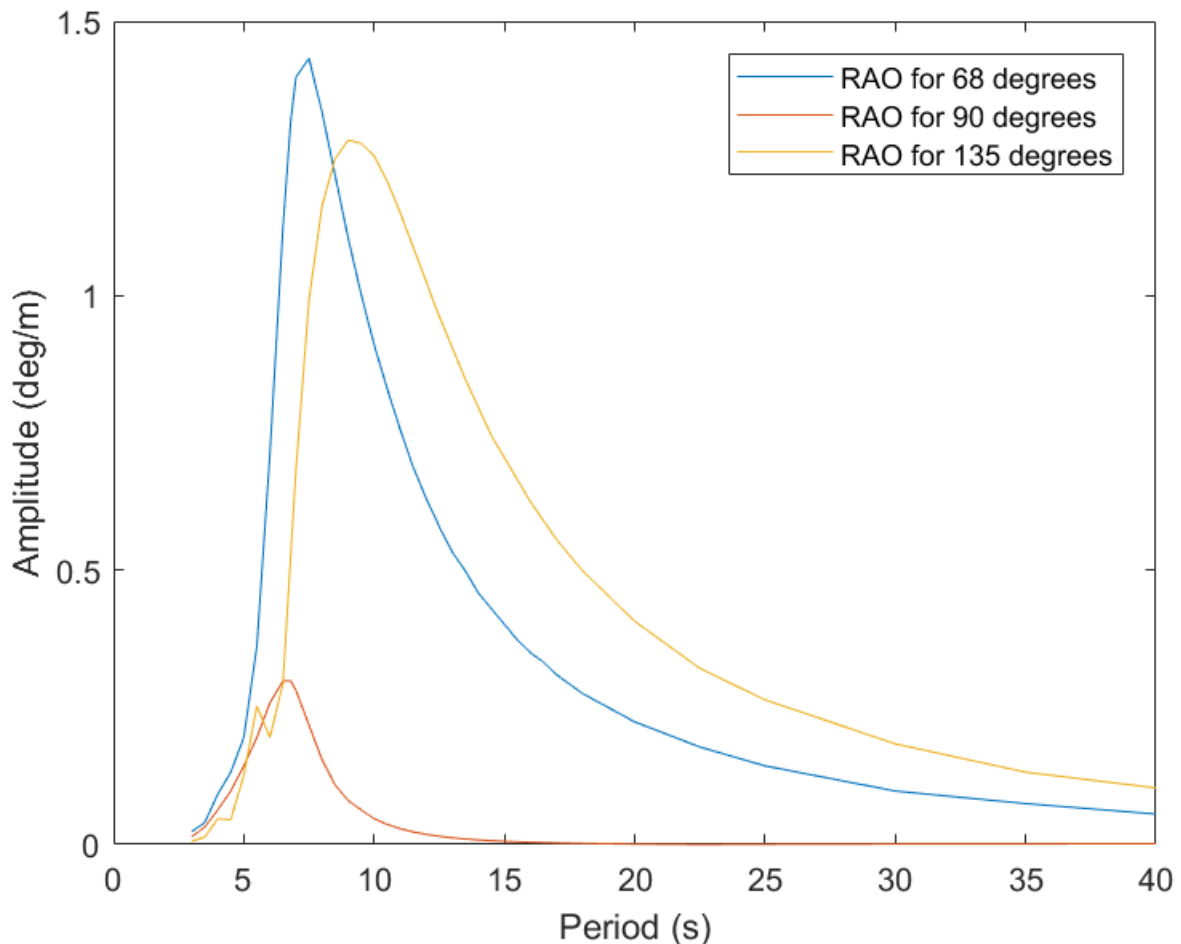


Figure 6.2.16: RAOs for pitch motion

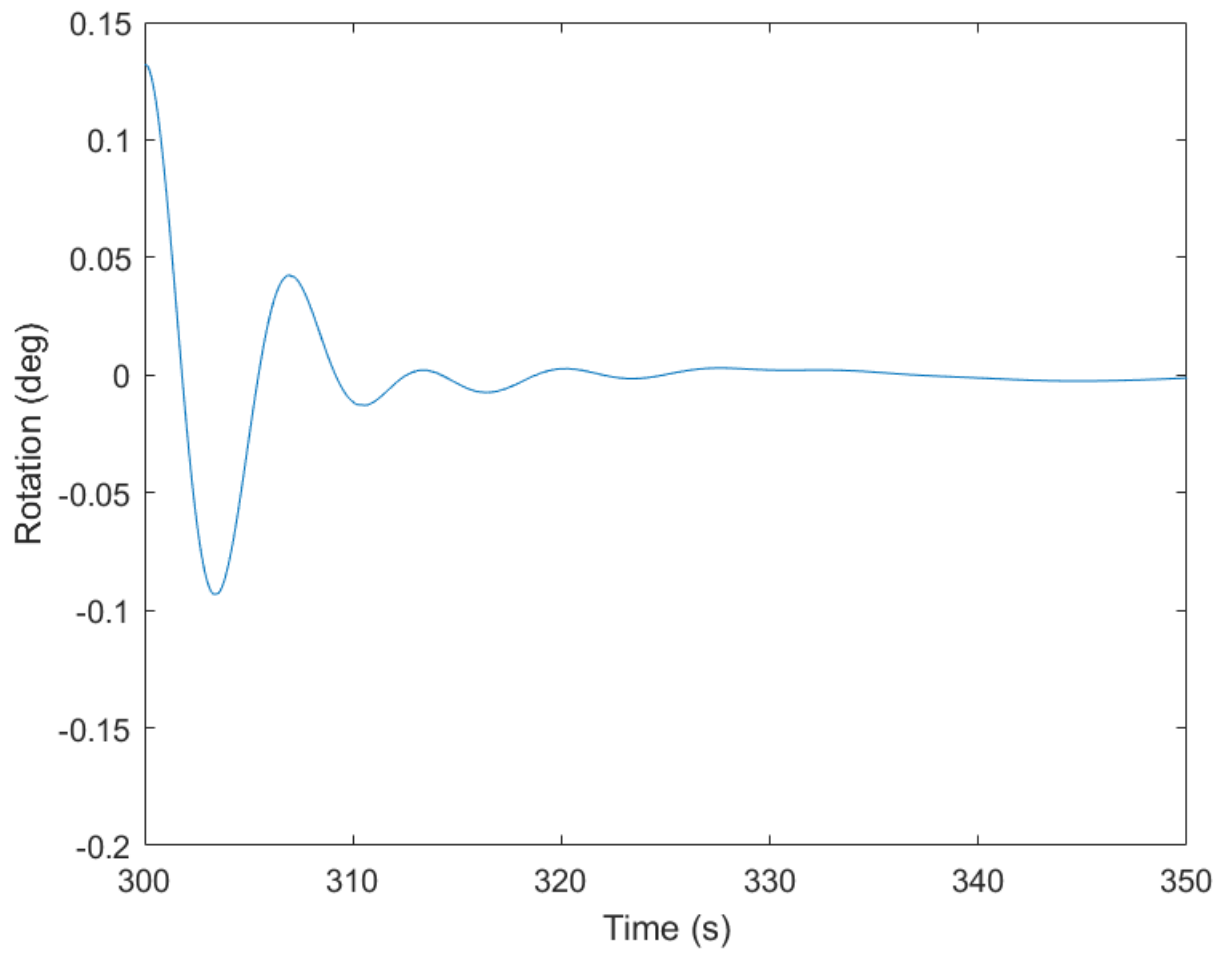


Figure 6.2.17: Decay test in pitch

RAO in yaw

RAOs for the vessels yaw motion is shown in Figure 6.2.18. Incoming waves with a heading of 113° result in an RAO with two peaks with a yaw amplitude of approximately 0.5 deg/m for periods of 8 s and 14.5 s. Incoming waves 135° to the vessel will have a similar curvature as the aforementioned one but with peaks around 9.5 s and 15 s. For incoming waves with heading 90° the yaw amplitude is much lower but has still similar curvature. The crane tip and the lifted object will have surge and sway motions during large yaw motions. Small surge motions do not have a huge impact on the operation, while large yaw motions should be avoided in order to prevent a potential collision between the lifted object and the vessel.

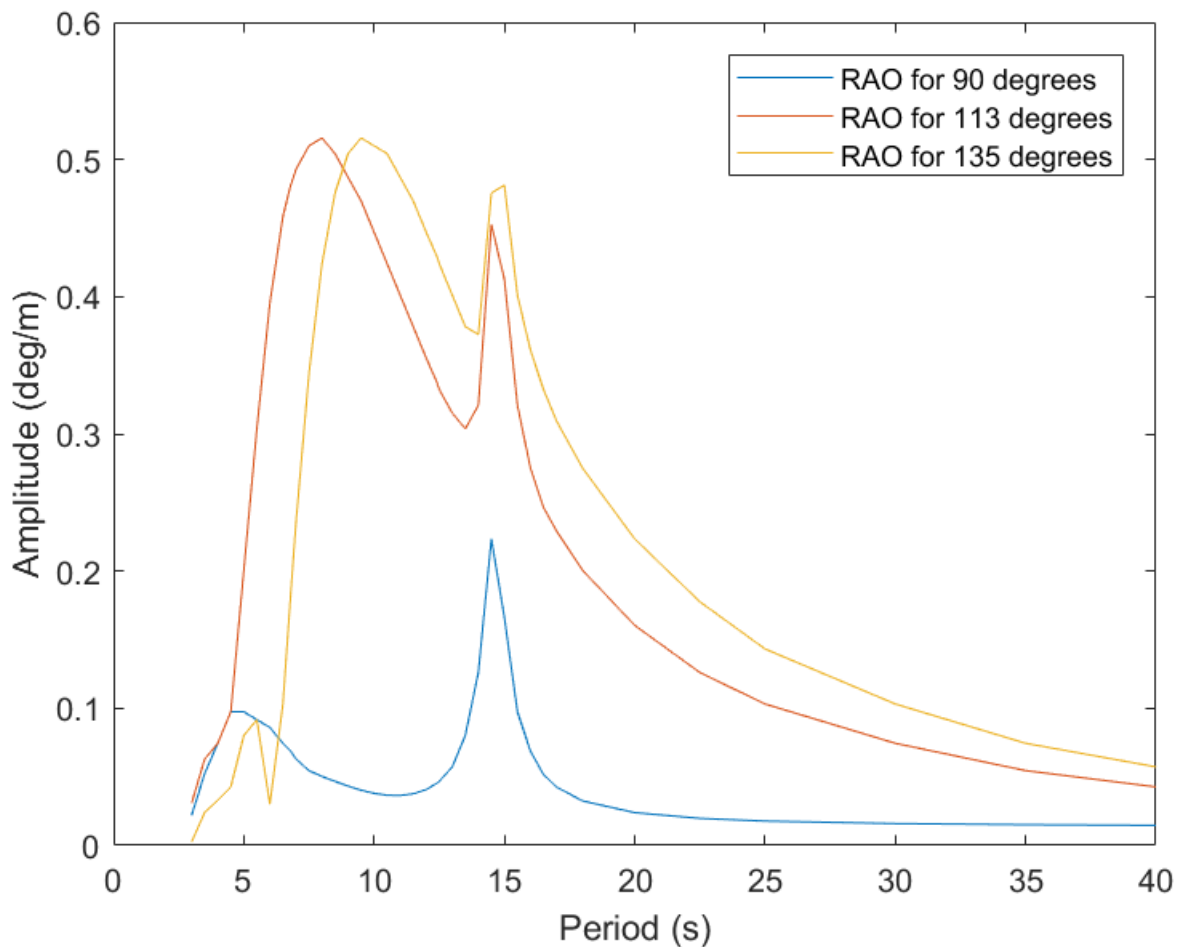


Figure 6.2.18: RAOs for yaw motion

6.2.5 Lifting Equipment

The set up of the lifting equipment is different for the suction anchor and the DPA. The set up for the DPA consist of a lifting wire connected to the centre of the top of the anchor, see Figure 6.2.19. For the suction anchor, the lifting wire is connected to a hook which is attached to three slings linked to the top of the anchor, see Figure 6.2.19.

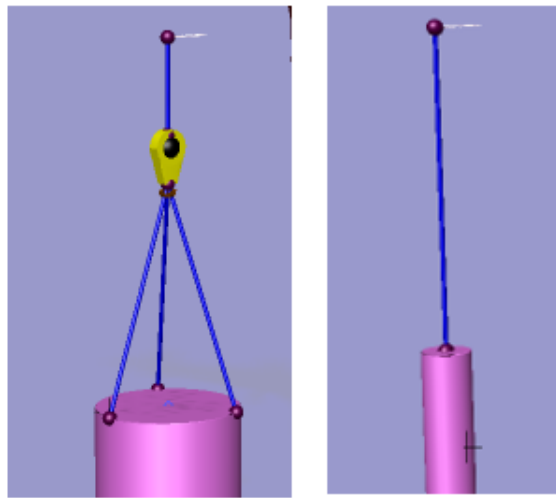


Figure 6.2.19: The crane set up from crane tip to anchor. To the left: the set up with hook and three slings for the suction anchor. The DPA on the right connected directly to lifting wire.

The global coordinates for the crane tip are $(-25.5, 27.9, 32.6)$. The crane wire is connected to the crane tip and either to the hook top or directly to the DPA. The material properties of the wire and slings are assumed to have the same properties and are found from BRIDON (2013). The Diamond Blue rope has been used and the complete guidance can be found in Appendix A.1. Table 6.14 displays the properties used in the simulation. The damping is assumed to be 1% of the cross-section axial stiffness.

Table 6.14: Properties of the crane wire and the slings

Property	Value	Unit
Diameter	0.8	m
Cross area	3167	mm^2
Cross-Section Axial Stiffness EA	$3.33 \cdot 10^5$	kN
Material Damping	$3.33 \cdot 10^5$	kNs
Breaking strength	$5.28 \cdot 10^3$	kN

The hook has a mass of 12 tons and has two local connection points; the hook top located at $(0.0, 0.0, 0.5)$ and the hook bottom located at $(0.0, 0.0, -1.5)$. This gives a vertical length of 2.0

m for the hook. The hook is given mass properties as listed in Table 6.15. The mass moments of inertia are defined about the origin and there is no linear damping nor any hydrostatic stiffness data implemented in the simulation model.

Table 6.15: Structural mass of the hook

Parameter	Value	Units
Mass	12 000	kg
I_{xx}	48 000	kgm^2
I_{yy}	48 000	kgm^2
I_{zz}	24 000	kgm^2

Further, the hook bottom is connected to three slings for the suction anchor. The slings have a length of 9.77 m. The location of the couplings between the suction anchor and the slings is shown in Table 6.16.

Table 6.16: Body points on suction anchor to connect anchor with slings

Name	(x, y, z)
Point_1	(-3.0, 0.0, 15.0)
Point_2	(1.5, 2.6, 15.0)
Point_3	(1.5, -2.6, 15.0)

A crane winch is modelled in the crane tip and gives values for the lifting speed and acceleration. The lifting speed is set to 0.2 m/s and the acceleration 0.1 m/s^2 . The total lifting system set up for the simulation of the suction anchor is illustrated in Figure 6.2.20, and as seen from Figure 6.2.21, the angle between the sling and the suction anchor is 72° .

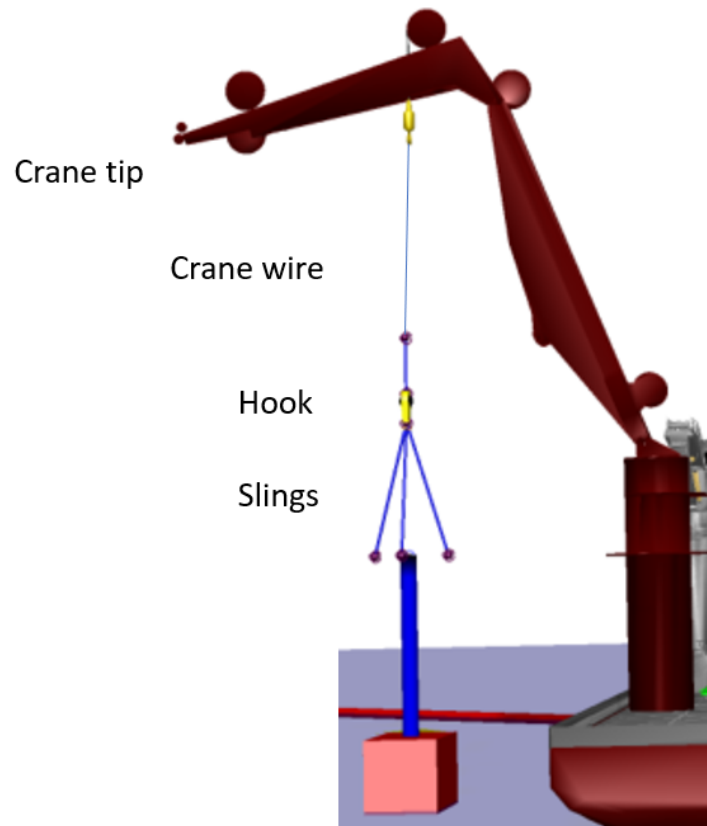


Figure 6.2.20: The crane set up for the suction anchor with crane tip, crane wire, hook and three slings.

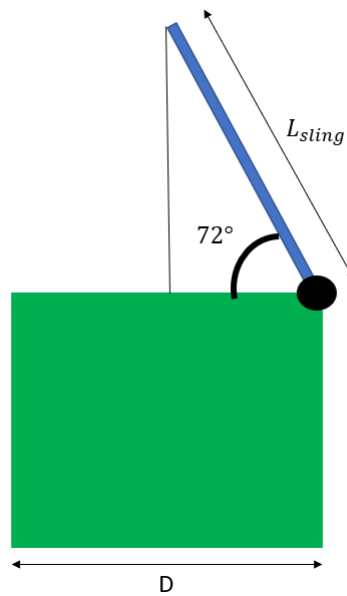


Figure 6.2.21: The angle between sling and suction anchor

Resistance and Capacity Checks

Further, one has to do overload checks for crane and hoisting line and rigging capacity for slings. In addition, the hoisting line slack check to avoid snap forces is to be done. Based on this, an upper and lower limit can be established for the tension in the wire during the simulation. The crane installed on Skandi Acergy has a safe working load (SWL) of 250 tons, which is the static capacity. Both the anchors have a weight lower than this. The global dynamic load effects may be accounted for by using a dynamic amplification factor (DAF). The dynamic capacity can be multiplied with a safety factor of 1.25 dependent on the offshore environment and the weight (DNV GL, 2014). This gives a maximum dynamic load of 313 tons.

Since the slings have the same EA as the wire, they will not be the weak link in the lifting system. Therefore, the capacity of the wire is important to find and consider. MBL is given as the breaking strength in Table 6.14. With the nominal safety factor set to 3, the criterion will be $F_{wire} < 1760 kN$, and the dynamic wire load shall never exceed 1760 kN. This is below the maximum dynamic load for the crane.

The requirement to avoid slack in the line will constitute the lower limit. For the suction anchor the, limit will be 107 kN and 49 kN for the DPA. They will have have different limit since the submerged weight is unlike due to the water filling and different buoyancy force.

Natural Period of The Hoisting Wire

The stiffness of the systems for the DPA and suction anchor is illustrated in Figure 6.2.22. To the right is the DPA with the lifting wire as the stiffer in the system. To the left is the suction anchor consisting of the wire and three slings that will contribute to the total stiffness. The natural period of the wire depends on the line length. The added mass for the suction anchor includes the water filling weight. The stiffness of the wire is found by dividing the wire cross-section axial stiffness with the length of wire released, from the crane tip to the anchor. For the suction anchor, the stiffness from the slings has to be added. The length of the slings is, however, constant, and the total stiffness for the suction anchor is found from

$$\frac{1}{K_{tot}} = \left(\frac{L_{wire}}{EA} + \frac{L_{sling}}{3EA} \right)$$

Figure 6.2.23a illustrates how the natural period changes with the length of the hoisting line for the suction anchor. The resonance period will lay between 1.8 s and 5.4 s for a water depth of 300m. For DPA, the natural period increases from 0.6 to 2.2 seconds for the same water depth, see Figure 6.2.23b.

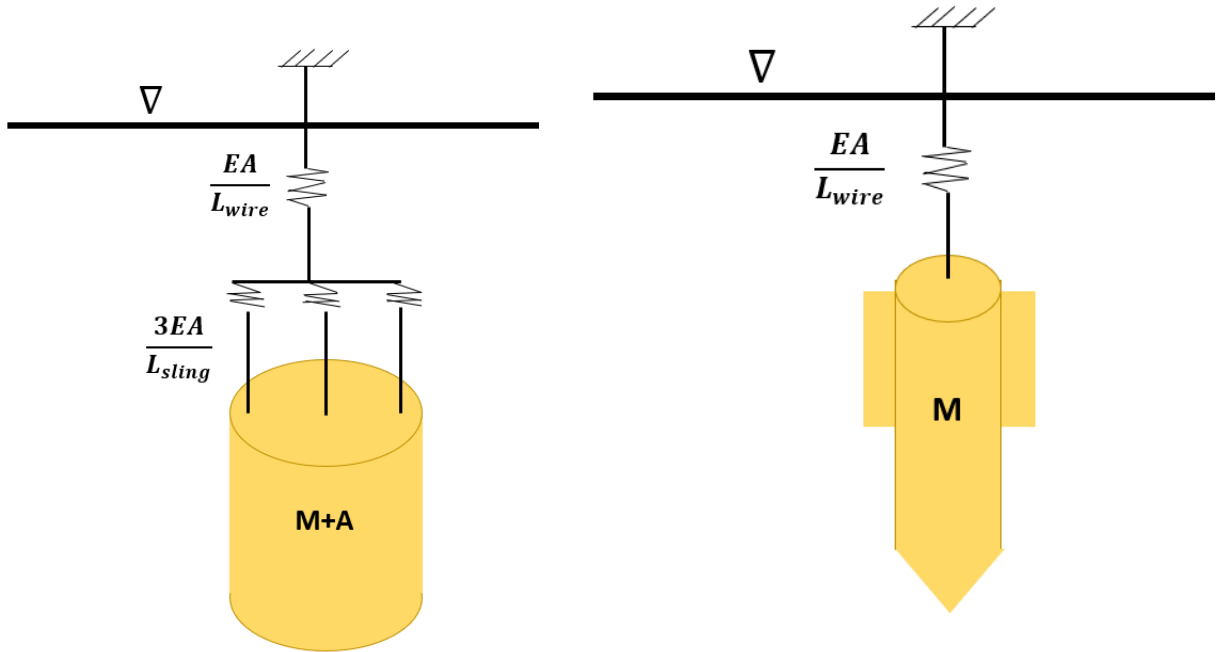


Figure 6.2.22: The stiffness in the lifting systems. To the left is the suction anchor and DPA to the right

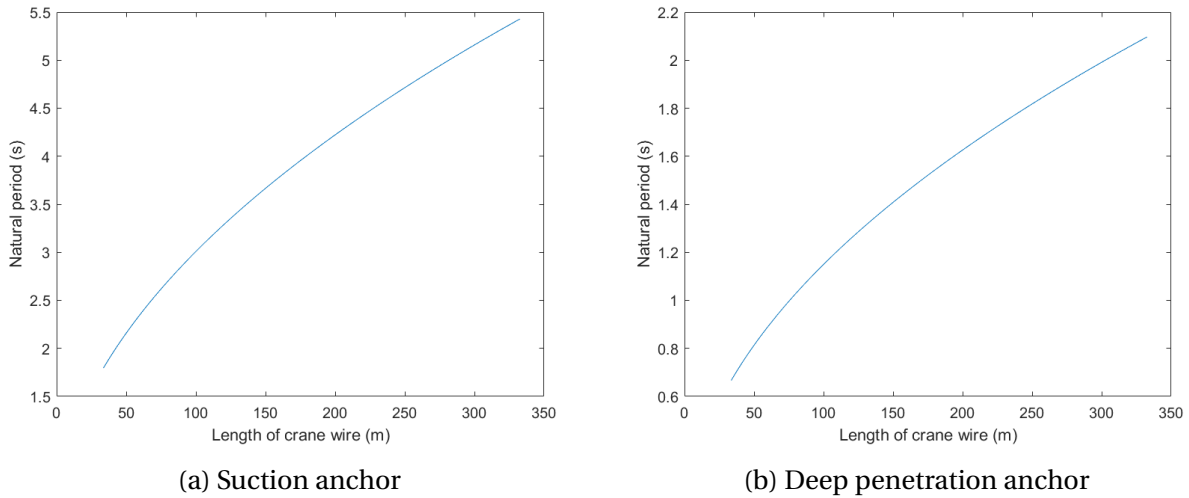


Figure 6.2.23: Resonance period of hoisting cable with varying length

Resonance can occur if the wave period and vertical crane tip period is close to the natural period of the wire. The natural period is low, and for the DPA this is not of a big concern, however, for the suction anchor some weather conditions may be particularly exposed and resonance can appear. This should be evaluated during the simulation.

Chapter 7

Simulation Results

In this chapter, the main results from the simulations defined in Chapter 6 are presented and discussed. The focus will be on the tension in the wire and the energy distribution.

7.1 Static Equilibrium

Before the dynamic simulation can take place, the static forces have to be checked. A static analysis is performed in SIMO, and Figure 7.1.1a presents the results for the suction anchor. For this purpose, the static analysis is taken as a dynamic simulation without any environmental effects. In the beginning, one can see that there are transient effects but they disappear after a few seconds. Figure 7.1.1b shows how the tension in the lifting line changes during the static analysis for the DPA. Here it is clearer when the anchor passes the water surface as the buoyancy increases, and the total submerged static line force is 788 kN .

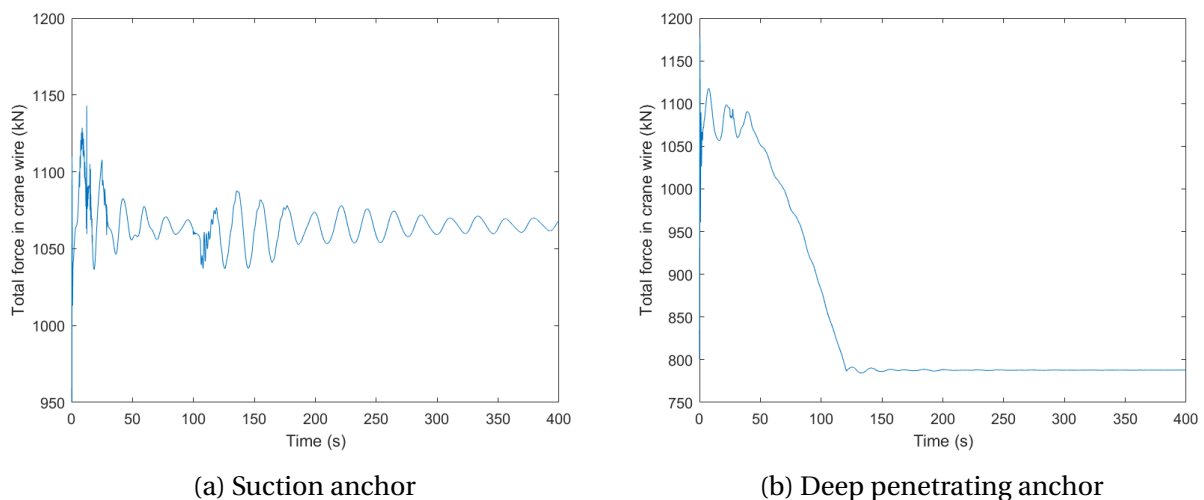


Figure 7.1.1: Static line force

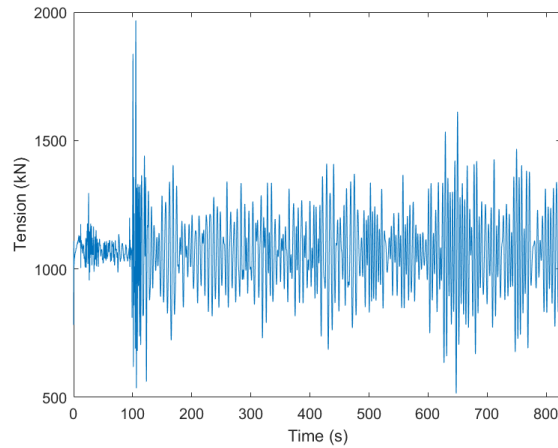
7.2 Tension in Wire

When deciding simulation length, the water particle movements are evaluated. In deep water and assuming a wave period of 14.5 seconds, the wave kinematics will have an effect until a water depth of approximately 160 meters. With a winch speed of 0.2 m/s in addition to 25 seconds before the lift starts, the simulation will last for about 825 seconds. All the simulations, both for the DPA and the suction anchor are simulated for 825 seconds. The simulations are performed for different wave headings. It is decided to evaluate head sea waves (180°) and waves with a changed angle of 20 and 45 degrees. From a quick sensitivity check, it is found that there are small differences for waves with same heading coming from port or starboard side due to symmetry. Waves from 160° and 135° are used further during the simulations.

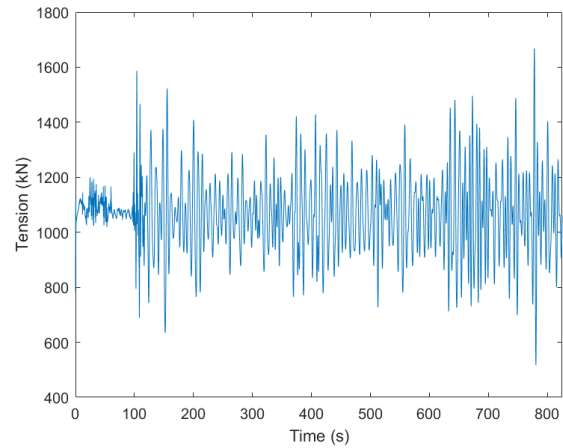
7.2.1 Suction Anchor

Figure 7.2.1 shows typical results from the simulation of the suction anchor with a significant wave height of 2 meters and varying peak periods at a heading of 160° . Here Figure 7.2.1a presents a peak period of 5.8 seconds, Figure 7.2.1b 8.7 seconds and Figure 7.2.1c 12.5 seconds. The maximum tension in the lifting wire is highest for T_p 5.8 s and reduces with increasing T_p . But the biggest difference is where the peaks appears. For the lowest peak period, a large peak occurs when the anchor is lowered through the splash zone illustrating the slamming force. This happens when the top of the anchor crosses the water surface. The load picture will thereby be dominated by the slamming forces since the rate of added mass is large and the relative velocity between the wave and the anchor is small. The impulse force (slamming) is not present for all simulations and the splash zone is thus less critical. The Morison's forces will dominate as the anchors are further lowered through the wave column. The wave particle motions diminishes further down the water column. To evaluate the wave loads, Morison's equation is used to find out that the suction anchor is inertia dominated. The suction anchor has a high added mass compared to the structural mass, and by increasing the hatch diameter the water will flow more freely, and the added mass is reduced.

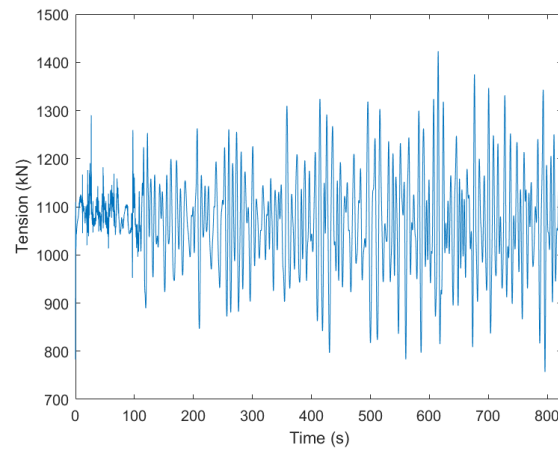
Figure 7.2.2a shows clearly the different phases through the lift for H_s 2m and T_p 5.8 s. First, the suction anchor is in air and then lowered through the splash zone. Here slamming forces can be of big concern. Further, the anchor is lowered through the water column. Here wave forces and Morison's forces will increase and can be classified as drag or inertia dominated. For deeper water depths resonance in the crane wire can be a hazard dependent on the wave period.



(a) Peak period 5.8 seconds



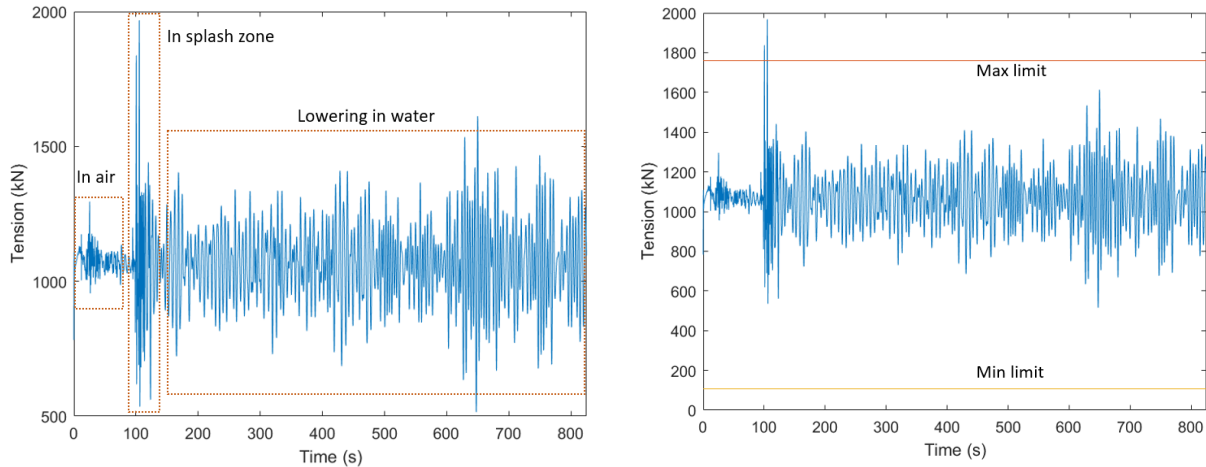
(b) Peak period 8.7 seconds



(c) Peak period 12.5 seconds

Figure 7.2.1: Simulation of suction anchor with significant wave height 2 meters and varying peak periods

Figure 7.2.2b shows the maxima and minimum requirements for the tension in wire for the suction anchor. Here significant wave height is 2 meters and peak period 5.8 seconds. In this case, the maximum tension in the wire is over the limit. It is the capacity of the wire that is the restricting limit during the simulations of the suction anchor, and it may look like there is no likelihood of slack.



(a) The different phases through a lift: in air, splash zone and further lowering (b) The maxima and minima requirement for the tension in the wire for the suction anchor

Figure 7.2.2: For significant wave height 2 meters and peak period 5.8 seconds

Since the simulations are run with different seed numbers, unlike maximum and minimum tensions appears. For significant wave height 1.5 m, five seeds are used for each weather condition. In Figure 7.2.3, nine different weather condition are evaluated for H_s 1.5 m. Here, the maximum tension in wire from each simulation is plotted and the figure shows how the maxima tension varies with peak period and headings for the suction anchor. The tension will be higher for lower periods and for waves not coming right on the bow. To get the most realistic result, the average of the peaks or the drops are compare against the settled limits and used further to set the design criterion.

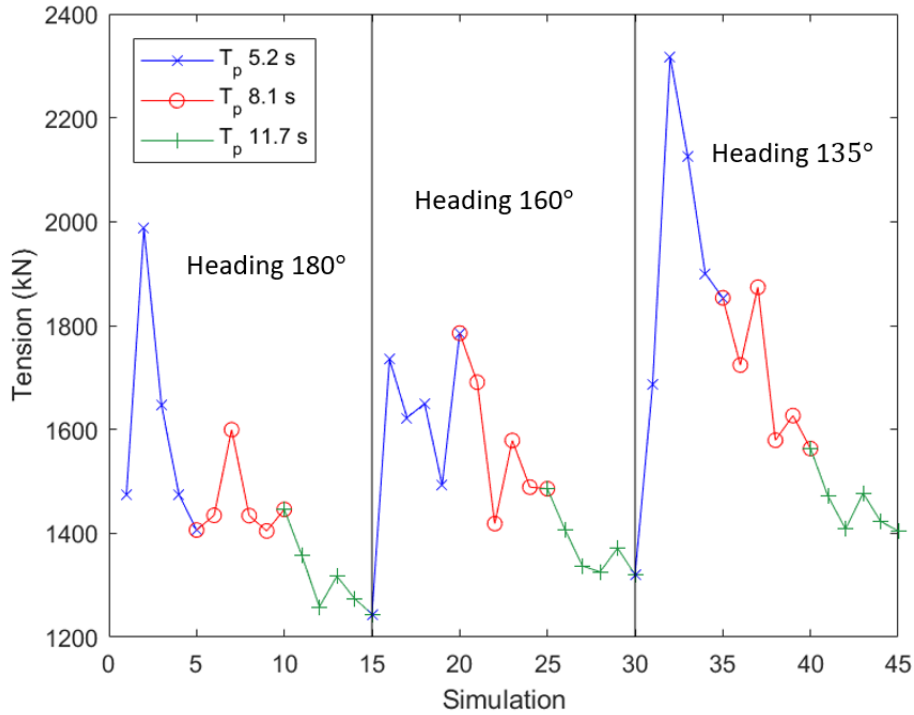


Figure 7.2.3: How the maximum tension varies with peak period and heading. This for significant wave height 1.5 m for suction anchor

The measured maximum and minimum tension in wire with related H_s and T_p are used to find the design criterion. These are established from the upper and lower limit regarding maxima tension in the wire and no slack. OP_{lim} is established from the significant wave height and depends on the heading and the wave period. Table 7.1 shows the points that makes up the design criterion for the suction anchor shown in Figure 7.2.4. The three values from each heading is based on the P5 T_p , T_p mean and P95 T_p . For the heading 135°, there are two limits with low T_p and H_s while the highest H_s is for a peak period of 14 second. It can thus be uncertainties for peak periods and significant wave height between here. The slamming force and Morison's forces have a greater impact to the wire for lower peak periods, while the crane tip is of large importance at higher periods as the ship will have large pitch, heave and roll movement. Lower peak periods give the highest tension in the wire and will, therefore, be more limiting for the operation, and to evaluate slamming and Morison's forces are therefore crucial.

Table 7.1: Significant wave height and peak periods that constitute the design criterion

	Heading 180°			Heading 160°			Heading 135°		
H_s (m)	1.86	3.15	4.00	1.74	2.27	3.94	1.00	0.88	3.36
T_p (s)	5.63	9.93	14.4	5.49	0.99	14.06	4.60	4.46	14.07

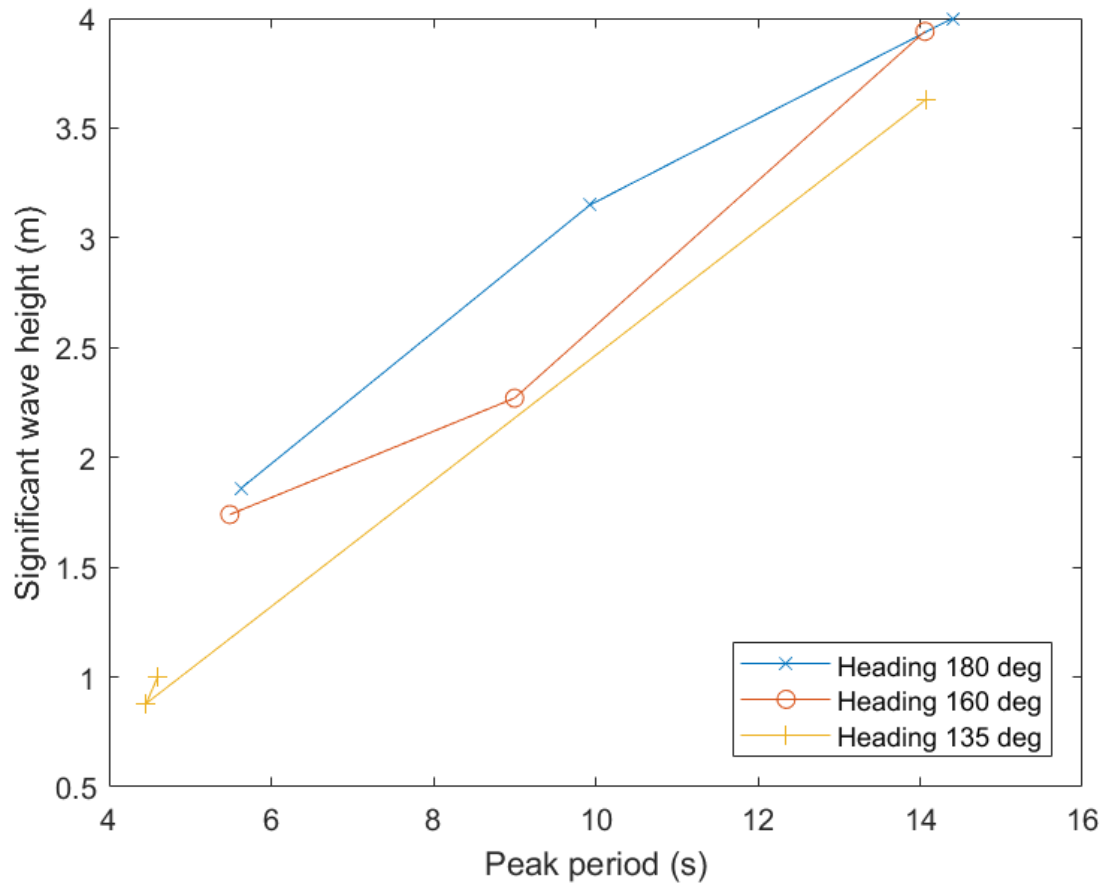


Figure 7.2.4: Design criterion for the suction anchor varying with the peak period and wave heading

7.2.2 Deep Penetration Anchor

The deep penetration anchor has to be simulated for higher weather conditions than the suction anchor since it does not reach the maxima and minima limit for the simulated weather conditions. Neither the slack or capacity criteria are violated. Figure 7.2.5 shows the simulation of deep penetration anchor with a significant wave height of 6 meters and varying peak periods. Here Figure 7.2.5a presents a peak period of 9.5 seconds, Figure 7.2.5b 12.4 seconds and Figure 7.2.5c 15.7 seconds. The tension in wire does not reach 1760 kN in any of the cases. In addition, there will not be that much variance in tension during the splash zone and no risk of slamming. The reason for this is the pointed end and the low added mass. Consequently, the lift may be defined as static. The motion in the crane tip will affect the lifting system.

Significant wave height higher than 6 m is acceptable for the DPA, however, there will be other factors limiting the design criterion, like the movement of the vessel. Handling on deck in harsh weather can be risky and a big hazard when it comes to falling objects and injuries of the

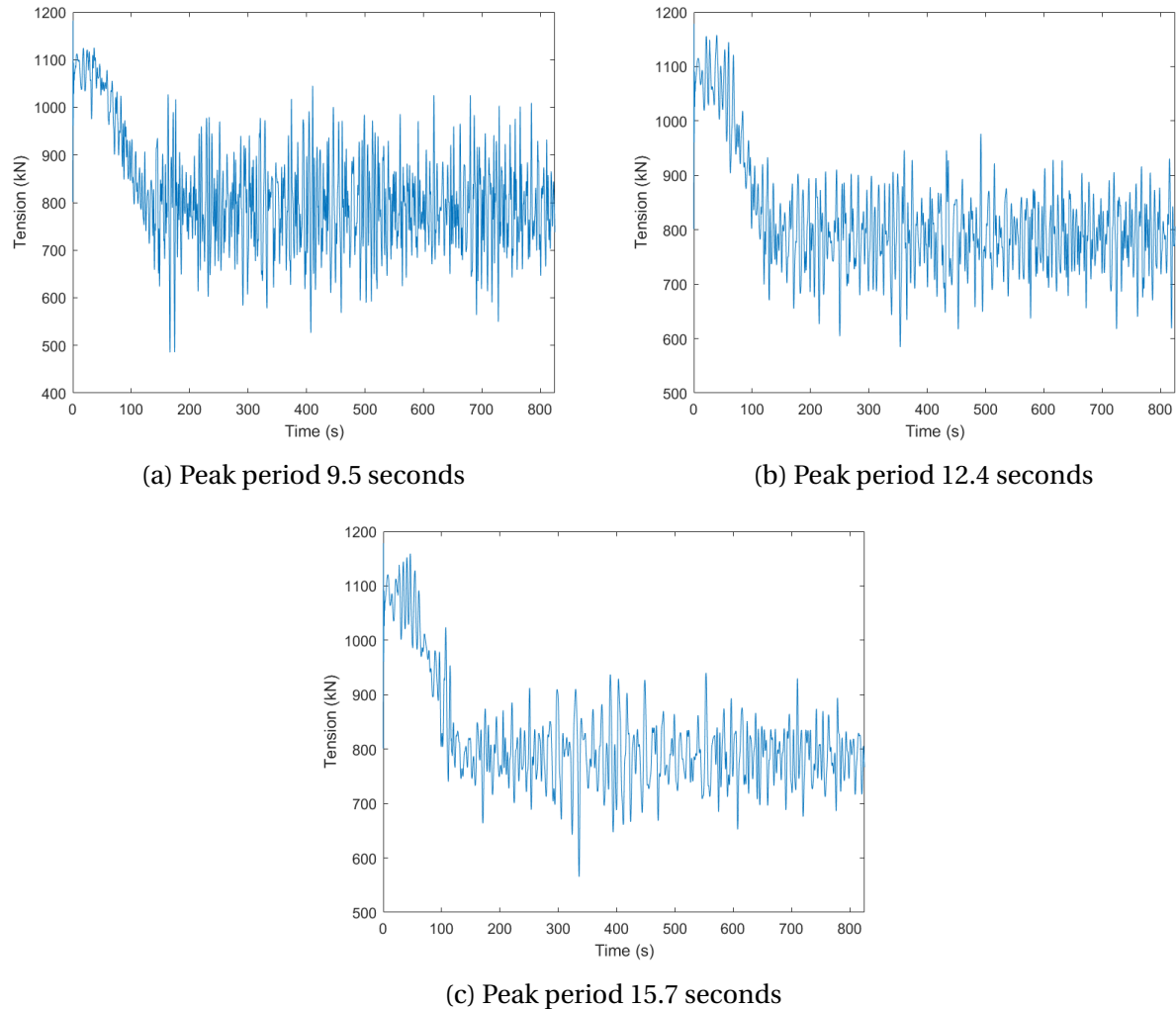


Figure 7.2.5: Simulation of deep penetration anchor with significant wave height 6 meters and varying peak periods

crew. As mentioned, the largest hazard when the anchor is in air and lifted from the deck and over the vessel is the pendulum movement. The resonance period of the pendulum is important to assess. With the crane tip z-coordinate 32.6 meters over the sea surface, the length of the wire will be between 0 and 32.6 meters when in air. This leads to a resonance period between 1 and 11.5 seconds. Comparing this to the roll period of the vessel, the critical period for both 180° , 158° and 135° is 14.7 seconds. The largest amplitude of the vessel is for beam sea. If the natural period of the anchor as a pendulum in the air is close to the roll period of the vessel, resonance can appear. In that case, one should install tugger winches to control the pendulum movement. Also wind can affect the anchor when in air, however, this is not considered during the simulations.

7.3 Evaluating Resonance - Fast Fourier Transformation

In this section, the resonance in the wire of the suction anchor is evaluated. This is as mentioned, not considered to be a risk during the lift of the DPA.

The weather condition of 1 m H_s and 4.6 s T_p can lead to resonance in wire since the wave period and the natural period of the wire is close. Figure 7.3.1 shows for which length of wire the natural period will be close to the wave period, and typically resonance can appear. The red horizontal line indicates the peak period.

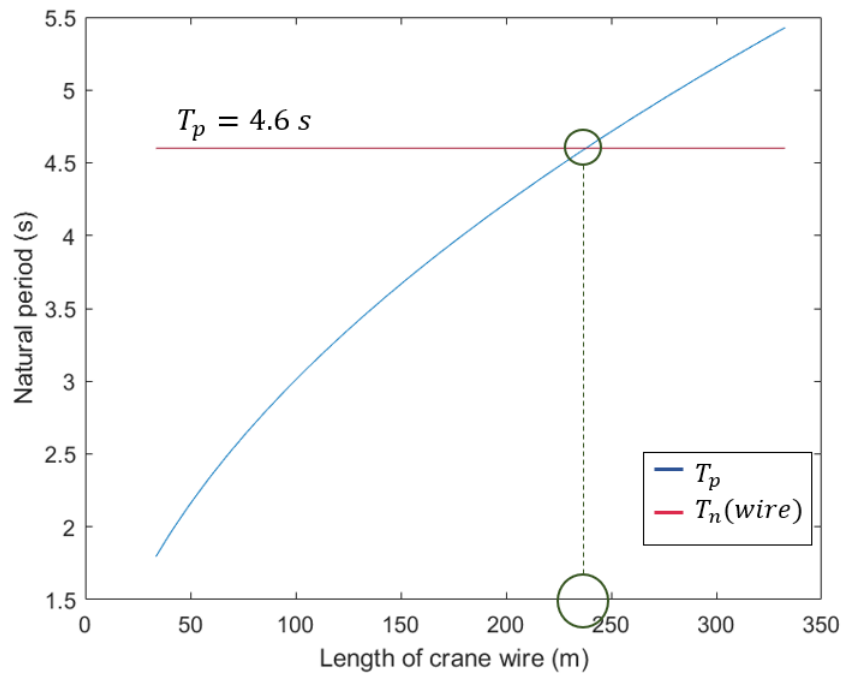
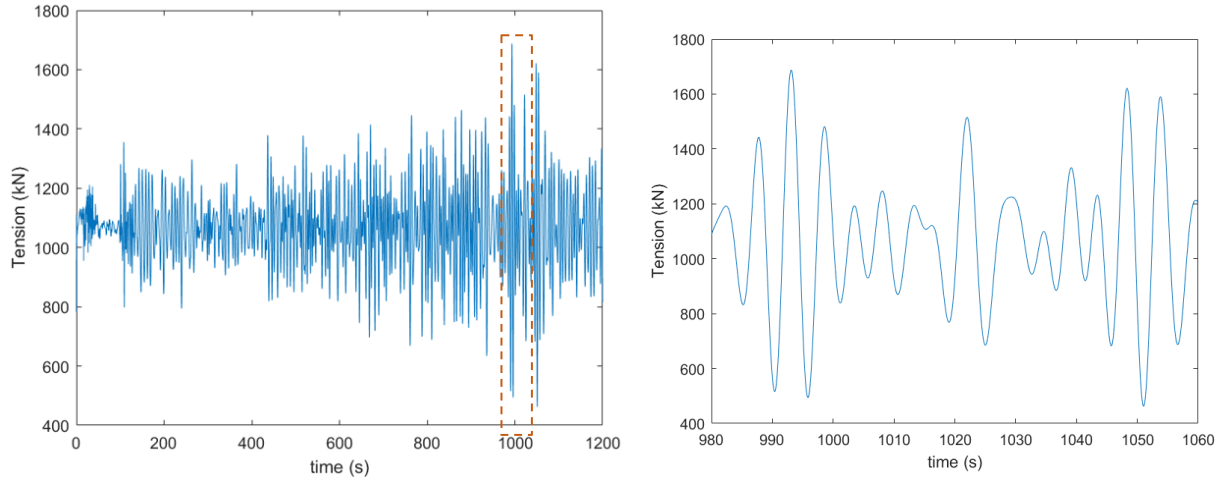


Figure 7.3.1: Natural period of the wire with varying length of crane wire for the suction anchor. A peak period of 4.6 s is highlighted.

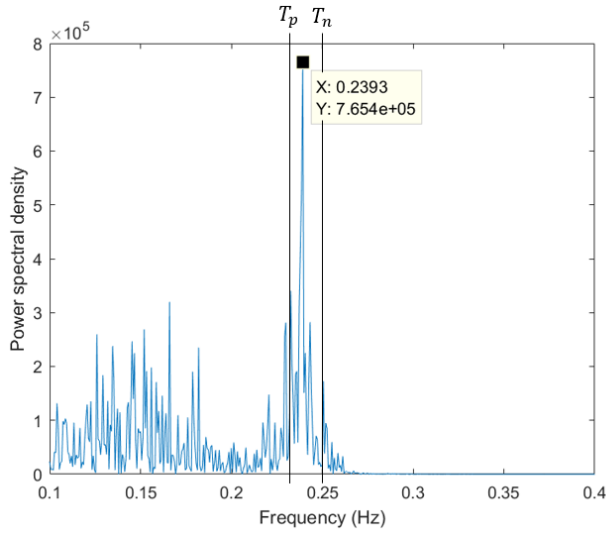
The figure shows that the critical length of wire is around 230-240 meters. A simulation is done past this water depth for the critical weather condition. Figure 7.3.2a shows the results from the simulation for a random seed number. Here, peaks or higher tension appears around the critical water depth around 1000 s, and it seems like the wire gets resonance. This resonance leads to tension in wire against the upper limit of 1760 kN. Therefore, one should be careful of doing the lift operation if the wave period is around 4.6 s. Figure 7.3.3b shows a snip of the simulation where the wire might get resonance. The wire will here oscillate with a period around 5 seconds.



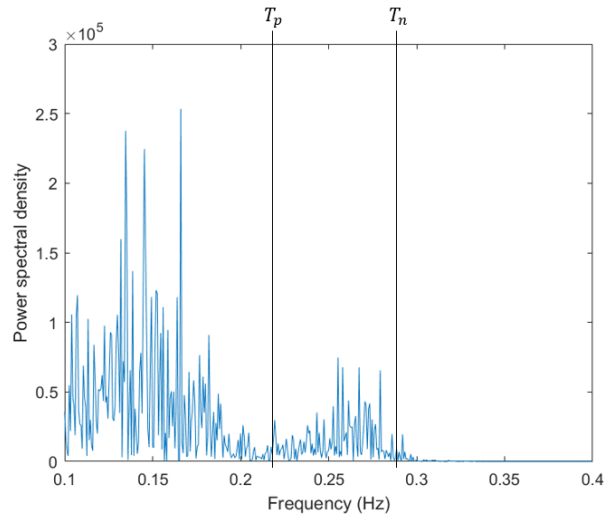
(a) H_s 1m, T_p 4.6 s and head sea waves to test if the wire will get resonance. (b) A snip of the simulation of H_s 1m, T_p 4.6 s and head sea waves

Figure 7.3.2: H_s 1m, T_p 4.6 s and head sea waves

Further, to evaluate where most of the energy is, FFT is performed for the suction anchor for on of the weather conditions that are critical with respect to resonance. For the condition with H_s 1 meters and T_p 4.6 seconds and head sea waves, water depth of 150 meters is evaluated. Here the natural period of the wire is about 4.0 seconds. Figure 7.3.3a shows the FFT with a peak for a frequency of 0.24 Hz equivalent to a period of 4.2 seconds. This is between the wave period and natural period which are marked in the figure, and it can be hard to evaluate the cause for this top. Therefore, one more water depth is to be considered. For a water depth of 100 meters, the natural period is 3.45 seconds, and the FFT is presented in Figure 7.3.3b. The peaks appear for frequencies around 0.15 Hz which equal a period of 7 seconds. This means that is not close to either wave period or the natural period. It seems like the tension is not affected by the natural period of the wire. On the other hand, the heave period is 7.4 seconds and can be the reason for the peaks in this area. These peaks are also present for the water depth of 150 meters with the same power spectral density but are small compared to the energy top. Figure 7.3.4 shows the time series for the simulations. The first part, coloured in red, is when the anchor is lowered to the correct water depth. These measurements are not considered for the power spectral density. The simulation is hold for 1500 seconds with the correct length of wire released. From Figure 7.3.4a with the time series for the simulation performed at the water depth 150 m, one larger top appears around 1100 s. This can be the reason for the resonance which caused a peak in the FFT. From Figure 7.3.4b, the time series shows no abnormalities.

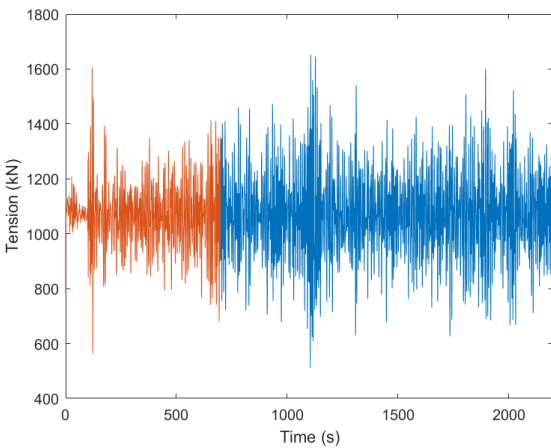


(a) Water depth 150 meters

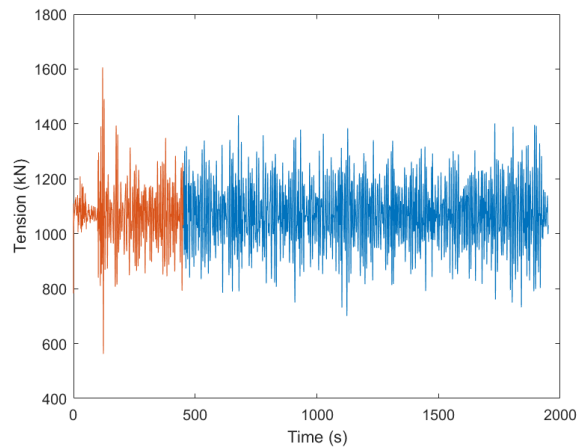


(b) Water depth 100 meters.

Figure 7.3.3: FFT for H_s 1 m T_p 4.6 s at water depth 150 and 100 meters. The wave period (T_p) and the natural period (T_n) are highlighted in the figures



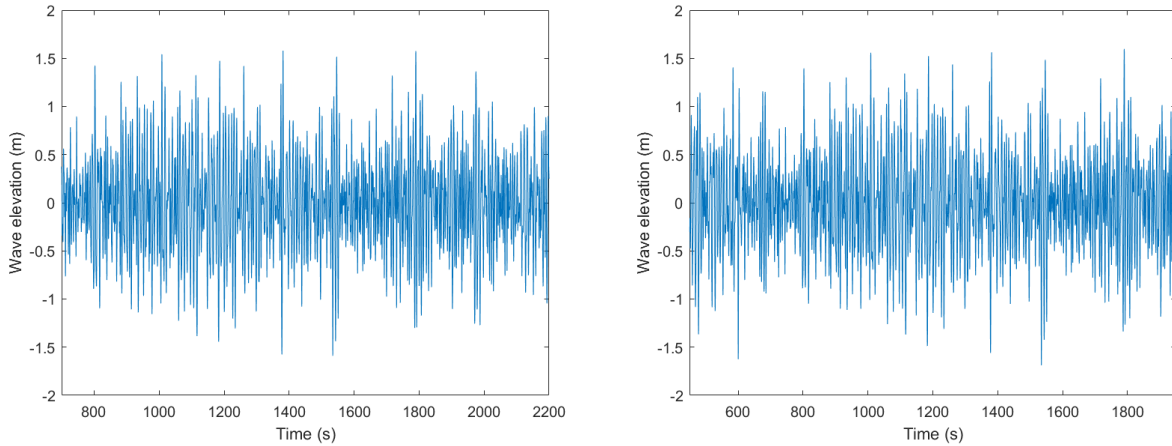
(a) Water depth 150 meters



(b) Water depth 100 meters

Figure 7.3.4: Time series for H_s 1 m and T_p 4.6 s - water depth 150 and 100 meters. The red part is when lowering anchor to desired water depth, and the blue part is used for the FFT.

By looking at the wave elevation for the same simulation, one can look for abnormal waves. This is presented in Figure 7.3.5, and both of the runs seem quite normal but with some larger waves now and then.



(a) Wave elevation for H_s 1 m T_p 4.6 s at water depth 150 meters. (b) Wave elevation for H_s 1 m T_p 4.6 s at water depth 100 meters.

Figure 7.3.5: Wave elevation for H_s 1 m T_p 4.6 s at water depth 150 and 100 meters.

For H_s 1.5 m and T_p 5.2 s for a water depth of 195 m, the FFT is presented in Figure 7.3.6. Here T_n of the wire is 4.5 s, and the figure shows a peak for the associated frequency. This means that resonance is triggered and the wire oscillates with the natural frequency and not only the load frequency from the waves. Resonance will thereby dominate the load and play an important role. The second peak at the frequency 0.1867 Hz is close to the wave peak period. Based on this, heave compensation should be evaluated to control the vertical motion of the anchor.

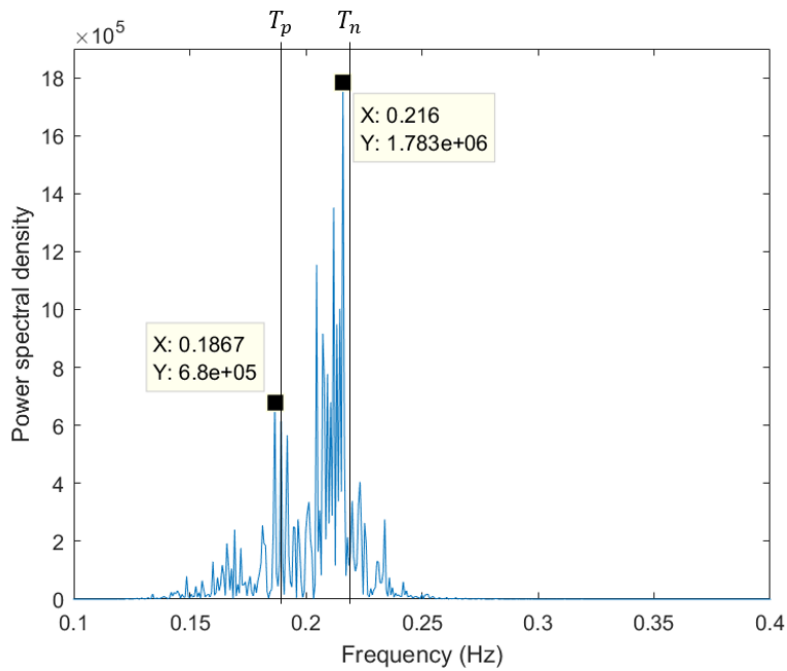


Figure 7.3.6: FFT for H_s 1.5 T_p 5.2 s at water depth 195 meters.

It can be more movement in the vessel with higher significant wave height, and the time series in Figure 7.3.7 shows some larger tension tops for the wire.

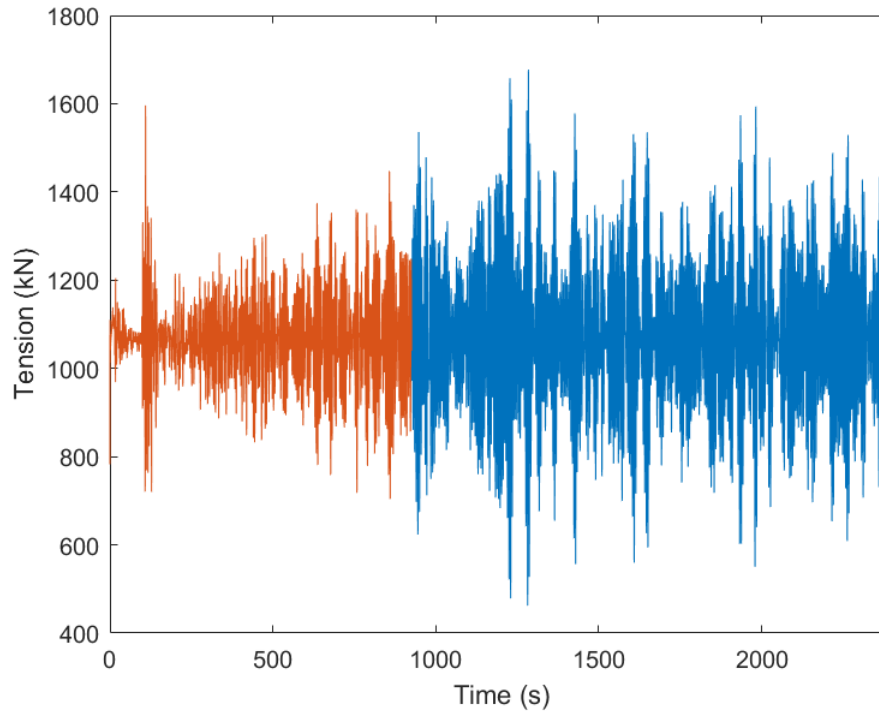


Figure 7.3.7: Time series for H_s 1.5 T_p 5.2 s - water depth 195 meters.

Moreover, the weather condition with H_s 4 m and T_p 14.4 s is the case with the highest allowed period for head sea waves. This period is close to the roll period of the vessel which is 14.7 seconds, and one can thus expect large movements of the vessel. Figure 7.3.8 illustrates the crane tip motion with head sea waves for H_s 4m and T_p 14.4 s as a function of heave, pitch and roll. Figure 7.3.9a presents the power spectral density for this weather condition. Here the roll period is marked T_{n_4} . The energy peak does not hit this period but is close. For beam sea waves might given a peak closer to the roll RAO. By looking at the energy distribution of the vertical crane tip motion, from Figure 7.3.9b, the peak appears at the same frequency. This peak is a result of the vessel's heave, pitch and roll, but for this period, the vessels heave motion is the dominating. Based on this, the wire is dominated by the crane tip motion for this weather condition. The RAOs will push the wave spectrum to the left. This is in line with the figure showing that the energy peak for the crane tip motion is moved to the left for the wave period. In general, the crane tip motion will move the energy of the wire towards lower frequencies.

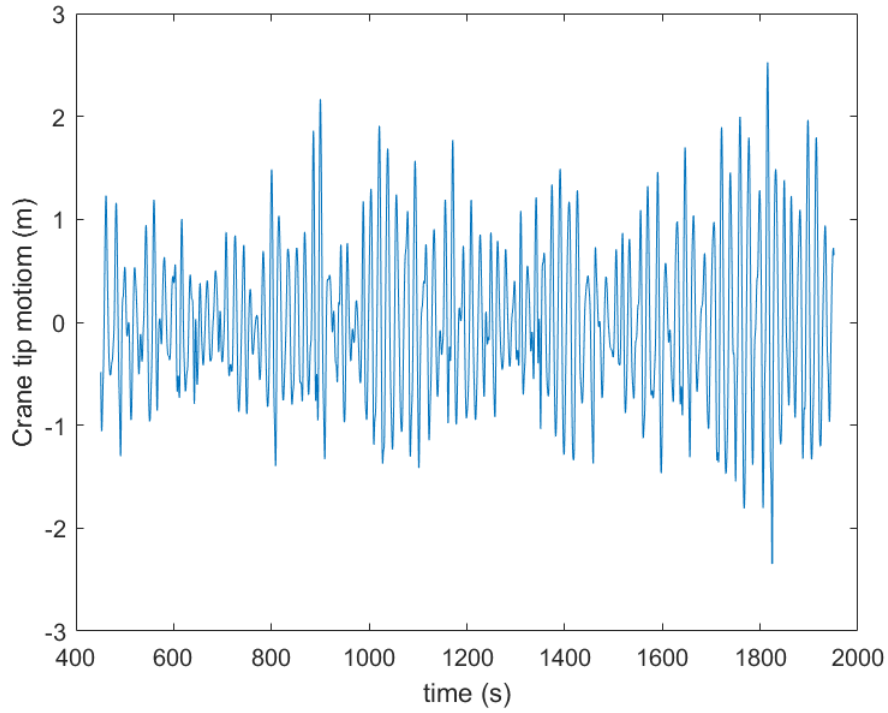
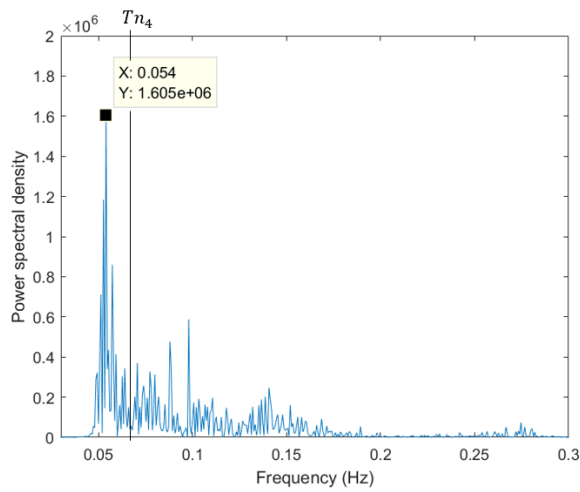
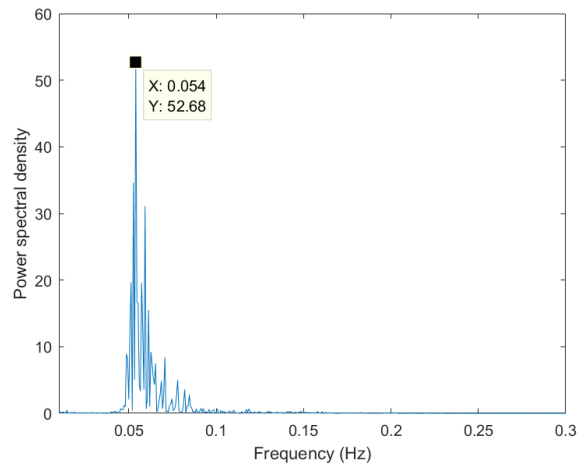


Figure 7.3.8: Crane tip movement for H_s 4m and T_p 14.4 s.



(a) FFT of the wire for H_s 4m and T_p 14.4 s. The roll period is marked as T_{n_4} .



(b) FFT for the crane tip motion

Figure 7.3.9: H_s 4m and T_p 14.4 s

Chapter 8

Operability

The lifting operations are further investigated with respect to operability, and this chapter will present the operational limits and discuss the availability to perform the marine operation by evaluating $P[(H_s \leq OP_{WF}) \cap (\tau_c > T_R)]$.

First, the planned time of the operation has to be settled to evaluate if it is weather restricted or unrestricted. Assumptions are made to decide T_{POP} , and can change as more information about exact equipment to be used is known. Cutting the sea fastening of the suction anchor will take about one hour and installing strips another hour. This can, however, often be done before the operation takes place, but is included here. Further on, the anchor is lifted off the deck before lowered into the water which takes about 30 minutes. By assuming a lowering speed of 0.2 m/s and a water depth of 300 m, the time from the splash zone to the sea bed is about 25 minutes. Then the anchor is to be sucked into the seabed which will take about 2 h. The duration of this operation will take 5 h per anchor. Also for the DPA, cutting of sea fastening and installation of strips will take 2 hours in total. The anchor is lowered to the drop height which will take 20 minutes and inspected by an ROV before it can be realised. The free fall and penetration into the ground are assumed to take 10 minutes. Finally, the ROV does a last inspection before the operation is in safe heaven. The total planned operation per anchor time will be 3 hours. To find the reference period, a contingency time is added to the planned time. T_C shall normally not be less than 6 h, and therefore it is set to 6 h for the installation of both anchors. Based on this, the operation can be classified as weather restricted since it is less than 72 h.

To establish the design criterion, the results from the simulations are used. Here, the design criterion is settled with respect to H_s , however, normally there shall be requirements for the peak periods as well. For the DPA, OP_{LIM} is based on other factors than the tension in the lifting wire, and is decided to be 6 m. The design criterion for the suction anchor depends on heading of waves and T_p . In this section it is decided to look at the T_p of 10 s and choose the strictest requirement for H_s which is at the heading of 135°. This gives a design criterion with respect to H_s of 2.5 m.

Table 8.1: Design criterion, α -factor, planned time for the operation, contingency time, reference time and operational criterion for suction anchor and DPA

	Suction Anchor	Deep Penetration Anchor
Design criterion ($OP_{lim}(H_s)$)	2.5 m	6 m
Planned time (T_{POP})	5 h	3 h
Contingency time (T_C)	6 h	6 h
Reference time (T_R)	11 h	9 h
α -factor	0.81	0.84
Operational criterion ($OP_{wf}(H_s)$)	2.02 m	5.04 m

As the design criterion and the planned duration of the operation is settled, the operational limit can be found. When calculating the operational limit for a weather restricted operation, an α -factor is used. There is no data to find this factor that accounts for the uncertainty of the measured weather forecasts in the Barents Sea. According to Orimolade and Gudmestad (2017), the wave forecasts for the Barents Sea are of good quality at lead times less than 30 hours and decreases rapidly beyond this lead time. In addition, it is stated that the wave conditions are found to be more reliable for the Barents Sea in the summer months compared to the North Sea and the Norwegian Sea wave conditions. One can thus assume that there are minor differences in the weather forecasts. Therefore, the α -factor presented in DNV GL (2011a) based on the North Sea is used. By use of weather forecast level B, the α -factors are found to be 0.81 and 0.84 for the suction anchor and DPA respectively. This leads to operational limits of 2.02 and 5.04 meters with respect to significant wave height. Table 8.1 shows the design criterion, α -factor, planned time for the operation, contingency time, reference time and operational criterion for both suction anchor and DPA.

8.1 Weather Hindcast for Johan Castberg

By studying weather hindcast data for a relevant location in the Barents Sea, the operability of the two anchor concepts can be compared. From measured significant wave heights, the duration of calms can be decided and evaluated with respect to the execution of an operation in this area. In this part, the logged data at the Johan Castberg field is collected by the Norwegian Meteorological Institute. Further on, this data is compared with the planned operation with related operational limits and reference periods. Weather data is collected every third hour for the Johan Castberg field located in the Barents Sea in the period from 2003 to 2013. The mean H_s for this location is 2.8 m and the maximum H_s measured in this period is 11.4 m. The mean H_s is thus higher than the OP_{WF} for the suction anchor. This is on the other hand, regardless of the time of year. Figure 8.1.1 shows logged H_s for the Johan Castberg field in 2010, and how it

changes with the months during the year. One can clearly see that the measured H_s are higher in the period between November and April.

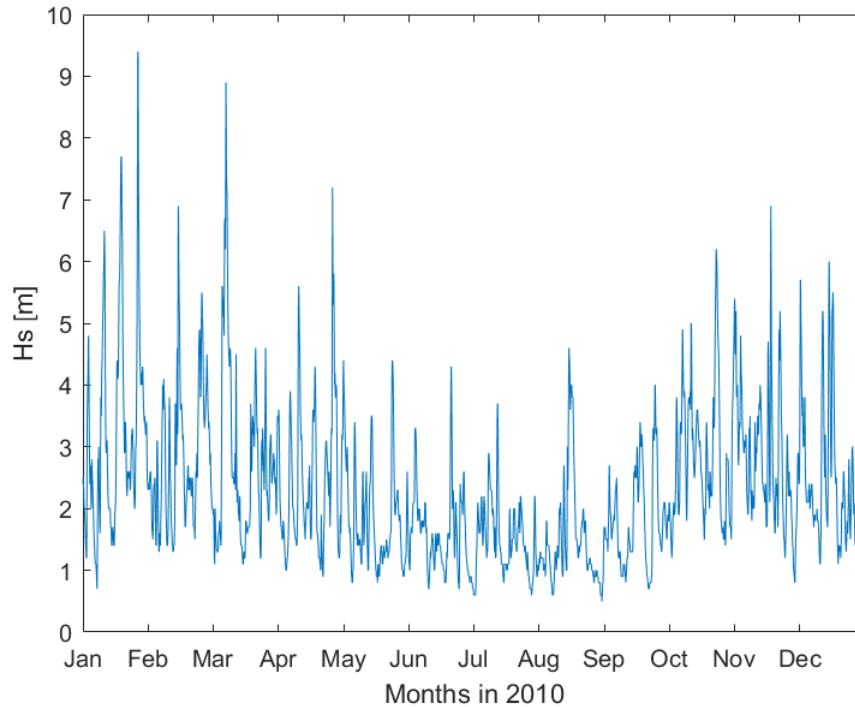


Figure 8.1.1: Measurements of H_s for the Johan Castberg Field during 2010

The length of a calm period will vary with Op_{WF} . Figure 8.1.2a shows $Op_{WF}(H_s)$ between 0 and 5 m with related calm periods independent on season. The number of periods with longer duration of calm increases with increasing Op_{WF} . The mean calm periods with respect to $Op_{WF}(H_s)$ is presented in Figure 8.1.2b, and shows clearly that the mean calm period increases with the operational limit. Since the DPA have a high Op_{WF} , the average calm is higher than T_R . Also, for the suction anchor is the average calm above T_R . On the other hand, for a FOWT or a park with several FOWTs, there will be more than one anchor to install. Since the vessel transports several anchors, a longer weather window is required to avoid waiting on weather for the entire job. It is therefore desirable to install several anchors consecutively. It will be safe heaven between each installation and a new evaluation against the weather forecast must be done.

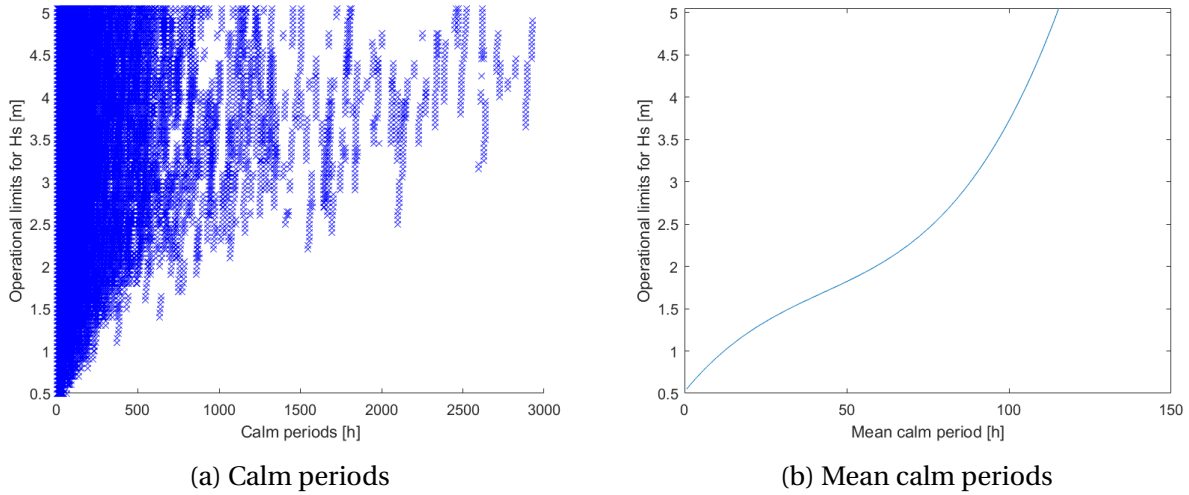


Figure 8.1.2: Calm periods independent on season

8.2 Probability Distribution

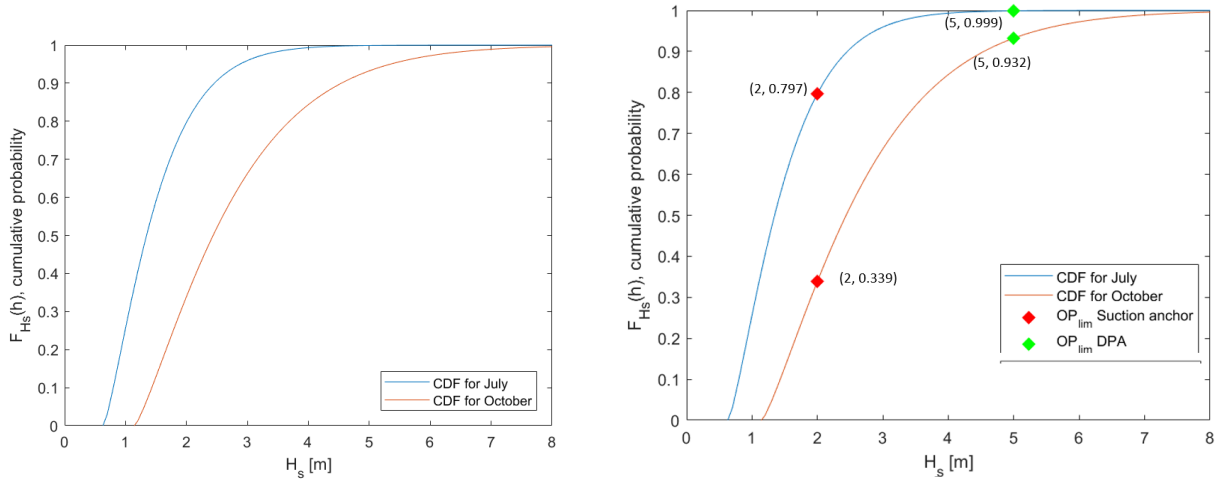
Further, the Weibull three-parameter distribution is used to evaluate the probability distribution. By use of data from Dezecot et al. (2016), the shape, scale and location parameters for the different months are listed. These are used for comparing the availability of the operation at different times throughout the year. It is decided to have a focus on comparing July and October, and the respective parameters can be found in Table 8.2.

Table 8.2: Monthly Weibull parameters for significant wave height at the Johan Castberg Field. Duration of event is 3 hours. Data from Dezecot et al. (2016)

Month	Annual prob.	Weibull parameters		
		Shape	Scale	Location
-	[%]	-	[m]	[m]
July	8.33	1.267	0.94	0.64
October	8.33	1.239	1.73	1.15

The cumulative probability with respect to H_s as the operational limit for July and October are shown in Figure 8.2.1a and can be used to evaluate $P[(H_s \leq OP_{WF})]$. The figure shows that the curve for July grows rapidly from the start, and start to diminish for H_s about 3m, and for H_s 4 m the F_{H_s} is close to one, in other words, the probability for having a H_s value equal or lower than 4 m is almost 100%. For October, the graph starts to increase for higher H_s values and with some smaller steepness. It will, therefore, be harder to perform the lifting operation in October. The $OP_{WF}(H_s)$ for the suction anchor and DPA are marked in Figure 8.2.1b. With the operational limit of 2 meters for the suction anchor, it is 80 % probable that the H_s is less than or equal to 2

meters in July. In October, the probability is 34 %, a decrease of 46 %. If the limit is reduced to 1.5 m, the probability will decrease with about 20 % for both July and October, and it can thus be quite difficult to get lower H_s in October. It is therefore important to not be precise, and not too conservative when finding the operational limit. For the DPA with a $OP_{WF}(H_s)$ of 5 m, the cumulative probability is over 0.9 in both months. In Figure 8.2.1b with CDF, the $OP_{WF}(H_s)$ for the suction anchor and DPA is marked.



(a) Cumulative probability for July and October (b) Cumulative probability for July and October with operational criterion for suction anchor and DPA

Figure 8.2.1: Cumulative probability with respect to H_s

Further, an expression for the average length of calms can be determined based on the CDF of wave length against average length of calms. The Weibull distribution will give an acceptable fit for this curve. The expression will be based on the formulation

$$\bar{\tau}_c(h) = A * [-\ln(F_{H_s}(h))]^{-\frac{1}{B}}. \quad (8.1)$$

where $\bar{\tau}_c(h)$ is the average length of calms and $F_{H_s}(h)$ the cumulative probability for a given H_s .

In July, the average duration of the calm for H_s 2 meters is 78.214 hours, and the corresponding $F_{H_s}(h)$ is 0.797. For H_s 5 meters, the F_{H_s} is 0.9991 and the average duration of the calm is 415.25 hours. By use of Equation 8.1, two expressions can be established

$$78.214 = A[-\ln(0.797)]^{-1/B}$$

and

$$415.25 = A[-\ln(0.999)]^{-1/B}$$

A and B is calculated to be 49.938 and 3.311 respectively. This gives the following formula for an average calm period for July

$$\bar{\tau}_c(h) = 49.938[-\ln(F_{H_s}(h))]^{-\frac{1}{3.311}}$$

For October, the average duration of the calm for H_s 2 meters is 51.033 hours, and the corresponding $H_{H_s}(h)$ is 0.339. For H_s 5 meters, the F_{H_s} is 0.932 and the average duration of the calm is 121.418 hours. The two expressions established are

$$51.033 = A[-\ln(0.339)]^{-1/B}$$

and

$$121.418 = A[-\ln(0.932)]^{-1/B}$$

A and B is calculated to be 52.301 and 3.158 respectively. This gives the following formula for an average calm period for July

$$\bar{\tau}_c(h) = 52.301[-\ln(F_{H_s}(h))]^{-\frac{1}{3.158}}$$

This can be plotted as a cumulative probability which can be used to find the $P[(\tau_c > T_R)]$. Figure 8.2.2 shows the CDF for both July and October with respect to the average length of calms. The difference in cumulative probability is quite small for July and October. One can notice that for both the months, the probability of having an average length of calm up to 30 hours are 100 %. Based on this, it will not be challenging to install either the DPA or suction anchor. But as the desired weather window increases with numbers of anchors installed, the probability decreases. This will be the case for a FOWT park, where the capacity on the vessel sets the limit.

The relationship between the cumulative probability of H_s and $\bar{\tau}_c(h)$ can be illustrated in Figure 8.2.3. The H_s which corresponds to the operating limit can be read and the average length of calm can be found. In this figure, the $OP_{WF}(H_s)$ for the suction anchor and DPA is marked.

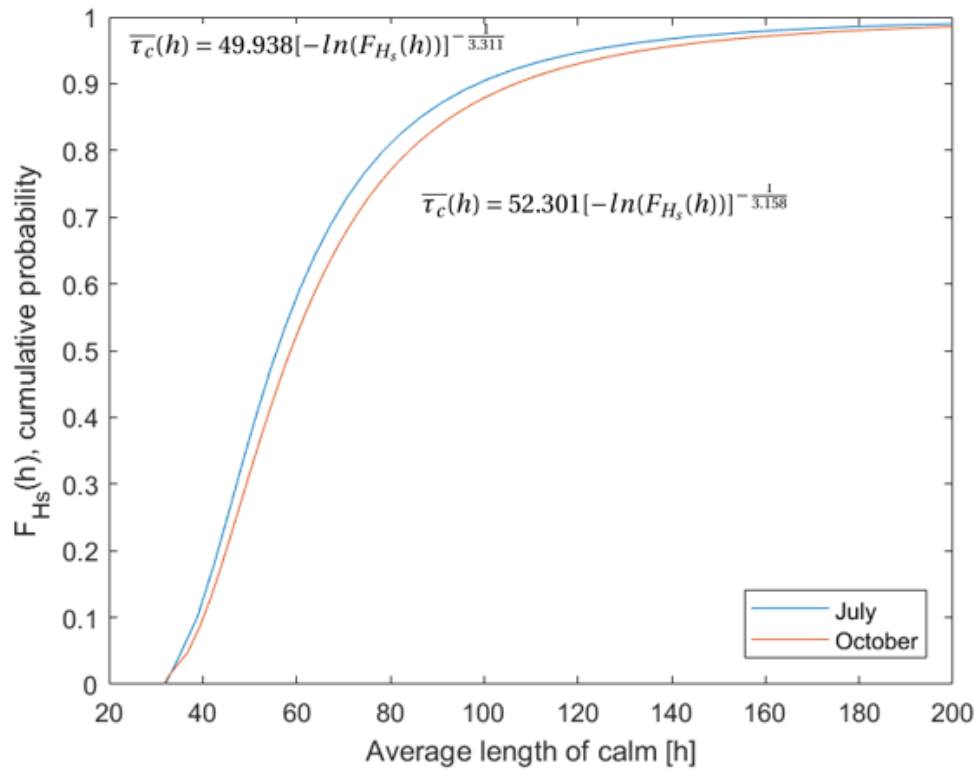


Figure 8.2.2: Cumulative probability with average length of calm for both July and October.

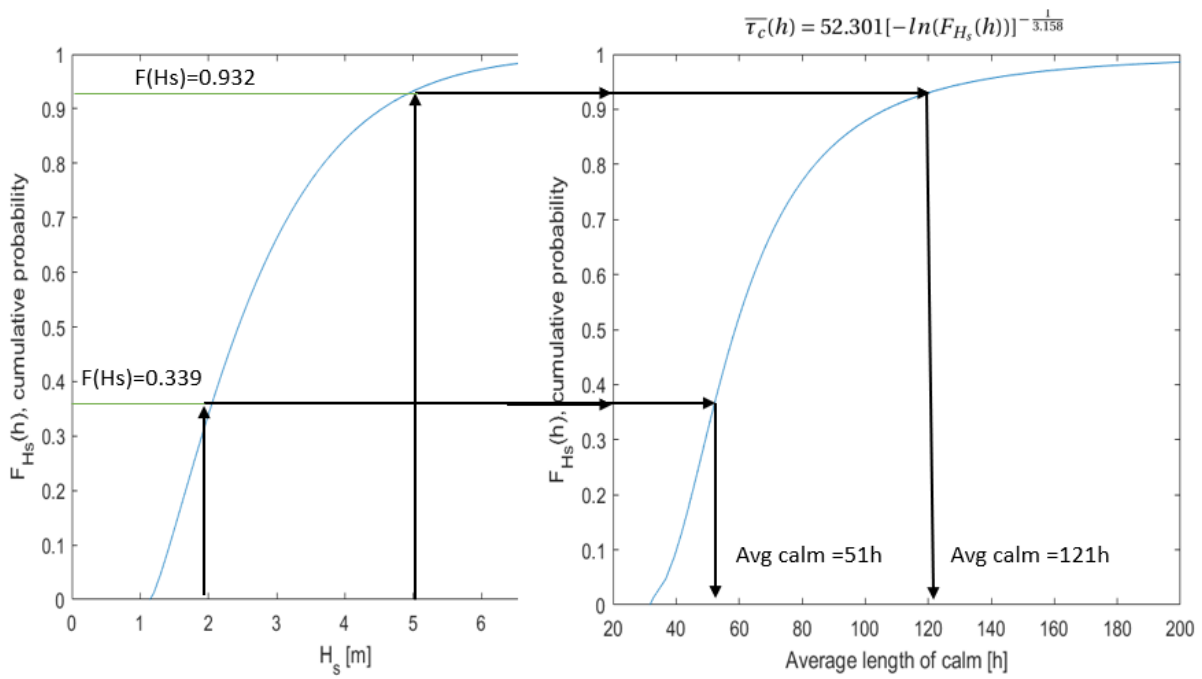
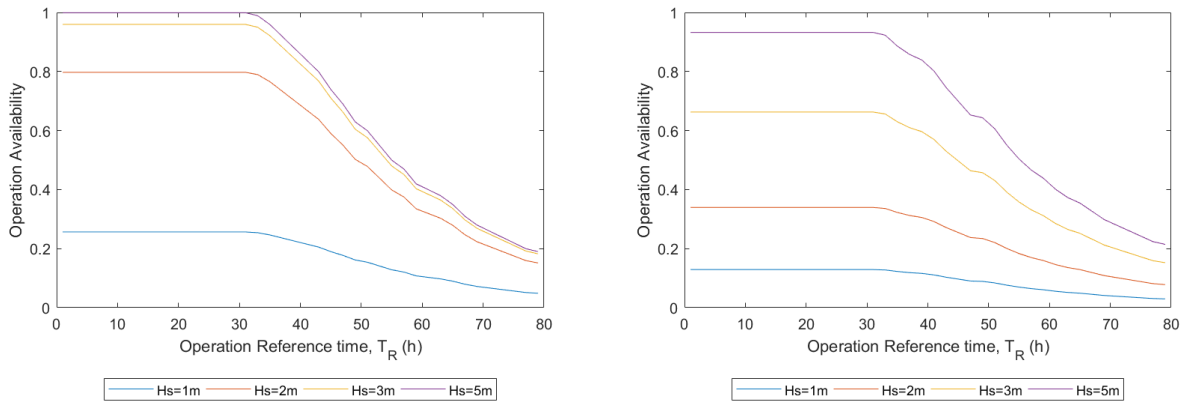


Figure 8.2.3: Relationship between cumulative probability of H_s and $\bar{\tau}_c(h)$

Based on this, the availability of the operation can be assessed. This is done by multiplying $F_{H_s}(OP_{wf}) \cdot Q_{\tau_c(OP_{wf})}(T_R)$, where $Q_{\tau_c(OP_{wf})}(T_R)$ equals $P(\tau(OP_{wf}) > T_R)$ meaning that the exceedance probability of the calm period is larger than the operation reference period. The availability for July can be found in Figure 8.2.4a and for October in Figure 8.2.4b. This shows how the availability increases with increasing $OP_{wf}(H_s)$ and decreasing T_R . For July, the operational limits with H_s 2 m, 3m and 5 m have high availability for T_R lower than 30 hours and drops rapidly for higher T_R . H_s 1 m will have low availability from the start but less drop for T_R higher than 30 h. In October, the availability decreases for all the operational limits. For H_s 2 m, which is the $OP_{wf}(H_s)$ for the suction anchor, the availability is reduced with over 40%. Thereby, the installation of the suction anchor is more dependent on season due to lower OP_{wf} compared to the DPA. Especially with increased number of anchors to install, operation during July is preferred for the suction anchor. For DPA with a OP_{WF} of 5 m, a increased T_R will be the main challenge.



(a) Operation availability with varying reference time for July

(b) Operation availability with varying reference time for October

Figure 8.2.4: Cumulative probability with respect to H_s

Chapter 9

Conclusion

This thesis has looked at the marine operation of installing anchors used for FOWT and compares a suction anchor and a deep penetration anchor by use of numerical simulations.

The simulation results show that for the suction anchor, the capacity of the wire is the limiting factor, and it seems like there is no risk of slack. The added mass term for a suction anchor is large compared to the structural mass since it includes the mass of the entrapped water which leads to higher hydrodynamic forces when passing the splash zone. The simulation results show that the splash zone is the most critical phase of the lift when it comes to the dynamic forces in the lifting wire and slamming forces appear. The combined effect from crane tip motion and wave kinematics will induce the overall largest vertical hydrodynamic forces on the structure to be installed when the structure is close to the surface. The results show that lower peak periods gives a higher maximum tension in the wire. The main reason for this is that slamming typically appears for smaller peak periods and larger accelerations. This means that the slamming force and Morison's forces have a greater impact to the wire for lower peak periods, while the crane tip is of large importance at higher periods as the ship will have large pitch, heave and roll movement. Since the lower peak periods have the highest tensions, it is, therefore, most important to assess the slamming and Morison's forces. For the suction anchor, the lifting wire can get resonance which is a risk. This emerges from the energy spectra of the wire for some weather conditions. For higher H_s and T_p it is clearer that the vessel's RAO affects the wave spectrum and pushes the energy towards lower frequencies.

DPA is simulated up to a weather condition of H_s 6 m and T_p 15.7 s and does still not reach the settled maximum or minimum limit. Consequently, the design criterion is limited by other factors like vessel movement, handling on deck and the pendulum motion when in air. The DPA does have less added mass compared to the suction anchor due to the tipped end and the solid inside. As a consequence, the lifting wire can be considered as static. The crane tip motion due to RAO of the vessel will affect the lifting system while slamming and Morison's forces are less important. The natural period of the wire is that low for the lifting system of the DPA and it is

therefore considered not to be critical with respect to resonance in the wire.

Based on the simulations, the design criterion is established to be 2.5 meters for the suction anchor and 6 meters for the DPA. The reference times are respectively 11 and 9 hours for installing one anchor. By use of data from the North Sea, the α -factor is found and gives an operational limit of 2.0 and 5.0 meters. The probability that the H_s is less than the operational criterion will be higher for the DPA. Also, execution during October is harder compared to July. When evaluating the probability that the calm period is shorter than the reference period, the same trend appears. The operation availability is higher for the DPA and the biggest difference is in October with over 50%. For the DPA the available weather window is acceptable for installation both during summer and autumn, while for the suction anchor the seasonal differences play a more important role. In July, it will normally not be a challenge for installing one anchor as the duration is less than 30 hours. However, as one wants to install several anchors in a sequence, the required weather window increases to avoid waiting on weather.

In conclusion, the deep penetration anchor is recommended in a marine operation view. It is less affected by the hydrodynamic forces during the lift, and the tension in the wire is lower which gives a higher design criterion compared to the suction anchor. In addition, the reference time is shorter and thereby the required weather window is shorter. It will, therefore, be the most cost-effective anchor concept.

9.1 Recommendations for Further Work

DNV GL's guidance is used to establish the added mass for the DPA and drag for both of the anchors. These can be some conservative since they have to be on the safe side. To achieve more realistic simulations and thereby results, the added mass and drag coefficients used in the simulation model should be found by model test. This is even more essential as the structures of the anchors are complex. Also, Computational Fluid Dynamics (CFD) simulations can give good indicates of the hydrodynamic coefficients.

Further, the simulations are not performed as the anchor is lifted from the deck and over vessel side. Nor is the landing on sea bed evaluated for the suction anchor. The added mass will increase here due to wall effect. This is not considered.

For the deep penetration anchor, the lifting operation does not necessarily have to be performed by a crane. If using a winch and an A-frame at the vessel's stern, one would avoid the lifting phase with the pendulum and the splash zone. On the other hand, the splash zone was not considered to be a critical phase of the lifting of a DPA.

When concluding that the deep penetration anchor is recommended, this is in a marine operation aspect. Also, when deciding which anchor to use for the FOWT, the soil and capacity of the anchors have to be assessed.

References

American Bureau of Shipping (2018). Design and installation of drag anchors and plate anchors.

BRIDON (2013). *Oil and Gas, Wire and fibre rope solutions for the world's most demanding applications*, 6 edition.

Chakrabarti, S. K. (2005). *Handbook of Offshore Engineering*. Elsevier.
<https://www.sciencedirect.com/book/9780080443812/handbook-of-offshore-engineering>.

Cruz, J. and Atcheson, M. (2016). *Floating offshore wind energy: the next generation of wind energy*. Springer.

de Aguiar, C. S., de Sousa, J. R. M., Ellwanger, G. B., de Campos Porto, E., Júnior, C. J. d. M., and Foppa, D. (2009). Undrained load capacity of torpedo anchors in cohesive soils. In *ASME 2009 28th International Conference on Ocean, Offshore and Arctic Engineering*, pages 253–265. American Society of Mechanical Engineers.

de Araujo, J. B., Machado, R. D., and de Medeiros Junior, C. J. (2004). High holding power torpedo pile: results for the first long term application. In *ASME 2004 23rd International Conference on Offshore Mechanics and Arctic Engineering*, pages 417–421. American Society of Mechanical Engineers.

Deep Sea Anchors (Downloaded April 2019a). Principles of concept.
<http://www.deepseaanchors.no/principles-of-concept/>.

Deep Sea Anchors (Downloaded April 2019b). Products. <http://www.deepseaanchors.no/product-and-services/>.

Deep Sea Anchors and Equinor (2009). Torpedo anchor installation (DPA). [Picture].

Dezecot, C., Eik, K. J., Teigen, S. H., and Øystein Braathen (2016). Johan Castberg Metocean Design Basis Rev 6.

DNV GL (2011a). DNV-OS-H101. *Marine Operations, General*.

- DNV GL (2011b). DNV-RP-H103. *Modelling and Analysis of marine operations*.
- DNV GL (2014). DNV-OS-H205. *Lifting Operations*.
- Equinor (2017). Full story of Hywind Scotland – world’s first floating wind farm. [video], Downloaded from: <https://www.youtube.com/watch?v=PUIfvXaISvc>.
- Faltinsen, O. (1993). *Sea loads on ships and offshore structures*, volume 1. Cambridge university press.
- Froese, M. (2018). First Subsea supplies platform mooring connectors for Windfloat Atlantic Project. <https://www.windpowerengineering.com/construction/first-subsea-supplies-platform-mooring-connectors-for-windfloat-atlantic-project/>.
- Gao, F., Li, J., Qi, W., and Hu, C. (2015). On the instability of offshore foundations: theory and mechanism. *SCIENCE CHINA Physics, Mechanics & Astronomy*, 58(12):124701.
- Gilbert, R. B., Morvant, M., and Audibert, J. (2008). Torpedo piles joint industry project—model torpedo pile tests in kaolinite test beds. *Prepared for the Minerals Management Service, The University of Texas at Austin, Austin, TX, Final Project Report*, (575).
- Greco, M. (2018). TMR4215: Sea Loads. Blackboard.
- Hagen, D., Andenæs, E., Korstad, G., et al. (1998). Innovative suction anchor design and installation. In *Offshore Technology Conference*. Offshore Technology Conference.
- IRENA (2016). Innovation outlook, Offshore Wind. Technical report, The International Renewable Energy Agency.
- Landhaug, D. L. (2015). Dynamic simulation of dart anchor installation. Master’s thesis, Norwegian University of Science and Technology. [Picture].
- Larsen, C. M. (2015). Marine dynamics. Department of Marine Technology, NTNU.
- Larsen, K. (2018a). STATION KEEPING and MOORING of Floating Structures. [PowerPoint].
- Larsen, K. (2018b). SUBSEA LIFTING and CRANE OPERATIONS. [PowerPoint].
- Lieng, J. T., Kavli, A., Hove, F., Tjelta, T. I., et al. (2000). Deep penetrating anchor: further development, optimization and capacity verification. In *The Tenth International Offshore and Polar Engineering Conference*. International Society of Offshore and Polar Engineers.
- McCool, J. (2012). *Using the Weibull distribution : reliability, modeling, and inference*, volume v.950 of *Wiley series in probability and statistics*. Hoboken, N.J.

- Næss, T., Havn, J., and Solaas, F. (2014). On the importance of slamming during installation of structures with large suction anchors. *Ocean Engineering*, 89:99–112.
- Nielsen, F. G. (2012). Installation of sub-sea structures - estimation of hydrodynamic forces. Technical report, Norsk Hydro O&E. Research Centre, Bergen, Field Development.
- Orimolade, A. and Gudmestad, O. (2017). On weather limitations for safe marine operations in the Barents Sea. In *IOP Conference Series: Materials Science and Engineering*, volume 276. IOP Publishing.
- Pettersen, B. (2007). TMR4247 marin teknikk 3, hydrodynamikk. Department of Marine Technology, NTNU.
- PrinciplePower (Downloaded October 2018). Key markets overview. <http://www.principlepowerinc.com/en/key-markets-projects?location=9>.
- Randolph, M. F., Gaudin, C., Gourvenec, S. M., White, D. J., Boylan, N., and Cassidy, M. J. (2011). Recent advances in offshore geotechnics for deep water oil and gas developments. *Ocean Engineering*, 38(7):818–834.
- Reinholdtsen, S.-A., Luxcey, N., and Sandvik, P. C. (2018). Simulations of Marine Operations using SIMA. [PowerPoint].
- SINTEF Ocean (2018). *SIMO 4.15.0 User Guide*.
- Solaas, F. and Sandvik, P. C. (2017). Hydrodynamic coefficients for suction anchors during installation operations. In *ASME 2017 36th International Conference on Ocean, Offshore and Arctic Engineering*, pages V009T12A031–V009T12A031. American Society of Mechanical Engineers.
- Solaas, F., Sandvik, P. C., Pákozdi, C., Kendon, T. E., Myhre, E., et al. (2017). Dynamic forces and limiting sea states for installation of grp protection covers. In *ASME 2017 36th International Conference on Ocean, Offshore and Arctic Engineering-Volume 9: Offshore Geotechnics; Torgeir Moan Honoring Symposium*. ASME Digital collection.
- SPT Offshore (Downloaded April 2019). Suction piles for moorings. <http://www.sptoffshore.com/en/solutions/floating-facilities/suction-piles-for-moorings>.
- Thurston, K. W., Swanson, R. C., and Kopp, F. (2011). Statistical characterization of slacking and snap loading during offshore lifting and lowering in a wave environment. In *ASME 2011 30th International Conference on Ocean, Offshore and Arctic Engineering*, pages 269–277. Citeseer.
- TSI (Downloaded April 2019). Wave energy and wave changes with depth. <https://manoa.hawaii.edu/exploringourfluidearth/physical/waves/wave-energy-and-wave-changes-depth> [Accessed 20 April 2019].

Vryhof Anchors (2010). *Anchor Manual 2010*.

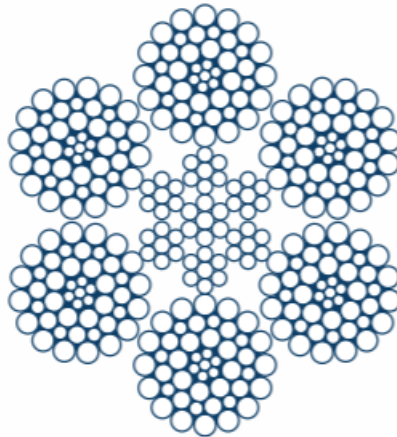
WILDE, B. (2009). Torpedo pile anchors enter the gom. *Hart's E & P*, 82(10):65–66.

Appendix A

Hardware properties

A.1 Diamond Blue

The material properties for the Diamond Blue rope are found from BRIDON (2013). The first illustration shows how the rope is build up and the table below shows the diameter with associated nominal mass, minimum breaking force, axial stiffness and nominal cross-sectional area. This data is used for the wire and slings in the simulation model.



Rope Diameter		Nominal rope length mass (M)				Minimum Breaking Force (Fmin)			Axial Stiffness at 20% Load		Torque Generated at 20% Load		Nominal metallic cross-sectional area (A)	
		In air (M)		Submerged		1960 grade					Ordinary Lay			
mm	in	kg/m	lbs/ft	kg/m	lbs/ft	kN	Tonnes	Tons	MN	Mlbs	kN.m	lbs/ft	mm ²	in ²
52		11.7	7.86	10.2	6.84	2231	227	251	140	31	1.51	1112	1338	2.074
54	2.1/8	12.6	8.48	11.0	7.38	2406	245	270	151	33	1.69	1245	1443	2.236
56		13.6	9.12	11.8	7.93	2587	264	291	163	36	1.88	1389	1552	2.405
57.2	2.1/4	14.2	9.51	12.3	8.28	2699	275	303	170	37	2.01	1480	1619	2.509
60		15.6	10.5	13.6	9.11	2970	303	334	187	41	2.32	1708	1781	2.761
60.3	2 3/8	15.7	10.6	13.7	9.20	3000	306	337	189	42	2.35	1734	1799	2.789
63.5	2 1/2	17.5	11.7	15.2	10.2	3326	339	374	209	46	2.75	2025	1995	3.093
64		17.7	11.9	15.4	10.4	3379	344	380	213	47	2.81	2073	2027	3.141
66.7	2 5/8	19.3	12.9	16.8	11.3	3670	374	413	231	51	3.18	2347	2201	3.412
68		20.0	13.4	17.4	11.7	3815	389	429	240	53	3.37	2487	2288	3.546
69.9	2 3/4	21.2	14.2	18.4	12.4	4031	411	453	254	56	3.66	2701	2418	3.747
72		22.4	15.1	19.5	13.1	4277	436	481	269	59	4.00	2952	2565	3.976
76		25.0	16.8	21.8	14.6	4765	486	536	300	66	4.71	3471	2858	4.430
76.2	3	25.1	16.9	21.9	14.7	4790	488	538	302	67	4.75	3499	2873	4.453
80		27.7	18.6	24.1	16.2	5280	538	593	333	73	5.49	4049	3167	4.908
82.6	3 1/4	29.5	19.8	25.7	17.3	5629	574	633	354	78	6.04	4457	3376	5.233
84		30.6	20.5	26.6	17.8	5821	593	654	367	81	6.36	4687	3491	5.412
88		33.5	22.5	29.2	19.6	6389	651	718	402	89	7.31	5389	3832	5.939
88.9	3 1/2	34.2	23.0	29.8	20.0	6520	665	733	411	91	7.54	5556	3911	6.061
92		36.6	24.6	31.9	21.4	6559	669	737	440	97	7.85	5785	4188	6.491
95.3	3 3/4	39.3	26.4	34.2	23.0	7038	717	791	472	104	8.72	6430	4494	6.965
96		39.9	26.8	34.7	23.3	7142	728	803	479	106	8.91	6573	4560	7.068
100		43.3	29.1	37.7	25.3	7750	790	871	520	115	10.1	7429	4948	7.669
101.6	4	44.7	30.0	38.9	26.1	8000	815	899	536	118	10.6	7791	5108	7.917
108	4 1/4	50.5	33.9	43.9	29.5	8306	847	934	606	134	11.7	8598	5771	8.946
114.3	4 1/2	56.6	38.0	49.2	33.0	9303	948	1046	679	150	13.8	10193	6464	10.020
120.7	4 3/4	63.1	42.4	54.9	36.8	10374	1057	1166	757	167	16.3	12003	7208	11.173
127	5	69.8	46.9	60.8	40.8	11485	1171	1291	838	185	19.0	13982	7981	12.370

Note: Tonnes = 1000kg Tons = 2000lbs

Figures shown are for guidance purposes only. For specific applications requirements please contact Bridon.

This table is for guidance purposes only with no guarantee or warranty (express or implied) as to its accuracy. The products described may be subject to change without notice, and should not be relied on without further advice from Bridon.





Appendix B

Hydrodynamic Coefficients

B.1 Added Mass Coefficients

This Section shows added mass coefficients for three-dimensional bodies theoretically, and how to find the total added mass. This is taken from DNV GL (2011b), Recommended practice DNV- RP-H103.

Table A-2 Analytical added mass coefficient for three-dimensional bodies in infinite fluid (far from boundaries). Added mass is $A_{ij} = \rho C_A V_R$ [kg] where V_R [m³] is reference volume

Body shape		Direction of motion	C_A				V_R
Flat plates	Circular disc 	Vertical	2/π				$\frac{4}{3} \pi a^3$
	Elliptical disc 	Vertical	b/a	C_A	b/a	C_A	$\frac{\pi}{6} a^2 b$
			∞	1.000	5.0	0.952	
			14.3	0.991	4.0	0.933	
			12.8	0.989	3.0	0.900	
10.0			0.984	2.0	0.826		
7.0	0.972	1.5	0.758				
6.0	0.964	1.0	0.637				
Rectangular plates 	Vertical	b/a	C_A	b/a	C_A	$\frac{\pi}{4} a^2 b$	
		1.00	0.579	3.17	0.840		
		1.25	0.642	4.00	0.872		
		1.50	0.690	5.00	0.897		
		1.59	0.704	6.25	0.917		
		2.00	0.757	8.00	0.934		
		2.50	0.801	10.00	0.947		
3.00	0.830	∞	1.000				
Triangular plates 	Vertical	$\frac{1}{\pi} (\tan \theta)^{3/2}$				$\frac{a^3}{3}$	


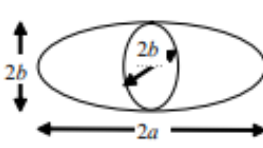
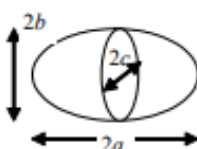
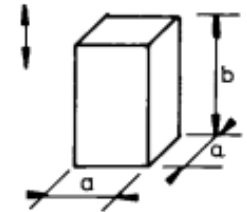
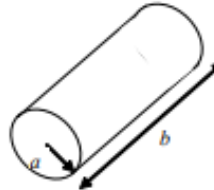
Bodies of revolution	Spheres 	Any direction	$\frac{1}{2}$		$\frac{4}{3} \pi a^3$
	Spheroids 	Lateral or axial	a/b	C_A Axial Lateral	$\frac{4}{3} \pi b^2 a$
		1.0	0.500 0.500		
		1.5	0.304 0.622		
		2.0	0.210 0.704		
		2.5	0.156 0.762		
		4.0	0.082 0.860		
		5.0	0.059 0.894		
		6.0	0.045 0.917		
		7.0	0.036 0.933		
		8.0	0.029 0.945		
Ellipsoid	 Axis $a > b > c$	Axial	$C_A = \frac{\alpha_0}{2 - \alpha_0}$ where $\alpha_0 = \varepsilon \delta \int_0^{\pi} (1+u)^{-3/2} (\varepsilon^2 + u)^{-1/2} (\delta^2 + u)^{-1/2} du$ $\varepsilon = b/a$ $\delta = c/a$		$\frac{4}{3} \pi abc$
Square prisms		Vertical	b/a	C_A	$a^2 b$
			1.0	0.68	
			2.0	0.36	
			3.0	0.24	
			4.0	0.19	
			5.0	0.15	
			6.0	0.13	
			7.0	0.11	
			10.0	0.08	

Table A-2 Analytical added mass coefficient for three-dimensional bodies in infinite fluid (far from boundaries). Added mass is $A_{ij} = \rho C_A V_R$ [kg] where V_R [m³] is reference volume (Continued)

Body shape		Direction of motion	C_A		V_R
			$b/2a$	C_A	
Right circular cylinder		Vertical	1.2	0.62	$\pi a^2 b$
			2.5	0.78	
			5.0	0.90	
			9.0	0.96	
			∞	1.00	

B.1.1 Effect of height (3D structure)

From DNV GL (2011b), the simplified approximation of the added mass in heave for a three-dimensional body with vertical sides may be applied

$$A_{33} \approx \left[1 + \sqrt{\frac{1 - \lambda^2}{2(1 + \lambda^2)}} \right] A_{33o} \quad [\text{kg}]$$

and

$$\lambda = \frac{\sqrt{A_p}}{h + \sqrt{A_p}} \quad [-]$$

Here, A_{33o} is the added for a flat plate with a shape equal to the horizontal projected area of the object with, h the height of the object and A_p the area of submerged part of object projected on a horizontal plane.

B.1.2 Effect of perforation

This part is taken from DNV GL (2011b). The effect of perforation on the added mass may roughly be estimated by the following guidance:

$$A_{33} = A_{33s} \quad \text{if } p \leq 5$$

$$A_{33} = A_{33s} \left(0.7 + 0.3 \cos \left[\frac{\pi(p-5)}{34} \right] \right) \quad \text{if } 5 < p < 34$$

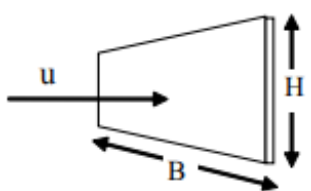
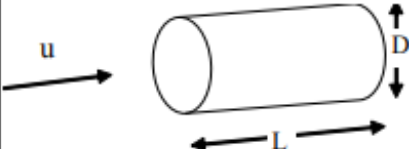
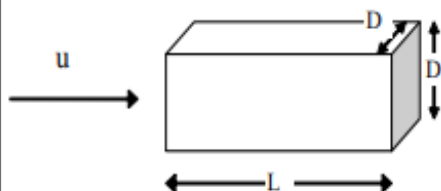
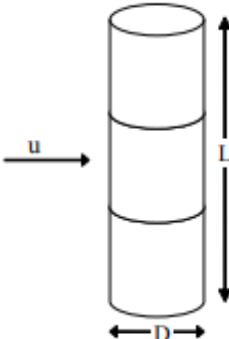
and

$$A_{33} = A_{33s} e^{\frac{10-p}{28}} \quad \text{if } 34 < p < 50$$

where A_{33s} is the solid added mass (added mass in heave for a non-perforated structure) in kilogram, and p is the perforation rate in percentage.

B.2 Drag Force Coefficients

This Section shows drag coefficients for three-dimensional bodies theoretically, and how to find the total drag force. This is taken from DNV GL (2011b), Recommended practice DNV-RP-H103.

Table B-2 Drag coefficient on three-dimensional objects for steady flow C_{DS} . Drag force is defined as $F_D = \frac{1}{2}\rho C_{DS} S u^2$. S = projected area normal to flow direction [m ²]. $R_e = uD/\nu$ = Reynolds number where D = characteristic dimension.			
Geometry	Dimensions	C_{DS}	
Rectangular plate normal to flow direction 	B/H 1 5 10 ∞	1.16 1.20 1.50 1.90 $R_e > 10^3$	
Circular cylinder. Axis parallel to flow. 	L/D 0 1 2 4 7	1.12 0.91 0.85 0.87 0.99 $R_e > 10^3$	
Square rod parallel to flow 	L/D 1.0 1.5 2.0 2.5 3.0 4.0 5.0	1.15 0.97 0.87 0.90 0.93 0.95 0.95 $R_e = 1.7 \cdot 10^5$	
Circular cylinder normal to flow. 	L/D 2 5 10 20 40 50 100	Sub critical flow $R_e < 10^5$	Supercritical flow $R_e > 5 \cdot 10^5$
		κ 0.58 0.62 0.68 0.74 0.82 0.87 0.98	κ 0.80 0.80 0.82 0.90 0.98 0.99 1.00
$C_{DS} = \kappa C_{DS}^\infty$			
κ is the reduction factor due to finite length. C_{DS}^∞ is the 2D steady drag coefficient.			

Appendix C

α -factor

From DNV GL (2011a), the North Sea and the Norwegian Sea should normally select the α -factor according to Table 4-1 through 4-5. Table 4-1 is applicable for weather forecast Level C, while Table 4-2 through Table 4-5 cover special cases. The table(s) can also be used as a guideline for other offshore areas.

Table 4-1 α -factor for waves, base case							
Operational Period [h]	Design Wave Height [m]						
	$H_s = 1$	$1 < H_s < 2$	$H_s = 2 = 2$	$2 < H_s < 4$	$H_s = 4$	$4 < H_s < 6$	$H_s \geq 6$
$T_{POP} \leq 12$	0.65	Linear Interpolation	0.76	Linear Interpolation	0.79	Linear Interpolation	0.80
$T_{POP} \leq 24$	0.63		0.73		0.76		0.78
$T_{POP} \leq 36$	0.62		0.71		0.73		0.76
$T_{POP} \leq 48$	0.60		0.68		0.71		0.74
$T_{POP} \leq 72$	0.55		0.63		0.68		0.72

Table 4-2 α -factor for waves, Level B highest forecast							
Operational Period [h]	Design Wave Height [m]						
	$H_s = 1$	$1 < H_s < 2$	$H_s = 2$	$2 < H_s < 4$	$H_s = 4$	$4 < H_s < 6$	$H_s \geq 6$
$T_{POP} \leq 12$	0.68	Linear Interpolation	0.80	Linear Interpolation	0.83	Linear Interpolation	0.84
$T_{POP} \leq 24$	0.66		0.77		0.80		0.82
$T_{POP} \leq 36$	0.65		0.75		0.77		0.80
$T_{POP} \leq 48$	0.63		0.71		0.75		0.78
$T_{POP} \leq 72$	0.58		0.66		0.71		0.76

Table 4-3 α-factor for waves, Level A with meteorologist at site							
Operational Period [h]	Design Wave Height [m]						
	$H_s = 1$	$1 < H_s < 2$	$H_s = 2$	$2 < H_s < 4$	$H_s = 4$	$4 < H_s < 6$	$H_s \geq 6$
$T_{POP} \leq 12$	0.72	Linear Interpolation	0.84	Linear Interpolation	0.87	Linear Interpolation	0.88
$T_{POP} \leq 24$	0.69		0.80		0.84		0.86
$T_{POP} \leq 36$	0.68		0.78		0.80		0.84
$T_{POP} \leq 48$	0.66		0.75		0.78		0.81
$T_{POP} \leq 72$	0.61		0.69		0.75		0.79

Table 4-4 α-factor for waves, monitoring							
Operational Period [h]	Design Wave Height [m]						
	$H_s = 1$	$1 < H_s < 2$	$H_s = 2$	$2 < H_s < 4$	$H_s = 4$	$4 < H_s < 6$	$H_s \geq 6$
$T_{POP} \leq 4$	0.9	Linear Interpolation	0.95	Linear Interpolation	1.0	Linear Interpolation	1.0
$T_{POP} \leq 12$	0.72		0.84		0.87		0.88
$T_{POP} \leq 24$	0.66		0.77		0.80		0.82
$T_{POP} > 24$	According to Table 4-1 or Table 4-2 as applicable						

Table 4-5 α-factor for waves, monitoring & Level A with meteorologist							
Operational Period [h]	Design Wave Height [m]						
	$H_s = 1$	$1 < H_s < 2$	$H_s = 2$	$2 < H_s < 4$	$H_s = 4$	$4 < H_s < 6$	$H_s \geq 6$
$T_{POP} \leq 4$	0.9	Linear Interpolation	0.95	Linear Interpolation	1.0	Linear Interpolation	1.0
$T_{POP} \leq 12$	0.78		0.91		0.95		0.96
$T_{POP} \leq 24$	0.72		0.84		0.87		0.90
$T_{POP} > 24$	According to Table 4-3						